University of Nevada, Reno

Resilience Enhancement Strategies for Modern Power Systems

A dissertation submitted in partial fulfillment of the
requirements for the degree of Doctor of Philosophy in
Electrical Engineering

by

Michael Abdelmalak

Mohammed Ben-Idris, Dissertation Advisor

August 2022

THE GRADUATE SCHOOL

We recommend that the dissertation
prepared under our supervision by

Michael Abdelmalak

Entitled

Resilience Enhancement Strategies for Modern Power Systems

be accepted in partial fulfillment of the
requirements for the degree of

DOCTOR OF PHILOSOPHY

Mohammed Ben-Idris, Ph.D., Advisor

Hanif Livani, Ph.D., Committee member

M. Sami Fadali, Ph.D., Committee member

David Feil-Seifer, Ph.D., Committee member

Christopher Barile, Ph.D., Graduate School Representative

Markus Kemmelmeier, Ph.D., Dean, Graduate School

August 2022

Abstract

The frequency of extreme events (e.g., hurricanes, earthquakes, and floods) and man-made attacks (cyber and physical attacks) has increased dramatically in recent years. These events have severely impacted power systems ranging from long outage times to major equipment (e.g., substations, transmission lines, and power plants) destructions. Also, the massive integration of information and communication technology to power systems has evolved the power systems into what is known as cyber-physical power systems (CPPSs). Although advanced technologies in the cyber layer improve the operation and control of power systems, they introduce additional vulnerabilities to power system performance. This has motivated studying power system resilience evaluation and enhancements methods.

Power system resilience can be defined as "The ability of a system to prepare for, absorb, adapt to, and recover from disruptive events" [1]. Assessing resilience enhancement strategies requires further and deeper investigation because of several reasons. First, enhancing the operational and planning resilience is a mathematically involved problem accompanied with many challenges related to modeling and computation methods. The complexities of the problem increases in CPPSs due to the large number and diverse behavior of system components. Second, a few studies have given attention to the stochastic behavior of extreme events and their accompanied impacts on the system resilience level yielding less realistic modeling and higher resilience level. Also, the correlation between both cyber and physical layers within the context of resilience enhancement require leveraging sophisticated modeling approaches which is still under investigation. Besides, the role of distributed energy

resources in planning-based and operational-based resilience enhancements require further investigation. This calls for developing enhancement strategies to improve resilience of power grids against extreme events. This dissertation is divided into four parts as follows.

Part I: Proactive strategies: utilizing the available system assets to prepare the power system prior to the occurrence of an extreme event to maintain an acceptable resilience level during a severe event. Various system generation and transmission constraints as well as the spatiotemporal behavior of extreme events should be properly modeled for a feasible proactive enhancement plan. In this part, two proactive strategies are proposed against weather-related extreme events and cyber-induced failure events. First, a generation redispatch strategy is formulated to reduce the amount of load curtailments in transmission systems against hurricanes and wildfires. Also, a defensive islanding strategy is studied to isolate vulnerable system components to cyber failures in distribution systems.

Part II: Corrective strategies: remedial actions during an extreme event for improved performance. The negative impacts of extreme weather events can be mitigated, reduced, or even eliminated through corrective strategies. However, the high stochastic nature of resilience-based problem induces further complexities in modeling and providing feasible solutions. In this part, reinforcement learning approaches are leveraged to develop a control-based environment for improved resilience. Three corrective strategies are studied including distribution network reconfiguration, allocating and sizing of distributed energy resources, and dispatching reactive shunt compensators.

Part III: Restorative strategies: retain the power service to curtailed loads in a fast and efficient means after a diverse event. In this part, a resilience enhancement strategy is formulated based on dispatching distributed generators for minimal load curtailments and improved restorative behavior.

Part IV: Uncertainty quantification: Impacts of uncertainties on modeling and solution accuracy. Though there exist several sources of stochasticity in power systems, this part focuses on random behavior of extreme weather events and the associated impacts on system component failures. First, an assessment framework is studied to evaluate the impacts of ice storms on transmission systems and an evaluation method is developed to quantify the hurricane uncertainties for improved resilience. Additionally, the role of unavailable renewable energy resources on improved system resilience during extreme hurricane events is studied.

The methodologies and results provided in this dissertation can be useful for system operators, utilities, and regulators towards enhancing resilience of CPPSs against weather-related and cyber-related extreme events. The work presented in this dissertation also provides potential pathways to leverage existing system assets and resources integrated with recent advanced computational technologies to achieve resilient CPPSs.

Acknowledgements

"If you have a dream, dream it big", a quote that always inspired me in many ways. I still remember the day I applied for Ph.D. degree and how the destination seemed hard to reach, but now it is becoming a reality. It has been a long road but without the support of few people, I wouldn't have accomplished it.

First of all, I would like to thank my adviser, Dr. Mohammed Ben-Idris, for his great efforts and guidance throughout my Ph.D journey. He has been a source of encouragement and motivation to go the farther mile. I am very grateful for his insightful mentorship, constructive feedback, and personal advice. I would like to acknowledge my deepest appreciation to, Dr. Sami Fadali, for his support and motivation. Also, I would like to thank Dr. Hanif Livani for being a great mentor and advisor.

I also owe special thanks to Dr. Sami Fadali, Dr. Hanif Livani, Dr. David Feil-Seifer, and Dr. Christopher Barile for providing valuable insights to my research work and constructive feedback.

Moreover, I would like to thank all my family members; my parents and my siblings, who have been so much supporting and encouraging. They have pushed me forward and instilled in me sufficient enthusiasm to pursue a Ph.D. degree. Ultimately, guiding me to a clear future career plan, they have always shown great care.

I would like to thank the University of Nevada Reno (UNR) for having me as graduate student and Electric Power Research Institute (EPRI) for giving me the opportunity to conduct two summer internship during my degree studies. I would also like to acknowledge the funding agencies: National Science Foundation (NSF) and US Department of Energy (DOE) for their funding support through National Renewable Energy Laboratory (NREL) and City of Reno. I would also like to recognize EnerNex LLC and National Renewable Energy Laboratory for hosting me as an NSF contracted intern and bridging my academic knowledge to the industry.

Last but not least, I am grateful to everyone who has been part of this journey: my colleagues at the E-RESILIENCY Lab at UNR, Dr. MD Kamruzzaman (EDF Renewables Inc.), Dr. Narayan Bhusal (Quanta Technology), Mukesh Gautam, and Jitendra Thapa. Also, I would like to thank all my internship supervisors, Dr. Hossein Hooshyar (NYPA), Dr. Evangelos Farantatos (EPRI), Dr. Aaron Snyder (EnerNex LLC), Mr. Sean Morash (EnerNex LLC), Mrs. Eliza Hotchkiss (NREL), and Dr. Jordan Cox (NREL).

Contents

List of Tables

List of Figures

Chapter 1

Introduction

1.1 Motivation

The frequency and impacts of severe events have increased dramatically in the last decade yielding increased power outages and catastrophic economic losses [2, 3]. These extreme events are usually classified into weather-related and cyber-related events. Each extreme event has distinct impacts on the performance of power systems [4, 5] as well as the associated impacts on the society [6, 7, 8, 9, 10]. The motivation for the work presented in this dissertation is explained as follows.

Weather-related Events. Annual economic losses due to extreme weather-related outages in the United States have exceeded $20 billion [11]. During the last seven years, the United States has been exposed to seven wildfires, eight droughts, 75 severe storms, 19 tropical cyclones, 16 floods, five winter storms, and one freeze event with more than one billion-dollar anticipated costs [12]. In 2017, the costs of damages caused by hurricanes Harvey, Maria, and Irma are $142, $101, and $57 billion, respectively. In 2018, a statistical analysis on wildfires over the period 2000–2016 has shown that wildfires cost utilities more than $700 million in parts of California's transmission and distribution systems [13]. The risk of severe wildfire has forced electric utilities to cut off power to 800,000 customers in California, USA in 2019 [14]. The very recent hurricane Ida has caused damages and losses exceeding $75 billion over the course of three days. More than four million customers in Texas experienced power outages with an outage time of more than 105 hours in some places due to the Uri ice storm in February 2021 [15]. The recent Dixie wildfire in the West coast of the U.S. has lasted for more than 60 days, burned almost one million acres of land, and resulted in evacuation orders for thousands of families [16]. Also, since the beginning of 2022, an extreme winter storm has caused power outages to more than 400,000 customers for a few days in the Northeastern region of the United States [17]. The societal and economic losses caused by severe weather events necessitate building more resilient power grids and developing enhancement strategies to mitigate, reduce, or even eliminate some of these impacts.

Cyber-related Events. The extensive integration of communication, computation, and control technologies into cyber-physical power systems (CPPSs) has increased the vulnerabilities of CPPSs to cyberattacks [18, 19]. Though this integration has enabled diverse applications of automation and control for enhanced performance of CPPS, vulnerabilities of power systems to cyber failures and cyberattacks have increased dramatically [20, 21]. Blackouts due to cyber-attacks and cyber-related issues have also been increasing [22, 23]. For example, the cyberattack on the Ukrainian power grid on December 2015 resulted in a blackout that affected 225,000 residents [24, 25]. Recent (June 16, 2019) blackout in South America caused power outages to more than 48 million customers [26]. The most recent power outage (August 3, 2019) in the capital of Indonesia caused the power outage to more than 10 million customers [27]. In the United States, cyberattacks have successfully compromised waste water systems, as seen in Oldsmar, Florida in February 2021 [28] and San Francisco, California in January 2021 [29]. Though extreme weather events have counted for the majority of power outages and losses, cyber-induced failures can also result in catastrophic failures and blackouts given that a large part of the grid can be impacted [30].

Resilience Enhancement Strategies. Though several resilience enhancement strategies have been studied, there still exist some challenges with proper system and events modeling as well as associated uncertainties [31]. First, some generation and transmission constraints are usually relaxed to reduce modeling complexities, yielding higher resilience levels. In [32, 33], the impacts of load variations, system preparedness level, event attack time (i.e., the instant at which an extreme event hits the system), and future potential failures have been given less attention. Moreover, preparing power systems for potential $N - k$ (i.e., $k > 1$) contingencies is an important factor for enhancing power system resilience due to the fast sequential probabilistic component failures. In [34], a procurement plan of black start units has been studied assuring sufficient energy supply prior to events at minimal cost; however, the spatiotemporal characteristics of extreme weather events have not been considered. Also, the high penetration level of renewable energy resources (RESs) has introduced significant uncertainties in the operation and control of power systems especially during extreme weather events. The 2021 Texas ice storm has raised concerns about the capability and availability of RESs during extreme events [35]. In short, ignoring the role of uncertainties result in over-estimated resilience levels. This calls for developing resilience enhancement strategies that consider realistic system and event models as well as operational constraints. Also, an uncertainty quantification framework is crucial to assess the stochastic behavior of extreme weather events and the associated impacts on system performance.

1.2 Power System Resilience

Definitions. The intergovernmental panel on climate change has defined power system resilience in terms of anticipation, absorption, and quickly and efficiently recover after hazardous events [36]. In [1], United States' presidential policy directive–

21 has defined resilience in terms of prepare, adapt, withstand, and recover rapidly from disruptions. The disruption could be a natural threat or man-made misery such as cyber-attacks. Electric Power Research Institute (EPRI) has defined power system resilience in terms of three elements: prevention, recovery, and survivability [37]. The U.S. National Infrastructure Advisory Council (NIAC) has defined power system resilience as to prepare and plan, absorb, recover, and adapt to adverse events [38]. North America Electric Reliability Corporation (NERC) has adopted the definition of NIAC in [39]. More definitions for power system resilience can be found in [6, 40, 41, 42, 43].

Disturbance and System Response Curves. The concept of resilience through a disturbance and impact resilience evaluation (DIRE) curve has been provided in [44, 45] which is shown in Fig. 1.1. The DIRE curve illustrates the relative performance of a system to optimal and minimum performance level (resilient thresholds) that the system needs to maintain to be considered resilient. Several common terms such as robustness, agility, adaptive capacity, adaptive insufficiency, resilience, and brittleness have been presented in the DIRE curve. The DIRE curve provides temporal demarcation as follows: t_i is the disturbance starting instant; t_{Bi} indicates the time at which the performance of the system falls below a minimum normalcy; t_R is the instant at which the system reaches a minimum performance level; t_{Bf} indicates the time at which the performance of the system achieves minimum normalcy again; and t_{f1} indicates the time at which the restoration processes start. In these notations, i indicates the start of the event and f indicates the end of the event. Also, it is worth mentioning here that the restoration processes could take a long time (i.e., $t_{f2} >> t_{f1}$). Also, a conceptual resilience curve has been developed in [46] to define and quantify power system resilience. It shows the level of resilience as a time-dependent function with respect to disaster event as shown in Fig. 1.2. A set of metrics have been proposed in [47, 48] based on the resilience curve. These metrics are abbreviated as FLEP which stands for: how fast (F) and how low (L) resilience drop in phase I (disturbance progress); how extensive (E) the post-disturbance degraded state is in phase II (post-disturbance degradation); and how promptly (P) the network recovers in phase III (restorative). Accordingly, this work focuses on studying the resilience of power systems covering the whole three main phases of operational resilience including proactive, corrective, and restorative.

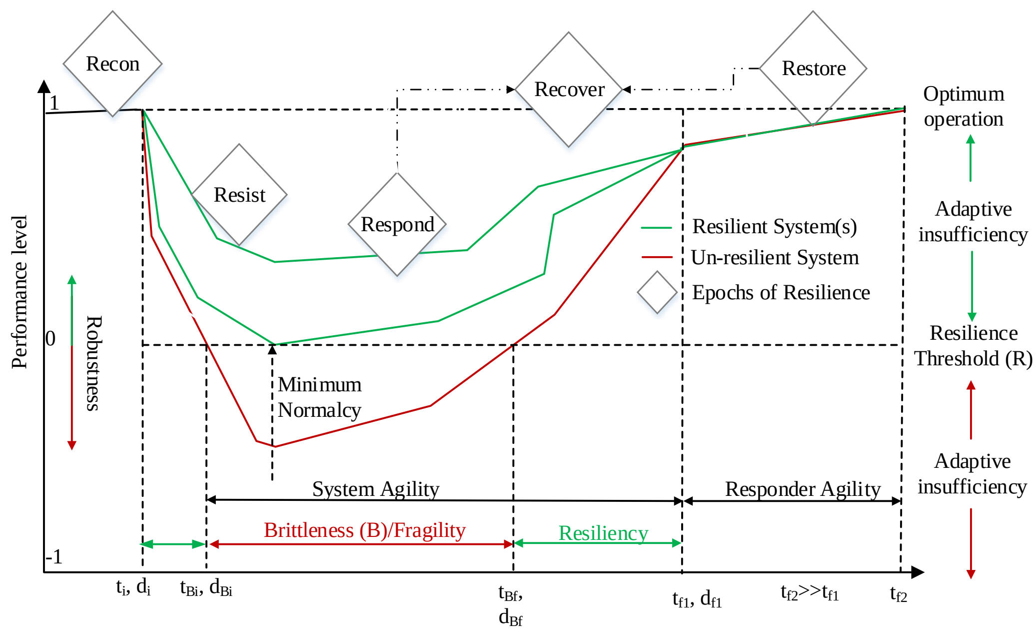

Figure 1.1: DIRE Curve (i=initial, f=final)

1.3 Objectives

The main goal of the dissertation is to develop resilience enhancement strategies for power grids. The proposed resilience enhancement strategies are classified into proactive, corrective, and restorative strategies. The goal of the dissertation is achieved via the following objectives:

- Develop various resilience enhancement strategies to improve the performance of power grids prior to, during, and after the occurrence of an extreme event.

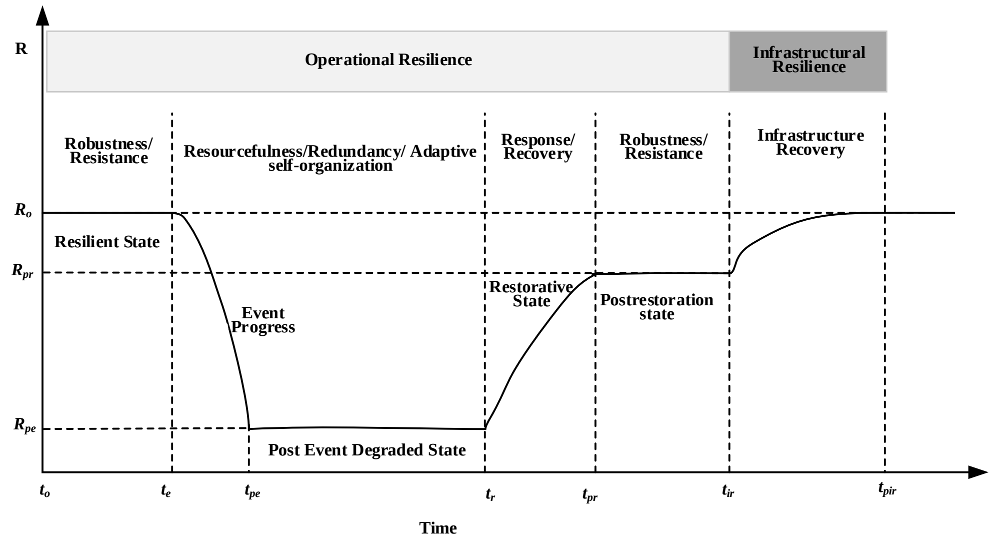

Figure 1.2: Resilience Curve

- Determine several approaches to formulate, solve, and assess the proposed enhancement strategies including optimization techniques, reinforcement learning (RL)-based techniques, simulation techniques, and statistical-based techniques.

- Develop uncertainty quantification models to evaluate the random behavior of extreme events and renewable energy resources.

The main thesis can be stated as follows: *Proper event- and time-based selection and implementation of proactive, corrective, or restorative resilience enhancement strategies will significantly improve the resilience the power supply.*

1.4 Organization

The description and organization of each chapter is provided as follows.

Chapter 2 describes modeling of extreme weather events and the fragility behavior of system components against weather parameters. First, the spatiotemporal characteristics of extreme weather events are explained including hurricane and ice storm events. A wind field model is used to simulate the propagation of a hurricane event, and an ice storm model is provided to emulate a freezing-rain ice storm event. Then, the concept of fragility model is explained to compute the failure probability of different system components due to diverse weather parameters.

Chapter 3 explains two proactive resilience enhancement strategies, which are proactive generation redispatch strategy and defensive islanding strategy. First, the mathematical model of the proactive generation redispatch strategy is formulated given generation and transmission constraints. Then, a Markov decision process (MDP) is leveraged to formulate the proactive generation redispatch strategy considering the uncertain failure behavior of system components. Various test cases are provided for validation. Moreover, the concept of defensive islanding as a resilience enhancement strategy is explained. The defensive islanding approach is proposed to reduce/mitigate the impacts of cyber-induced failures. Regarding cyber-induce failures, a correlation mapping model between cyber components and power system components is illustrated to simulate the propagation behavior of cyber-induced failures. The proposed clustering methodology aims to split the power grid into small grids considering the components' fragility and the system operating conditions.

Chapter 4 focuses on corrective resilience enhancement strategies leveraging reinforcement learning approaches. First, a detailed explanation of actor-critic algorithms is provided for a single and multi agent framework. Then, the proposed actor-critic algorithms are used to formulate three corrective resilience enhancement strategies including network reconfiguration, allocation of distributed energy resources (DERs), and dispatching shunt compensators. In the network reconfiguration strategy, it is required to control tie-switches and sectionalizers of a distribution feeder to improve resilience due to multiple line outages. The second strategy aims to determine the locations and sizes of DERs for enhanced resilience. The shunt dispatch strategy focuses on determining required reactive power to be injected into transmission systems to maintain the voltage levels within permissible range.

Chapter 5 provides a restorative strategy to improve resilience of distribution power systems after extreme events. The proposed strategy dispatches available distributed generators (DGs) due to multiple line failures of an islanded distribution feeder. A multi-agent deep deterministic policy gradient model is trained to minimize the amount of load curtailments. The proposed approach provides a preliminary results as a potential future extension of this dissertation.

Chapter 6 describes the role of uncertainties in resilience assessment methods. This chapter discusses the uncertainties associated with spatiotemporal characteristics of extreme weather events, fragility failure behavior of system components, and renewable energy unavailability. First, a resilience assessment framework is developed and used to quantify the stochasticity of ice storms on transmission system components. Then, a probabilistic model is proposed to quantify the uncertainty of hurricanes and their impacts on accuracy of the results. Proper probability distribution functions (PDFs) representing weather-related parameters are used to simulate diverse ice storm and hurricane events. Finally, the role of unavailability of RESs is evaluated for improved resilience performance.

Chapter 7 summarizes the main outcomes of the proposed resilience enhancement strategies. It also discusses future work of the developed approaches.

Chapter 2

Modeling of Extreme Events

Modeling of evolvements of extreme events and failure propagations is an important factor to evaluate the resilience of power systems—extreme events are defined in this dissertation as weather-related and cyber-induced events. Extreme weather events have different models depending on the type and intensity of the given event. For example, HAZUS (Hazards US) models are usually used to forecast hurricanes and floods. Modeling of failure propagations due to simulated weather extreme events is usually carried out using fragility curves. This chapter provides a brief illustration on modeling of extreme weather events. First, a description of the spatiotemporal propagation behavior characteristics is provided focusing mainly on hurricane and ice storm events. Then, the failure fragility of system components due to weather factors or cyber incidents is explained.

2.1 Introduction

Although power system resilience has been assumed to be related to High Impact Low Probability (HILP) events, HILP events are no longer low probability events [49]. Extreme weather events have catastrophic impacts on the society [6, 7, 8, 9, 10] as well as on the resilience of power grids [4, 5]. Man-made events such as cyber-attacks have also been considered as high impact events [50]. Each extreme event has distinct impacts on the performance of power systems. For example, earthquakes, wind storms, and hurricanes usually result in the failure of underground cables, transmission poles, and overhead transmission lines of power systems [51, 52, 53]. On the other hand, cyber-related events impact the power grid through communication channels and control centers [54]. A proper model is required for any extreme event to identify its propagation and impact. Both probabilistic [55] and deterministic [56] methods have been used to model weather-related events. Most of the studies in the field of resilience rely either on historical data of extreme events [57, 58, 59, 60] or forecasting models provided by meteorological agencies to model extreme events [61, 62]. The forecasting and historical weather data can be obtained from different sources including the National Weather Service (NWS), National Oceanic and Atmospheric Administration (NOAA) and Weather Research and Forecasting (WRF) model [63].

Modeling of Weather-related Events. Several models have been proposed in the existing work to model weather events. In [56], the Yang Meng wind field model has been used to calculate the wind speed for a moving typhoon and determine the duration of the event. Satellite big data has been used to identify the path of hurricane [52], whereas a tri-level scaled hourly historic wind profile during hurricane events has been applied in [4]. One of the most widely used hurricane models named HAZUS-MH2 has been developed to simulate a real hurricane event based on historical records [60]. The HAZUS-MH model has been developed by the federal emergency management agency (FEMA) to simulate flood scenarios based on historic data [64] and to simulate typhoon scenarios for critical infrastructure resilience assessment [57].

Though hurricane events have gained more interest compared to other extreme weather event, other studies have proposed models for earthquakes, wildfires, and floods. In [65], a model has been proposed based on the rate of spread, solar radiation, and radiative heat flux to model wildfire using historical data. A probabilistic earthquake energy transfer model has been proposed based on auto regressive (AR) estimation method in [66]. The proposed model can be used to estimate the peak ground acceleration parameter based on three main variables: earthquake intensity in Richter, the distance between the earthquake center and location of interest, and the ground type. In [61], a flood model has been used which is based on rainfall intensities using weather agencies' prediction model. A forecasting model has been used to estimate the ice thickness forecast error in [67]. An ice disaster model has been proposed in [68] to calculate the rate of ice accretion based on five main parameters: rate of precipitation, the content of the liquid water, speed of the wind, path, and moving speed.

Modeling of cyber-related Events. Cyber-attacks can severely impact the resilience of power systems especially if they are planned based on prior reconnaissance missions. Although there have been no sufficient historical data to model cyber-attacks, modeling of cyber layers and their interactions with physical layers can capture the extent to which cyber-attacks can impact the functionality of power systems. Cyber incidents can be classified as inefficiency in the communication, distortion in information, malfunction in the device, leakage in secrecy, and misconfiguration in applications. The main domains for cyber-attacks are application software, communication network, and field devices. Cyber-attack approaches have been reviewed focusing on illustrating several ways to create a cyber-attack event [54]. To simulate a cyber-attack, the control systems of 50 generators have been infected by a malware known as Erebos Trojan. A cyber vector represents the path that an attacker takes to target specific cyber elements. The malware was able to drive the generators to the overloading phase leading to the collapse of the system [50, 54].

Modeling of Impacts of Extreme Events. Most of the resilience-based studies have focused on modeling failure of system elements toward extreme weather events. The HILP events are difficult to model due to their stochastic behavior and lack of historical data [43, 59, 69]. The most well-known models to allocate failed elements are the random outage method, scenario-based method, and fragility curves [4, 31]. In random outage methods, several elements are selected randomly to be in the down state without considering a forecasted event scenario or real-time event scenario [70, 71, 72]. A scenario-based method implements either a historical real event or a simulated event on a geographical map to determine the impacted points on a real power system [71, 73, 74]. A fragility curve model has been used extensively to calculate the probability of failure of system elements for a given event parameter such as wind speed or earthquake ground acceleration [32, 41, 46, 48, 56, 66, 75, 76, 77].

A fragility curve provides a means to assess the impact of extreme events on various system elements and determine their unavailability. At every simulation instant, a forecasted weather profile is mapped to the fragility curve to obtain the failure probabilities [78]. Several fragility curves have been studied in weather-related resilience studies [56, 75, 79]. A seismic vulnerability assessment algorithm using four fragility curves based on peak ground acceleration due to the earthquake has been presented in [66]. A fragility curve model has been implemented in [48, 56] for transmission lines and towers based on wind speeds. In [59, 80, 81, 82, 83, 84, 85], a pre-developed fragility curve has been used for distribution poles and conductors. A fragility model, developed by the Resilient electricity Networks for Great Britain (RESNET), has been used to assess elements failure based on wind speed [4, 40]. A flood-induced fragility model based on rainfall intensity has been used for a microgrid proactive scheduling strategy in [61]. A detailed methodology has been studied in [86] to estimate the probability of line failure based on wind force and maximum rated line perpendicular stress resistance. A log-normal fragility curve has been presented in [86] to determine the probability of substation failures against wind storms. A fragility model has been used in [32, 68, 87] to determine the failures of transmission poles and lines against ice storms.

2.2 Spatiotemporal Propagation Characteristics

This section provides a description to models of extreme events. It explains the wind field model and the ice storm model representing the propagation of a hurricane and freezing rain storm, respectively.

2.2.1 Wind Field Model

Hurricanes are characterized by unique spatiotemporal properties that are governed by weather-related parameters such as wind speed, wind direction, and central pressure difference, and geographically-related parameters such as landing site [88]. Various stochastic wind field models have been identified [89], however, Batts model has been widely used [90]. In Batts model, hurricanes are assumed to vanish over time as a result of the reduction of the pressure difference between the center and the periphery of the hurricane. As a hurricane propagates, the pressure difference at a certain time t can be found as follows,

$$\Delta P(t) = \Delta P_0 - 0.02\,[1 + \sin(\phi - \delta)]t, \tag{2.1}$$

where $\Delta P(t)$ is the central pressure difference at time t, measured in $inHg$, ΔP_0 is the original central pressure difference before the hurricane lands, ϕ is the angle between coastline and the due north direction, and δ is the angel between the due north direction and the hurricane motion direction—the clockwise is positive. Accordingly, the maximum gradient wind speed is evaluated as follows,

$$v_g(t) = K\sqrt{\Delta P(t)}, \tag{2.2}$$

where K is a geographical location constant. The value of K is measured in $m/s/mm^{1/2}$ can be represented by a linear function that varies between 6.97 at latitude 23^o N to 6.93 at latitude 45^o N [90]. Note that the value of $\Delta P(t)$ in (2.2) is measured in $mmHg$. By multiplying (2.1) with a scaling factor of 0.75 to compensate for the the unit type difference and substituting in (2.2), the maximum gradient wind speed is computed as follows,

$$v_g(t) = K\sqrt{0.75\Delta P_0 - 0.508\,[1 + \sin(\phi - \delta)]t}, \tag{2.3}$$

The total duration of the hurricane (T) can be obtained when the $\Delta P(t)$ is equal to zero yielding the following,

$$T = 1.476\ \Delta P_0/\ [1 + \sin(\phi - \delta)], \tag{2.4}$$

where T is measured in seconds.

The maximum wind speed of the hurricane at time t is evaluated as follows,

$$v_{r_{max}}(t) = 0.865\ v_g(t) + 0.5\ V_T, \tag{2.5}$$

where V_T is the translational speed of the hurricane, measured in m/s.

The wind speed of a certain location varies based on the relative position between the determined location and the radius of maximum wind speed as follows,

$$v_r(t) = \begin{cases} v_{r_{max}}(t)d(t)/r_{max}(t), & d(t) \leq r_{max}(t) \\ v_{r_{max}}(t)(r_{max}(t)/d(t))^{0.6}, & d(t) > r_{max}(t) \end{cases} \tag{2.6}$$

where $d(t)$ is the euclidean distance between a location and the center of the hurricane at time t, measured in m, and r_{max} is the radius of maximum wind speed, which can be calculated as follows [91, 92],

$$r_{max}(t) = \exp(2.63 - 5.086 \times 10^{-5}(\Delta P(t))^2 + 0.0395y_h(t), \tag{2.7}$$

where $y_h(t)$ is the latitude of the center of the hurricane.

The distance between a specific geographical location and the hurricane center at time t can be evaluated as follows,

$$d(t) = \sqrt{[x_d - x_h(t)]^2 + [y_d - y_h(t)]^2}, \tag{2.8}$$

where x_d and y_d are the latitude and longitude coordinated of the component location, respectively, and x_c and y_c are latitude and longitude coordinates of the center of the hurricane at time t, respectively, which can be calculated as follows,

$$x_h(t) = x_0 + V_T\, t\, \sin(\delta), \tag{2.9}$$

$$y_h(t) = y_0 + V_T\, t\, \cos(\delta), \tag{2.10}$$

where x_0 and y_0 are the hurricane landing coordinates, respectively.

Fig. 2.1 displays the spatiotemporal characteristics of the hurricane across the system. It shows the relative distance between the center of a hurricane and a specific system component as the hurricane propagates.

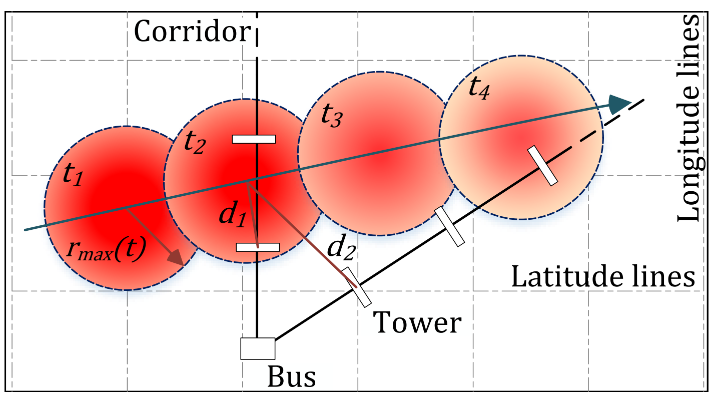

Figure 2.1: Wind field and ice storm propagation across power system components

The main parameters that affect the severity and propagation behavior of a hurricane are original pressure difference ΔP_0, translational speed V_T, hurricane motion direction δ, and landing site coordinates (x_0, y_0). Several hurricanes can be simulated using different parameter values. PDFs governing the behavior of such parameters can be obtained via extensive statistical analysis using measured weather data at the geographical location under study.

2.2.2 Ice Storm Model

The spatiotemporal characteristics of ice storms are governed by weather-related parameters and geographical-related parameters [88]. Their parameters can be used to identify the uncertainty behavior of an ice storm. Weather-related parameters include, but not limited to, wind speed, translational speed, and ice precipitation rate, whereas geographical-related parameters can be coordinates of the ice storm landing site. System components may fail as a result of increased ice accumulation and extended freezing temperature during an ice storm. In [93], a predicting model to calculate the snow loads on transmission lines has been presented. A freezing rain ice load model has been provided in [94]. The ice thickness on transmission lines and towers is calculated based on a freezing rain ice model provided in [89].

The level of ice thickness differs based on the relative position between the center of the ice storm and the component under study, which can be calculated as follows,

$$R_{ice}(t) = (N_h/\rho_i \pi)\sqrt{(P_{ice}\rho_w)^2 + (3.6V_w(t)W)^2}, \tag{2.11}$$

where $R_{ice}(t)$ is the ice thickness on the component under study, measured in inch, at time t, W is the liquid water content of rain-filled air ($W = 0.067P_{ice}^{0.846}$), $V_w(t)$ is the wind speed (m/s) at the component under study at time t, P_{ice} is the ice precipitation rate at the component under study, ρ_i is the density of ice (0.9 g/cm^3), and ρ_w is the density of water (1.0 g/cm^3).

Fig. 2.1 visualizes the propagation behavior of an ice storm crossing transmission lines and towers. It also shows the importance of a component location with respect to the ice storm propagation path. Since ice accumulation decreases radially as it gets farther from the center of an ice storm, components closer to the center of an ice storm will experience high ice accumulation level. Also, the impact of an ice storm on components lying outside the maximum impact radius will be very small and can be neglected. The main weather-related and geographical-related parameters that govern the behavior of an ice storm are ice precipitation rate, central pressure, translational speed, motion direction, wind speed, and landing site coordinates [88]. The behavior of ice storms varies based on the values of these parameters. Extensive statistical analysis can be applied to determine proper PDF for each parameter through recorded weather data at specified geographical locations.

2.3 Fragility Modeling

Transmission corridors are defined as sets of transmission line segments and transmission poles that connect two buses. A single corridor is decomposed of segments such that each segment comprises two corresponding towers and the part of transmission line carried by them. Since transmission corridors can be relatively long, the weather parameters of an extreme event change from one location to another along the same corridor. In other words, the wind speed at the head of a transmission corridor may hold different value than at the middle or the end of the corridor. Additionally, wind speed varies at sequential time instants for a specific geographical location.

2.3.1 Wind Speed Fragility

A fragility model from [89] is adopted to calculate the failure probability of each transmission corridor based on the wind speed at specific time instants. By dividing the total hurricane period (T) into N time steps, a set of discrete time instants can be obtained. Also, transmission corridors are decomposed of M towers and L line segments. The instantaneous failure rates of the transmission towers and line segments can be calculated as follows,

$$\lambda_{k,m}(t_d) = \begin{cases} 0, & v_{k,m}(t_d) \leq v_{to} \\ \exp[\gamma(v_{k,m}(t_d) - 2v_{to})], & v_{to} < v_{k,m}(t_d) \leq 2v_{to} \\ 1, & v_{k,m}(t_d) > 2v_{to} \end{cases} \tag{2.12}$$

$$\lambda_{k,n}(t_d) = \exp\left\{11 \times \frac{v_{k,n}(t_d)}{v_{li}} - 18\right\} \Delta l, \tag{2.13}$$

where t_d is discrete time instant, $v_{k,m}(t_d)$ is the wind speed, γ is the model coefficient [89], v_{to} is a threshold design wind speed of transmission tower, in this study $35m/s$, $v_{k,n}(t_d)$ is the wind speed at the midpoint of the n^{th} line segment, v_{li} is a threshold design wind speed of line segment, and Δl is the length of the line segment.

2.3.2 Ice Precipitation Fragility

A spatiotemporal fragility model from [89] is integrated with an ice storm model adopted from [68] to calculate the cumulative failure probability of each transmission corridor during the ice storm. The total ice storm duration period T can be divided into N time steps with a shorter duration period Δt, where component statuses can be evaluated at discrete time instants. For a transmission corridor i, which is split into L line segments through M towers, the failure rate $\lambda_{i,m}$ of the m^{th} tower of the i^{th} corridor at time t_j can be evaluated as follows,

$$\lambda_{i,m}(t_j) = \begin{cases} 0, & R_{i,m}(t_j) \leq R_{to} \\ e^{[\frac{0.6931(R_{i,m}(t_j) - R_{to})}{4R_{to}}]} - 1, & R_{to} < R_{i,m}(t_j) \leq 5R_{to} \\ 1, & R_{i,m}(t_j) > 5R_{to} \end{cases} \tag{2.14}$$

where $R_{i,m}(t_j)$ is the ice thickness, and R_{to} is a threshold ice thickness design of transmission tower (in this study 15 mm value is used).

The failure rate $\lambda_{i,n}$ of the n^{th} line segment of the i^{th} transmission corridor at time t_j can be evaluated as follows,

$$\lambda_{i,n}(t_j) = \exp\left\{11 \times \frac{R_{i,n}(t_j)}{R_{li}} - 18\right\} \Delta l, \tag{2.15}$$

where $R_{i,n}(t_j)$ is the ice thickness at the midpoint of the n^{th} line segment, and R_{li} is a threshold design ice thickness of line segment.

2.4 Failure Probability of System Components

The corresponding probability of failure of the transmission towers and line segments during the extreme event for a specific transmission corridor can be calculated as follows,

$$P_{k,m} = 1 - \exp\left\{-\sum_{d=0}^{N-1} \frac{\lambda_{k,m}(t_d)}{(1-\lambda_{k,m}(t_d))}\Delta t\right\}, \tag{2.16}$$

$$P_{k,n} = 1 - \exp\left\{-\sum_{d=0}^{N-1} \lambda_{k,n}\Delta t\right\}. \tag{2.17}$$

A whole transmission corridor will become out of service, if a single transmission segment fails. In this study, the failure of components on the same corridor are assumed independent. Therefore, the cumulative failure probability of the k^{th} corridor can be evaluated by combining (2.17) and (2.16) as follows,

$$P_k = 1 - \prod_{1}^{M}(1 - P_{k,m}) \prod_{1}^{L}(1 - P_{k,n}). \tag{2.18}$$

Chapter 3

Proactive Strategies

Proactive resilience enhancement strategies focus mainly on utilizing the available assets to prepare the power system prior to the occurrence of an extreme event to maintain an acceptable resilience level during the event. Various dynamic system constraints need to be considered for a feasible proactive enhancement plan such as availability of generation units and transmission lines, load variations, operational costs, generation ramping rates, and time-related constraints. Also, the spatiotemporal behavior of extreme event propagation should be modeled considering future potential failures, event attack time, and duration of impact. In this chapter, we propose two proactive strategies to enhance resilience of power systems prior to an extreme event. First, a probabilistic proactive generation redispatch strategy is formulated using MDP to minimize the amount of load curtailments and total operational costs. The proposed framework is studied for hurricane and wildfire events. The efficiency of the generation redispatch approach is validated through several case studies on IEEE 30-bus system. Moreover, a defensive islanding approach is studied to enhance robustness of distribution systems against cyber-induced failures. Defensive islanding aims to split a power system into smaller microgrids and isolate impacted parts of CPPS. The propagation behavior of cyber-induced failures to power system components is illustrated. The proposed algorithm is tested on a modified 33-node system integrated with DERs and cyber-related devices.

3.1 Introduction

Various strategies have been proposed to improve the resilience of power systems against extreme weather events. Such strategies have focused mainly on restoration approaches such as mobile energy storage systems, network reconfiguration, and microgrid formation [52, 53]. Proactive and corrective resilience-based enhancement strategies have not been sufficiently explored [95]. To reduce modeling complexities, some generation and transmission constraints are usually relaxed, yielding higher resilience levels [32, 33]. Impacts of load variations, system preparedness level, event attack time, and future potential failures have been given less attention [2]. Since extreme weather events may create sequential failures of system components, other studies have considered the role of system operators in the decision making process for improved resilience [32, 96]. The need of having a fast-acting decision tool to optimize system operations during extreme events has increased dramatically [97].

Resilience Enhancement through Proactive Preparations. Several operational resilience enhancement strategies have been proposed. Maintenance planning [31, 98, 99] and mobile energy storage allocation [4, 66, 73] strategies have been studied to prepare the system before an event. A decision-making framework based on an analytical hierarchy process has been proposed in [100] to evaluate possible locations of solar panels and battery energy storage systems for multiple contingencies to improve resilience of distribution systems and reduce operational costs. In [101], a graph theory-based approach integrated with Choquet integral has been used to quantify resilience enhancements and to maintain power supply to critical loads at the distribution level. In [34], a procurement plan of black start units has been studied assuring sufficient energy supply prior to events at minimal cost; however, the spatiotemporal characteristics of extreme weather events have not been considered.

A proactive generation redispatch strategy has been proposed in [32] to reduce load curtailments during hurricanes where operational costs and load variations are not considered. An approach for generation redispatch during hurricanes has been proposed in [33, 102], which takes into account event attack time, operational costs, and generation level prior to the event. Though several resilience enhancement strategies have been studied at the distribution level, developing resilience enhancement methods at the transmission level still requires further investigation [31]. The impacts of sequential probabilistic component failures create stressed operating conditions on the transmission system with the potential of cascading failures or blackouts. Also, preparing power systems for potential $N-k$ (i.e., $k>1$) contingencies is an important factor for enhancing power system resilience against extreme events.

Resilience Enhancement through Microgrid Formation. On the other hand, several methods have been proposed to enhance the resilience of power systems using islanding and microgrid formation strategies. A spectral clustering algorithm has been employed to determine optimal network partitions under tight potential $N-k$ (i.e., $k>1$) contingencies [103]. A risk-based defensive islanding approach has been studied in [78] to reduce the impact of cascading failures on transmission systems for enhanced resilience against hurricanes. In [104], a multi-layer constrained clustering technique has been investigated to split a power system into islands while minimizing power disruptions. Also, a clustering approach has been integrated with frequency measurements of inverter-based resources to create microgrids based on transient responses of RESs [105]. In [106], a resilience-based microgrid formation framework has been proposed to enhance the restoration of critical loads in both radial and meshed networks. Most of these studies have focused on transmission level due their highly meshed topology. Despite the significant contributions of these methods to enhance islanding strategies, impacts of cyber-induced failures on microgrid formation of distribution systems require further investigation.

Resilience Enhancement against Wildfires. A few studies have proposed several resilience enhancement strategies against wildfires [65, 107, 108, 109]. In [107], the impact of wildfires on the optimal power flow solution of transmission system has been studied based on propagation of flat fire surface toward a single transmission line. In [108], a proactive dispatch algorithm of DGs has been proposed considering uncertainties of wildfire progression and accompanied impacts on distribution line ratings. A stochastic programming approach has been used in [65] to determine the optimal utilization of RESs on the main feeder of a distribution system during a wildfire given uncertainties of weather parameters. In [109], a resilience-based enhancement strategy has been proposed to avoid spurious trip of inverter-based resources and eliminate the risk of wildfires. A probabilistic decision process has been proposed in [110] to improve resilience of power systems against wildfires; however, the propagation rate of a wildfire has not been considered. Although several enhancement strategies against wildfires have been proposed, only a few have tested the applicability of proactive generation redispatch considering probabilistic behavior of component failures due to spatiotemporal characteristics of wildfires.

Resilience Enhancement against Cyber-induced Failures. The impact of cyber-induced failures on the operational performance of CPPS has gained significant interest. A CPPS model representing the IEEE 118-bus system integrated with a communication network has been used to assess the impact of malware-induced cyberattacks [111]. An exploration approach to identify the most vulnerable components to malicious external attacks in nuclear power plants has been studied in [112]. A resilience-based mechanism to improve the recovery rate of communication links impacted by a cyberattack has also been proposed in [113]. A defensive enhancement scheme has been proposed in [114] to reduce the likelihood of cyber-induced failures in waste water treatment systems. In [115], the impact of cyber-induced failures on composite power system reliability has been investigated. Also, a CPPS model has been proposed in [116] to capture the propagation of cyber-induced failures into distribution power systems for reliability evaluation. The role of cyber-induced failures in islanding strategies is still underdeveloped. Also, most of these studies have focused on performance evaluation against cyber-induced failures rather than defensive islanding of CPPS. Therefore, an islanding method that captures the correlation between physical operating conditions and cyber fragility behavior in CPPSs is required for enhanced resilience.

The main contributions of this chapter are summarized as follows:

1. Develop and validate the efficiency of probabilistic proactive generation redispatch strategy to improve resilience of transmission systems against extreme events, specifically hurricanes and wildfires.

2. Develop a defensive islanding methodology to split distribution CPPS into microgrids to mitigate the negative impacts of cyber-induced failures.

3.2 Proactive Generation Redispatch

This section describes the proposed generation redispatch strategy to enhance resilience of transmission systems. First, it illustrates the impacts of propagation of a wildfire and a hurricane on power system components. Then, it explains the recursive MDP to formulate a probabilistic generation redispatch algorithm. Finally, it provides implementation and test cases for hurricane and wildfire events.

3.2.1 Impacts of Extreme Weather Events on System Components

Impacts on the performance of power system vary according to the type of the event and vulnerability and preparedness of the system. For example, earthquakes have high impacts on underground cables whereas hurricanes result in failure of transmission poles and lines [51]. For each extreme weather event, a proper model is required to identify its propagation properties and spatiotemporal characteristics.

3.2.1.1 Impacts of Hurricanes

Intensities of hurricanes change temporally and geographically with their progression trajectories, which can be used to identify their spatiotemporal properties [32]—various components in the system can be impacted at sequential time intervals. Fig. 3.1 shows a scenario where two system components are on the trajectory of a hurricane. At t_2, component A is subjected to potential failure resulting in noticeable disturbance in the system performance. Component B is expected to fail at t_4 imposing further impacts on system dynamics. Hurricanes are usually fast acting weather events that might impact more than one component at the same instant resulting in various system configurations. Also, it is usually difficult to restore failed elements during the hurricane time especially if maintenance crew dispatching is a must for the restoration process. In very severe hurricane conditions, maintenance of some failed components might extend from a few hours to a few days [32]. Therefore, at each time instant during the hurricane, the set of failed components will include the possible failed components from previous time intervals.

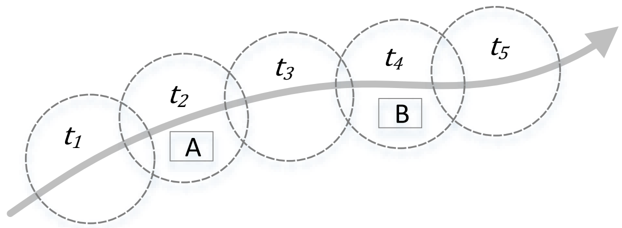

Figure 3.1: Two components on the trajectory of a hurricane

3.2.1.2 Impacts of Wildfires

Wildfires are characterized by the possibility to change path, to be completely extinguished, or to have less intensity at any time instant [95]. Fig. 3.2 shows a scenario where three system components (A, B, and C) are on the potential trajectory of a wildfire at five time instants (t_1 to t_5). Also, the restoration time of failed components is usually high due to the significant damage and destruction caused by wildfires [65].

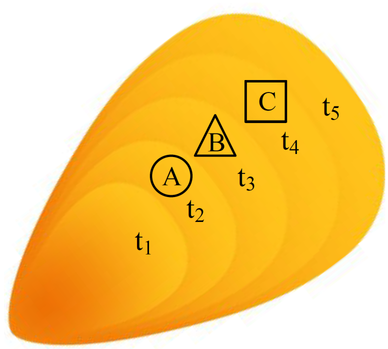

Figure 3.2: Three components on the trajectory of a wildfire

3.2.2 The Concept of Generation Redispatch

Failure of system components results in noticeable changes in the performance of the power grid such as power flow between transmission lines, generators output level, and overall operating costs. When the number of failed elements increases, the severity of the situation arises dramatically. In some cases, power grid can withstand low impact failures but when it comes to fast sequential failure scenarios, some loads must be curtailed to maintain more resilient operation. Moreover, during extreme weather events, the priority should be given to the reduction of load curtailment rather than operational costs. However, some existing strategies ignore the future potential failures of system components. This leads to implementing a less resilient strategy and increasing the negative consequences on the system performance. For instant, if a generating unit is expected to be impacted by a hurricane at upcoming future time, it is preferable to reduce the utilization of this unit before the extreme weather event hits the system.

Proactive generation redispatch relies mainly on determining the optimal generation levels of each operating generator unit for a specific period of time given the current and forecasted future system conditions. During normal operation, minimum operating costs should be imposed whereas during abnormal conditions, load curtailments and their associated costs should be minimized. Integrating the two objectives for two different operation conditions (i.e., to minimize both generation costs and load curtailment costs) requires consideration of several system constraints and varying factors such as ramping rates, minimum up and down times, and forecasted event progression. For example, load demand at each time instant has a direct role in generation output levels. Assurance of assets availability, such as generating units and transmission lines, during and after an extreme weather event is a vital constraint to maintain reliable operation of the system. On the other hand, restoring the curtailed load in a fast, efficient, and economical way, enhances the overall operational resilience level of the system. Also, the power grid could be split into several islanded microgrids where the generation level at each microgrid should be sufficient to supply all or most of its loads. Using generation redispatch, generator levels can be adjusted to meet the goal of each islanded microgrid.

3.2.2.1 System States during Extreme Event

Various components in the system can be impacted at sequential time intervals during an extreme weather event[32]. Fig. 3.3 shows a scenario where three system components are on the trajectory of a hurricane. As a result, the power grid might have different operating states at each time instant. A Markov state can be defined to represent a unique system topology based on the available components. Total number of Markov states is $2^{N_{c,t}}$ where $N_{c,t}$ is the total number of impacted components at time t. Assuming that failed components are not recovered during the hurricane period, the set of impacted components at time t lists the current and previously impacted components. Fig. 3.3 describes the propagation of component failures on Markov states during hurricane. S_o represents Markov state with no component failure, whereas S_{ABC} denotes Markov state where all components are in failure state. Utilizing Markov process to represent the behavior of power system from one time instant to another requires evaluating transition probabilities from one state to another. The transition probability from state $S_{i,t}$ to $S_{i',t+1}$ can be evaluated as follows.

$$P(S_{i,t}, S_{i',t+1}) = \prod_{m \in \Omega_{C,t+1}} P(o_{m,t}, o_{m,t+1}),\ i \in \Omega_{S,t}, \tag{3.1}$$

$$P(o_{m,t}, o_{m,t+1}) = \begin{cases} 1 & o_{m,t} = 0,\ o_{m,t+1} = 0 \\ 0 & o_{m,t} = 0,\ o_{m,t+1} = 1 \\ 1 - \lambda_{m,t+1} & o_{m,t} = 1,\ o_{m,t+1} = 1 \\ \lambda_{m,t+1} & o_{m,t} = 1,\ o_{m,t+1} = 0 \end{cases} \tag{3.2}$$

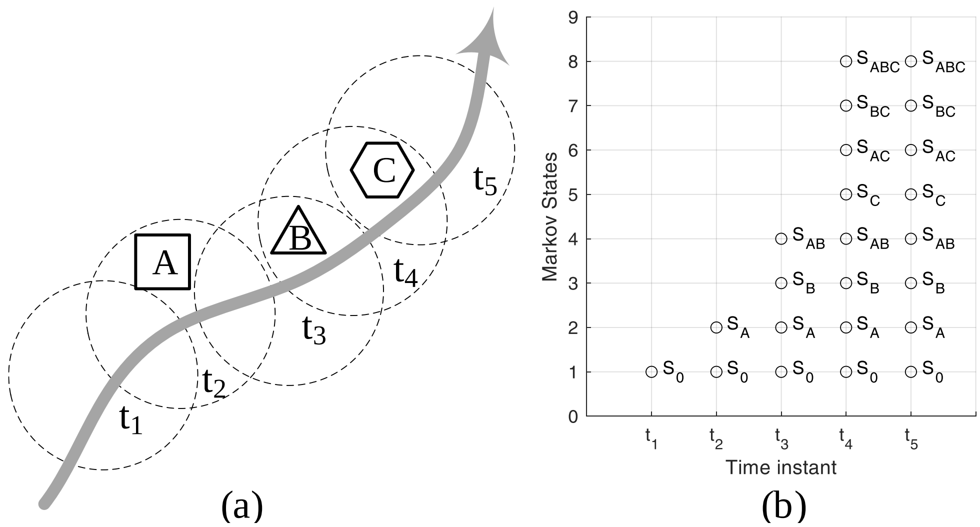

Figure 3.3: Markov states on the trajectory of a hurricane

where $\Omega_{S,t}$ is the set of all system states at a given time t; $\Omega_{C,t+1}$ is the set of all impacted components at time $t+1$; $\lambda_{m,t+1}$ is the failure probability of component m at time $t+1$; and $o_{m,t}=0$ and $o_{m,t+1}$ are the statuses of the component m at times t and $t+1$, respectively.

3.2.2.2 Recursive Markov Process

Uncertainties of component failures during extreme weather events impose additional burden for system operators to determine the best decision, according to current and future system states. Each decision impacts the overall performance of the system during the entire period of an event. Since generation dispatch usually takes place in terms of minutes, a discrete-time MDP can be used to model the whole process. The MDP determines the optimal action (decision) at each time instant based on current system states as well as possible future states. The backward induction method and the value iteration method [117] have been used to find solution for each state in MDP. However, when time-dependent constraints correlating Markov states at sequential time instants are considered, linear scalarization method can be used to transform the multi-objective optimization problem into a single objective optimization problem [32].

Fig. 3.4 shows the progression behavior of an extreme event on system components. Prior to the event, no failure state is observed. All Markov states are encountered and their transition probabilities are calculated. At each time instant, the optimization model takes into account all possible observable states. An action is made and the system holds a new Markov state with a new set of observable states. An action represents the supplied real power by operating generators. This process is repeated for all time instants.

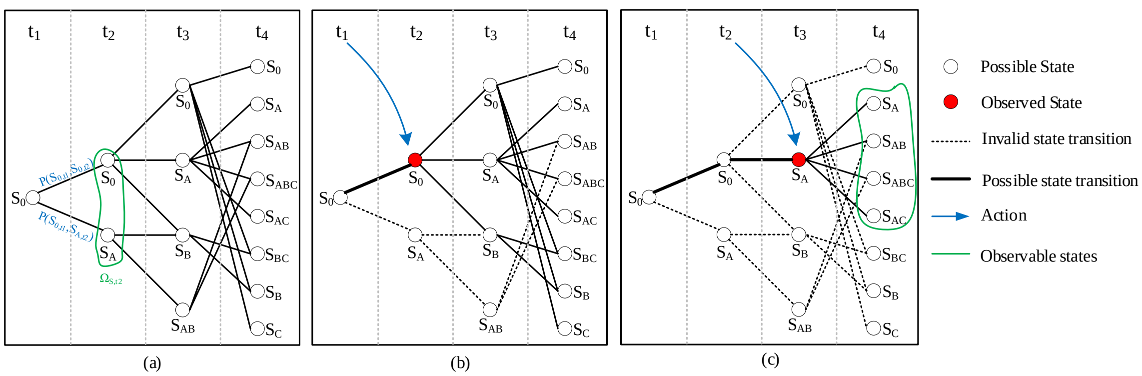

Figure 3.4: (a) Markov states prior to the event, (b) Markov decision at t_1, and (c) Markov decision at t_2.

3.2.3 Markov Decision Process Formulation

This section explains the formulation of the MDP-based optimization problem to minimize the overall operating costs and load curtailments. Various system constraints and event spatiotemporal properties are considered in the proposed algorithm.

3.2.3.1 Objective Function

The optimal generation redispatch strategy for a specific system state $S_{i,t}$ at a given time t is expressed as follows.

$$v_t^*(S_{i,t}) = \min\{v_t(S_{i,t}, A_{a,t}), a \in \Omega^A\}, i \in \Omega_{S,t}, t \in \Omega^T, \tag{3.3}$$

where $A_{a,t}$ denotes a set of actions, i.e., generators output power; $v_t(S_{i,t}, A_{a,t})$ is the expected overall cost for state $S_{i,t}$ under a specific action $A_{a,t}$; Ω^A represents the set of all possible actions; $\Omega_{S,t}$ is the set of all system states at a given time instant t; and Ω^T is the set of all time instants.

The value of each state in MDP can be evaluated as follows.

$$v_t(S_{i,t}, A_{a,t}) = C_t(S_{i,t}, A_{a,t}) + \sum_{i' \in \Omega^S_{i,t+1}} [P(S_{i,t}, S_{i',t+1}) \,.\, v_{t+1}(S_{i',t+1}, A_{a',t+1})]. \tag{3.4}$$

In (3.4), $\{a, a'\} \in \Omega^A$, $i \in \Omega_{S,t}$, and $\{t, t+1\} \in \Omega^T$ where $P(S_{i,t}, S_{i',t+1})$ is the transition probability from state $S_{i,t}$ to all possible states in the proceeding time instants; and $C_t(S_{i,t}, A_{a,t})$ represents the immediate cost of state $S_{i,t}$ given action $A_{a,t}$, which can be expressed as follows.

$$C_t(S_{i,t}, A_{a,t}) = W_1 \,.\, C_{cu} \,.\, \sum_{n \in \Omega^N} Cu_{n,t,i} \; + W_2[\sum_{j \in \Omega^G} C_f(P^G_{j,t,i}) + C_{su}(T^{ON}_{j,t,i}) + C_{sd}(T^{OFF}_{j,t,i})], \tag{3.5}$$

where $Cu_{n,t,i}$ represents the amount of load curtailment at node n; C_{cu} is the cost of curtailed loads; $C_f(P^G_{j,t,i})$ is the fuel cost of generator j; Ω^N represents the set of all buses; Ω^G represents the set of all generators; and $C_{su}(T^{ON}_{j,t,i})$ and $C_{sd}(T^{OFF}_{j,t,i})$ are the startup and shutdown cost of generator j, respectively.

3.2.3.2 Constraints

Several constraints are considered as follows.

1. Power Balance: The power balance of system state $S_{i,t}$ at time t can be expressed as follows.

$$\sum_{j\in\Omega_n^G} P^G_{j,t,i} - (L_{n,t,i} - Cu_{n,t,i}) + \sum_{n'\in\Omega_n^N} P^L_{n,n',t,i} = 0, \forall n \in \Omega^N, \tag{3.6}$$

where Ω_n^G represents the set of generators connected to bus n; $P^G_{j,t,i}$ is the j^{th} generator real power at bus n; $L_{n,t,i}$ is the amount of load in MW at bus n; $Cu_{n,t,i}$ is the amount of load curtailed at bus n; Ω_n^N represents the set of all buses connected to bus n; and $P^L_{n,n',t,i}$ represents the power flow from bus n to bus n' at time t.

2. Transmission Flow Limits: The power flow through a specific line connected at bus n of system state $S_{i,t}$ can be defined as follows.

$$B_{n,n'}.(\theta_{n,t,i} - \theta_{n',t,i}) - P^L_{n,n',t,i} \leq P^{Max}_{n,n',t,i} \ \forall n \in \Omega^N, \tag{3.7}$$

$$B_{n,n'}.(\theta_{n,t,i} - \theta_{n',t,i}) - P^L_{n,n',t,i} \geq P^{Min}_{n,n',t,i} \ \forall n \in \Omega^N, \tag{3.8}$$

where $B_{n,n'}$ represents the susceptance of the line connecting nodes n and n'; $\theta_{n,t,i}$ and $\theta_{n',t,i}$ are the voltage angles at buses n and n', respectively; and $P^{Max}_{n,n',t,i}$ and $P^{Min}_{n,n',t,i}$ are the maximum and minimum line flow ratings, respectively.

3. Load Curtailment Limits: For each $S_{i,t}$ during a hurricane, the amount of load curtailment at each bus should be less than or equal the total amount of load at the same bus as follows:

$$0 \leq Cu_{n,t,i} \leq L_{n,t,i} \ \ \forall n \in \Omega^N, \ \forall t \in \Omega^T. \tag{3.9}$$

4. Ramping Rates of Generating Units: The ramping rates of each generator should be satisfied as follows.

$$P^G_{j,t+1,i} - P^G_{j,t,i'} \leq (2 - u_{j,t,i} - u_{j,t+1,i'}).P^{G,Min}_j + (1 + u_{j,t,i} - u_{j,t+1,i'}).R^{UP}_j \ \ \forall i' \in \Omega^S_{i,t+1}, \tag{3.10}$$

$$P^G_{j,t,i} - P^G_{j,t+1,i'} \leq (2 - u_{j,t,i} - u_{j,t+1,i'}).P^{G,Min}_j + (1 - u_{j,t,i} + u_{j,t+1,i'}).R^{DN}_j \ \ \forall i' \in \Omega^S_{i,t+1}, \tag{3.11}$$

where for the j^{th} generator, $P^G_{j,t+1,i'}$ is generated power in state $S_{i',t+1}$; $u_{j,t,i}$ and $u_{j,t+1,i'}$ are generator statuses at states $S_{i,t}$ and $S_{i',t+1}$, respectively; $P^{G,Min}_j$ and $P^{G,Max}_j$ are the minimum and maximum generation power; and R^{UP}_j and R^{DN}_j are the up and down ramping rates, respectively.

5. Generators Minimum Up/Down Time: Since the proactive redispatch is time-dependent, minimum up and down times for each generator should be satisfied as follows.

$$\sum_{t-UT+1}^{t} T^{ON}_{j,t,i} \leq u_{j,t,i''} \ \ \forall t \in \{UT, \cdots, T\}, \tag{3.12}$$

$$\sum_{t-DT+1}^{t} T^{OFF}_{j,t,i} \leq 1 - u_{j,t,i''} \ \ \forall t \in \{DT, \cdots, T\}, \quad \forall j \in \Omega^G, \ \forall i'' \in \Omega^S_{i,t+}, \tag{3.13}$$

where $T^{ON}_{j,t,i}$ and $T^{OFF}_{j,t,i}$ are the turn on/off signals of j^{th} generator at state $S_{i,t}$, respectively; UT and DT are the minimum up/down times for same generator, respectively; and $\Omega^S_{i,t+}$ is the set of all possible transition states starting at state $S_{i,t}$.

6. Power Limits of Generating Units: The generated power of each generator can be as expressed as follows.

$$P^{G,Min}_j.u_{j,t,i} \leq P^G_{j,t,i} \leq P^{G,Max}_j.u_{j,t,i} \ \ \forall j \in \Omega^G, \tag{3.14}$$

where $P^{G,Min}_j$ and $P^{G,Max}_j$ are the lower and upper limits of j^{th} generator, respectively; and Ω^G is the set of all generators.

7. Generator Status: The status of each generator at state $S_{i,t}$ is represented by a binary number as follows.

$$u_{j,t,i} \in \{0,1\}, \ \forall j \in \Omega^G, \tag{3.15}$$

8. Voltage Angle Limits: Voltage angle at bus n at state $S_{i,t}$ can be expressed as follows.

$$\theta_n^{Min} \leq \theta_{n,t,i} \leq \theta_n^{Max}, \ \forall n \in \Omega^N, \tag{3.16}$$

3.2.4 Implementation and Results for Hurricane Event

The proposed approach is applied on the IEEE 30-bus system. The MDP is formulated using CPLEX solver integrated with MATLAB. The hurricane is assumed to pass through the system as shown in Fig. 3.5 and to last for 25 minutes sampled in set of 5 minutes. At each time instant, components may fail due to the spatiotemporal properties of the hurricane. The set of impacted components and their failure probabilities are given in Table 3.1, using the approach given in [32].

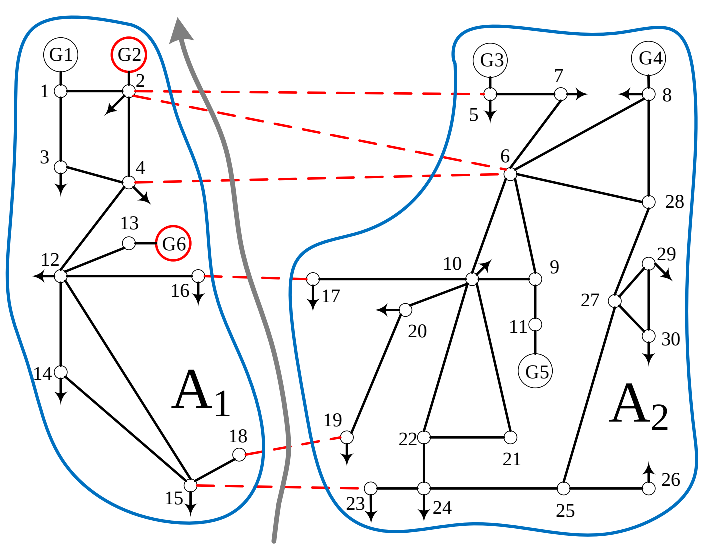

Figure 3.5: Hurricane propagation on IEEE 30-bus system

Table 3.1: List of Impacted Components with their Probability of Failure for Hurricane Event

Time Instant	Component No.	Description	Failure Probability
t_1	–	–	–
t_2	C_1	Line 15-23	0.25
	C_2	Line 18-19	0.22
t_3	C_4	Line 16-17	0.2
t_4	C_6	G_6	0.08
	C_7	Line 4-6	0.18
t_5	C_8	G_2	0.08
	C_9	Line 2-6	0.15
	C_{10}	Line 2-5	0.12

Several test cases are simulated to validate the accuracy and effectiveness of the proposed method. The impact of load variations is considered by scaling the system nominal load based on load demand profile obtained from [118] as shown in Fig. 3.6. The hurricane event is assumed to take place during load peak time to create more severe circumstances. On the other hand, proper scaling weights are used to prioritize the cost of load curtailment over the operational costs. Two simulation cases are considered to assess the sensitivity between the initial generation level and algorithm performance.

3.2.4.1 Predefined Initial Generation Level

In this case, initial generation levels are obtained by solving optimal power flow under normal operating conditions. The calculated initial generation profile is integrated into the optimization problem to determine the optimal generation redispatch scenarios. Fig. 3.7 shows the optimal generation strategy for three scenarios compared with the generation dispatch under normal operation conditions. The three scenarios are selected as follows: (a) no component fail, (b) only transmission lines fail, and (c) all components on the hurricane path fail. The overall cost of each redispatch strategy is evaluated and compared with normal operation cost as illustrated

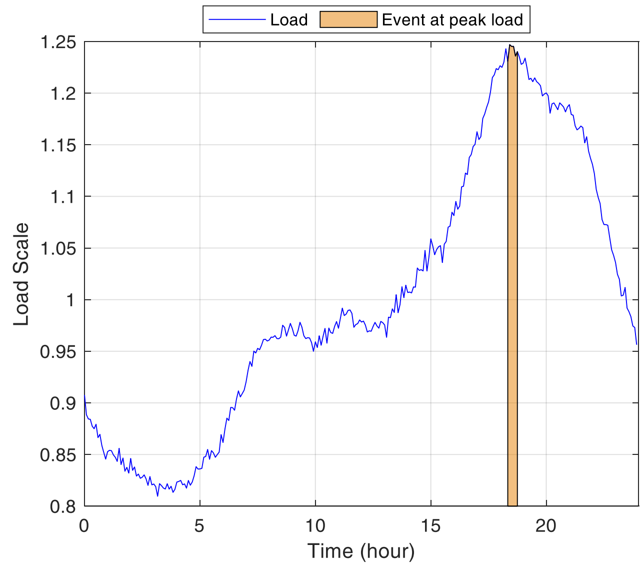

Figure 3.6: Load profile with hurricane landing time

in Fig. 3.9.

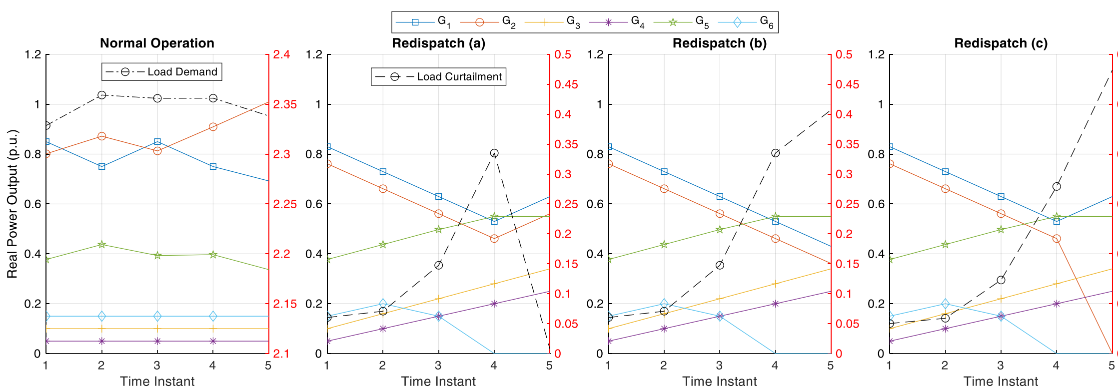

Figure 3.7: Optimal strategies under predefined initial generation level

It is noticeable that the MDP takes in consideration the potential future failures of system components. Both G_1 and G_2 are ramping down in all studied redispatch scenarios to shift the reliance of the system on the largest generation unit. Although G_3, G_4, and G_5 are ramping up to compensate for the reduction of generation from G_1 and G_2 as well as achieve the increasing demand, the net ramp up/down of all generators is not sufficient to supply all load demands resulting in some load curtailments. On the other hand, G_6 does not continue to ramp up for the whole period because the possibility to fail at t_4. Although system components do not fail in scenario (a), load is curtailed at earlier time instants to avoid much larger curtailment in proceeding instants. Also scenario (b) describes the generation portfolio when islanding occurs at t_5 which shows further curtailment due to insufficient power for each region. The total amount of load curtailment increases in scenario (c) due to the loss of G_2. The impact of the generation level prior to the event on the performance of the redispatch strategy has been noted clearly in scenario (a) and (b). For instant, if G_2 was producing much less power, it would have behaved as G_6 and shut down earlier in time.

3.2.4.2 Unknown Initial Generation Level

Due to the sensitivity of generation redispatch and ramping to initial generation levels, MDP algorithm is used to determine the optimal initial generation level as well as the dispatch profile to reduce the amount of load curtailment. Fig. 3.8 shows the optimal initial generation level and redispatch strategy for scenarios (b) and (c) from the previous case. Also, the overall cost is compared with results of the previous case as illustrated in Fig. 3.9.

The obtained generation dispatch strategies for scenario (b) and (c) are significantly different than previous results in many ways. All generation units are initialized to deliver 40% to 70% of their maximum capacity resulting in higher initial generation of G_3, G_4, and G_5. Also, the initial generation level of G_2 has been reduced to be able to completely shut down by reaching t_5. The MDP algorithm utilizes G_2 as long as possible since it has lower overall operating costs than other units. The obtained strategies for scenarios (b) and (c) are identical reflecting the effectiveness of the MDP algorithm to consider future potential generation outage. The ramping of G_3, G_4, and G_5 is mainly due to increase in load demand. G_6 reaches

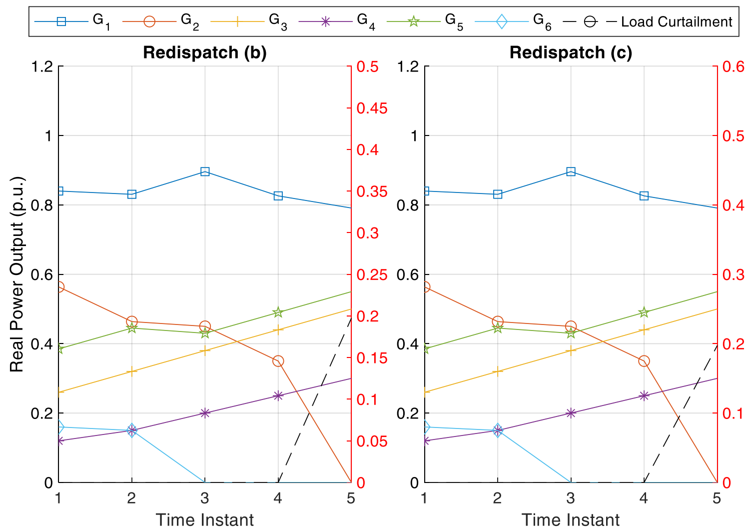

Figure 3.8: Optimal strategies under unknown initial generation level

a complete shutdown state at t_3 before it is potentially impacted at t_4. Although a significant reduction in load curtailment profile is obtained, both scenarios encounter small amount of load curtailment at the last time instant t_5.

Fig. 3.9 describes the variation of cost values for all scenarios under various constraints. Three feasible initial generation conditions are used to assess the performance of the redispatch algorithm: (1) 40% to 70% of maximum generation capacity; (2) 100% to 230% of minimum generation capacity; and (3) minimum to maximum generation capacity. Condition (2) imposes more curtailment costs than condition (1) and (3) because generators are initialized at low levels. When the initial generation level constraint is relaxed, the algorithm reaches very close total cost compared to normal operation costs in case of scenario (a).

3.2.5 Implementation and Results for Wildfire Event

The proposed approach is applied to the IEEE 30-bus system for validation [119]. Generator data are provided in Table 3.2. In this study, the wildfire is assumed to propagate across the system as shown in Fig. 3.10. Due to the spatiotemporal

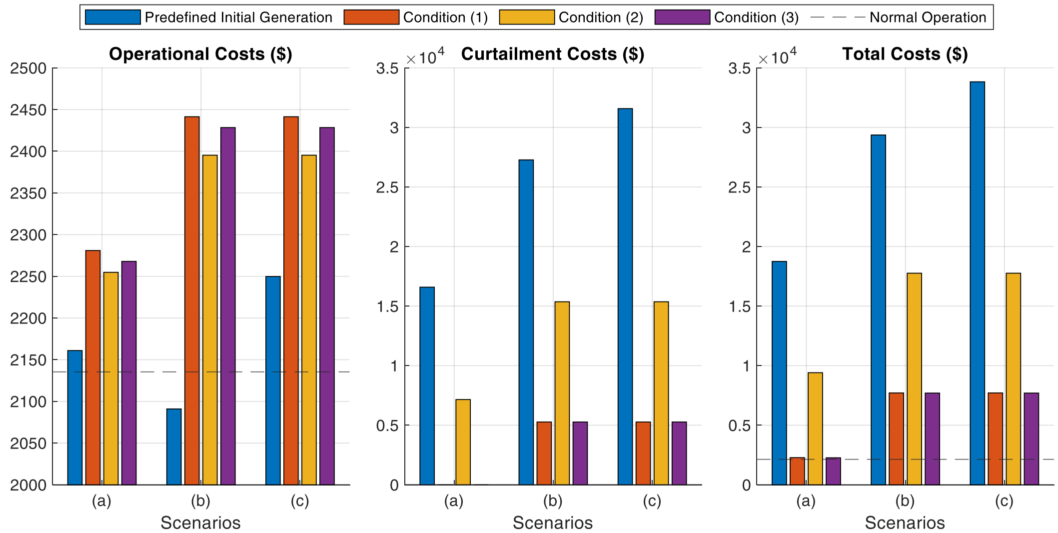

Figure 3.9: Cost analysis

characteristics of wildfires, system components may fail at each time instant. Table 3.3 lists the set of impacted components and their failure probabilities. Although the propagation speed of a wildfire varies based on weather factors, fuel data (e.g., land type), and wildfire data, the scope of this work is resilience enhancement strategy under a given wildfire scenario. The impact of load variation is considered by scaling the system nominal load using load demand profile obtained from [118] as shown in Fig. 3.6.

Table 3.2: Generator Parameters

Unit	Cost ($)			Time (min)		Power (MW)		Ramp
	b	C_{su}	C_{sd}	UT	DT	Min	Max	(MW/hour)
G_1	2.00	70	176	15	15	30	120	12.0
G_2	1.75	74	187	15	15	35	140	12.0
G_3	2.00	50	113	15	15	10	50	7.2
G_4	3.25	110	267	15	15	5	30	6.0
G_5	3.00	72	180	15	15	10	55	7.2
G_6	3.00	40	113	15	15	15	40	6.0

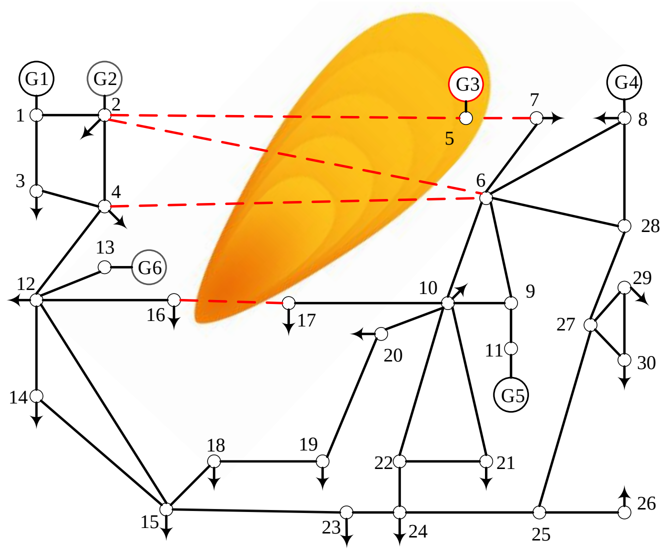

Figure 3.10: Wildfire propagation on IEEE 30-bus system

Table 3.3: List of Impacted Components with their Probability of Failure for Wildfire Event

Time Instant	Component No.	Description	Failure Probability
t_1	–	–	–
t_2	C_1	Line 16-17	0.7
t_3	C_2	Line 4-6	0.4
t_4	C_3	Line 2-6	0.6
t_5	C_4	Line 2-5	0.3
t_6	C_5	G_3	0.7
	C_6	Line 5-7	0.3

The performance and effectiveness of the proposed method are tested and validated through several test cases. To induce more severe circumstances, the wildfire event is assumed to take place during the peak load period. The wildfire duration for crossing the indicated lines is assumed to be 25 minutes sampled at 5 minute intervals for the recursive discrete decision epochs. As previously mentioned, to ensure that the algorithm prioritizes reducing load curtailments over operational costs, the scaling weight of W_1 is selected to be significantly higher than W_2. In this work,

W_1 equals 100 and W_2 is 1. The performance of the proposed algorithm is tested through three simulation cases, which are: 1) corrective strategy, 2) immediate proactive strategy, and 3) predictive proactive strategy. The impact of the propagation rate of a wildfire is assessed to validate the effectiveness of the proposed algorithm under diverse circumstances. Also, the impacts of different generator ramping rates are studied to assess their role in resilience enhancement. The optimal generation dispatch during normal operation (no wildfire) is computed and used for comparison.

3.2.5.1 Corrective Strategy

Since the system may experience actual failures during a wildfire, the generation dispatch has to be readjusted to adapt to such failures and fulfill system generation and transmission constraints. In this case, no redispatch is applied prior to the event attack time; however, dispatching is applied at each time instant during the wildfire event to fulfill the current system constraints. In other words, the decisions are made to fulfill the current system constraints ignoring future impacts. This case is used for comparison and validation of the proactive generation redispatch algorithm and to highlight the importance of proactive resilience enhancement strategies.

Fig. 3.11(a) and Fig. 3.11(b) show the generation dispatch solution during normal operation and corrective strategy, respectively. For Fig. 3.11(b), the amount of load curtailment (dashed line) keeps growing throughout the wildfire duration for several reasons. First, G_3 (yellow line) ramps down to avoid any constraint violation starting at 18:45 due to sequential failures of transmission lines 2–5 and 5–7. Also, the failures of lines 2–5, 2–6, 4–6 and 16–17 impose stressful burden on the amount of transferable power from G_1, G_2 and G_6 to the load spots on the right side of the grid and results in ramping down of G_1 and G_2. As a result, the generation profile of all units have changed significantly. It is obvious that proactive strategies are required to improve the system performance and reduce the amount of load curtailments. Also, the generation and transmission constraints impose further complexities which should be considered during the enhancement strategy.

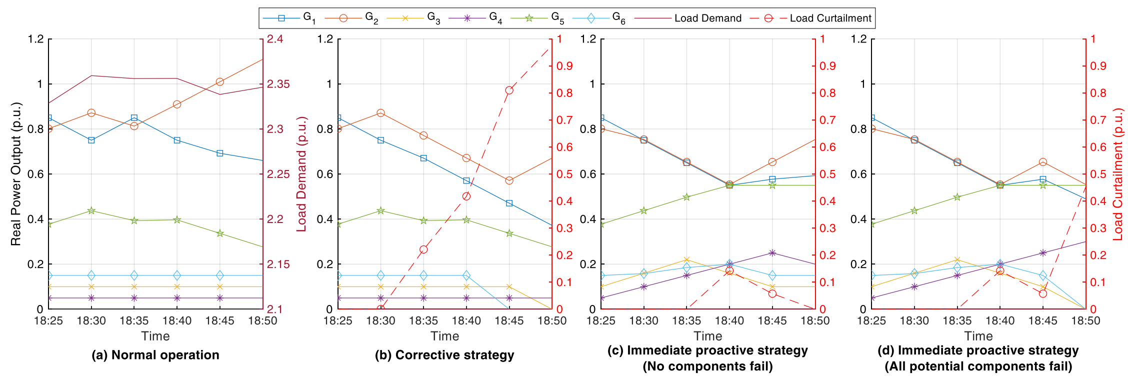

Figure 3.11: Optimal generation dispatch under (a) normal operation, (b) corrective strategy, (c) immediate proactive strategy given no components fail during wildfire, and (d) immediate proactive strategy given all potential components fail during wildfire

3.2.5.2 Immediate Proactive Strategy

In this case, the MDP algorithm proactively dispatches generators *when* a wildfire *occurs* based on the predicted direction and speed of the wildfire and potential failures of system components. The formulated MDP considers all possible component failures due to the wildfire, which were ignored in case 1. The initial generation levels are obtained from the scheduled generation dispatch solution under normal operation and integrated into the MDP to ensure that the optimization problem is initialized with the proper system status prior to strategy implementation. Fig. 3.11(c) and Fig. 3.11(d) show the optimal generation dispatch for two scenarios: S_1—no components fail, and S_2—all potential components fail, respectively.

In this case, generation profiles for all generators have changed significantly, as shown in Fig. 3.11(c) and Fig. 3.11(d) compared to the corrective strategy case. Considering the results in Fig. 3.11(c), high reliance on the right-side generators (G_4

and G_5) compared to the left-side generators (G_1 and G_2) is observed during the first few instants to avoid violating the ramping constraints of large generation units, G_1 and G_2, which are highly utilized prior to the event due to their low operational costs. A very fast ramping up behavior of G_4 and G_5 is observed to compensate for the ramping down of G_1 and G_2 as well as increase in load demand. G_3 supplies high generation level at early instants utilizing its low operational costs; however, it ramps down at 18:35 to prepare for possible shutdown at 18:50. This highlights the capability of MDP to utilize low-operational cost generators. Since G_6 has high operational costs, it ramps down at 18:40 to reduce the operational costs during severe situations. Generators G_1 and G_2 ramp up at 18:40 while G_4 ramps down at 18:45 to reduce the overall operational costs since no failure takes place. On the other hand, G_1 and G_2 ramp up momentarily between 18:40 and 18:45 to utilize their low-operational costs even with decreasing in load demand. As a result, MDP utilizes low-operational cost generators as long as all generation and transmission constraints are not violated.

For scenario S_2 (Fig. 3.11(d)), the loss of G_3 and islanding of bus 5 results in non-avoidable curtailments at 18:50, yielding higher load curtailments compared to S_1. Although system components do not fail in S_1 (Fig. 3.11(b)), load is curtailed at earlier time instants to avoid much larger curtailments in proceeding instants. From the results, the proposed MDP algorithm provides much less load curtailments compared to the corrective strategy.

Our work shows that MDP selects the optimal generation redispatch at each instant that ensures not only minimal load curtailments at the current instant but less negative impacts on the following time instants. In other words, the load curtailment profile for both scenarios is the same for all time instants till 18:45, which highlights the capability of MDP to consider future impacts and mitigate the worst case scenario earlier in time. The proposed algorithm is able to reduce the total amount of load curtailments more than 50%. Additionally, MDP prioritizes reducing amount of load curtailments over operational costs in present and future instants.

3.2.5.3 Predictive Proactive Strategy

Similar to case 2, the proposed strategy utilizes MDP to proactively dispatch generators given a predicted wildfire event. In other words, the optimal redispatch is determined *prior* to the *potential* wildfire. The MDP algorithm is used to determine the optimal initial generation level prior to the event so that if an event happens, further load curtailments will be avoided. Fig. 3.12 compares generation profile for S_2 under immediate and predictive proactive strategies.

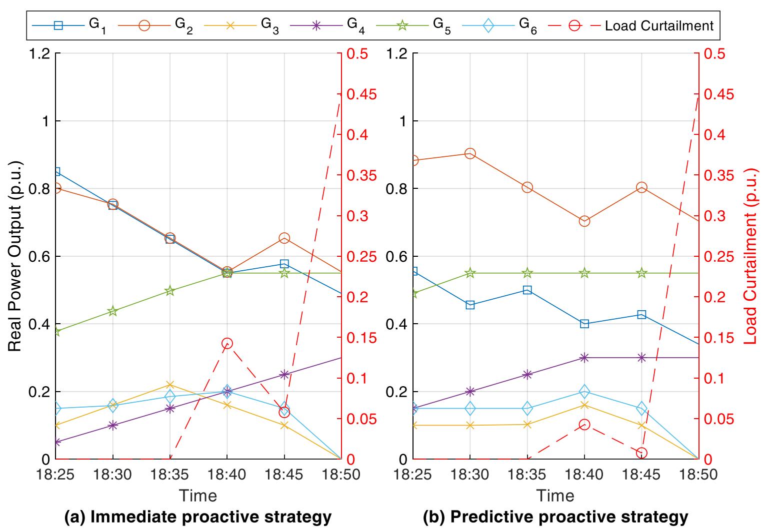

Figure 3.12: Optimal generation dispatch for S_2 under (a) immediate proactive strategy and (b) predictive proactive strategy

The impact of the generation level prior to the event on the performance of the redispatch strategy is clearly noticed. The obtained generation dispatch profiles, shown in Fig. 3.12(b), are significantly different compared to Fig. 3.12(a). In this case, G_2, G_4 and G_5 have higher initial generation levels than G_1 compared to case 2. The full utilization of G_4 and G_5 earlier in time results in lower load curtailments at 18:40 and 18:45. MDP has prioritized G_5 over G_4 due to its lower operational costs. Also, MDP has selected a higher initial generation level for G_2 since it has the lowest operational costs and highest generation capacity. Although G_3 is expected to fail at 18:50, it is optimally utilized prior to that instant due to its low operational costs, which highlights the effectiveness of MDP to differentiate between low– and high–operational cost generators. MDP provides a proactive resilience enhancement approach to determine the proper allocation of sources prior to extreme weather events and avoid large curtailments.

The total amount of load curtailment during the event duration (18:30 to 18:50) is lower in Fig. 3.12(b) implying higher resilience level; however, both strategies show same amount of load curtailments at 18:50. Deeper investigation shows that the shared spots of load curtailment at 18:50 for both strategies are buses 8, 12, 14, 15, 29, and 30. Such curtailments are deemed non-avoidable due to either insufficient generation supply or exceeding transmission capabilities. For instance, the load demand at bus 8 at 18:50 of almost 37 MW—calculated by scaling the base load using provided load profile—can be supplied through G_4 and transferable power through transmission lines connected to bus 8. If G_4 has a capacity lower than the load demand, the remaining load demand should be supplied through transferable power over transmission lines; however, that might not be feasible if these lines are fully occupied due to other load requirements. Regardless of the non-avoidable curtailments, case 3 provides better resilience level represented by fewer load curtailments. The obtained strategies reflect the effectiveness of the MDP algorithm to consider future potential generation outages and transmission failures. Also, MDP can be used to determine the most vulnerable spots due to extreme events and provide proper proactive planning.

To show the significance of the proposed algorithm on the overall costs, Table 3.4

describes the variation of cost values for S_2. The operational cost is higher in case 3 than in case 2. The curtailment cost is less in case 3 compared to case 2. This implies the capability of MDP to prioritize reducing load curtailment costs over operational costs. Also, relaxing the initial generation level constraint results in less total cost. The cost analysis can be used to determine optimal decisions taking into account the energy market regulations during extreme weather events.

Table 3.4: Cost Analysis

Cost ($)	Normal operation	Proactive strategy	
		Immediate (Case 2)	Predictive (Case 3)
Operational	2562	2711	2751
Curtailments	0	17454	13447
Total	2562	20165	16199

3.2.5.4 Role of Wildfire Propagation Rate

Due to the large geographical distance between some components at the transmission level, the sequential failure behavior might take several hours instead of a few minutes [107]. In this case, the wildfire event is assumed to propagate across the system in 5 hours. The decisions are made at the start of each hour. To create more stressed operating conditions and show the importance of the proposed algorithm, a few extra constraints are imposed. First, the wildfire is assumed to ignite prior to peak load demand period. Each generator ramping rate (MW/hour) is assumed to be 25% of maximum power capacity [120]. Line 4–12 replaces line 16–17 in the list of potential components at t_2 (Table 3.3) to create an islanding scenario and potential isolation of the two largest generators.

Fig. 3.13 compares the immediate proactive strategy and the corrective strategy with the normal operating conditions for a 5-hour wildfire event. The total amount of load curtailment is reduced dramatically by applying the proactive redispatch strategy as noticed in Fig. 3.13(c) and 3.13(d). The islanding of buses 1, 2, 3, and 4 due to wildfire shows insufficient generation capability, yielding non-avoidable load curtailments. On the other hand, the MDP selects G_2 over G_1 in the proactive strategy compared to the corrective strategy revealing the effectiveness of MDP to consider low-cost generators. Fig. 3.11 and Fig. 3.13 confirm the capability of the proposed algorithm to provide feasible solution and better resilience for fast and slow-paced extreme weather events.

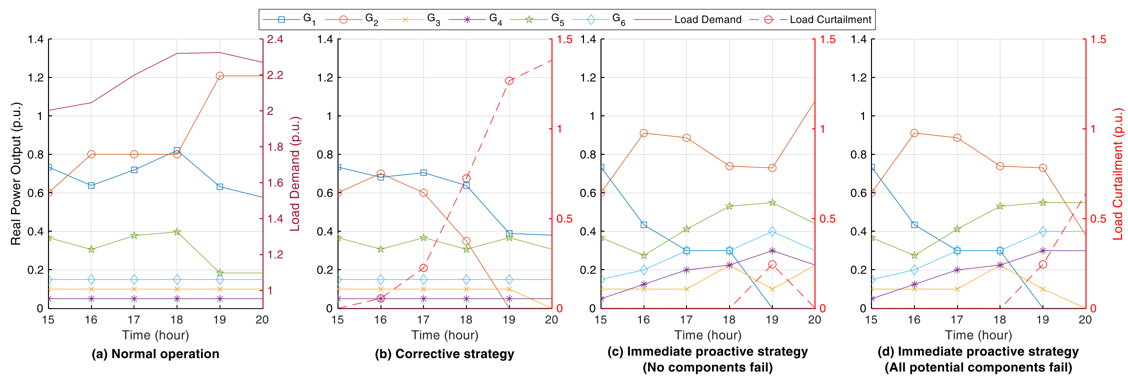

Figure 3.13: Optimal generation dispatch for slow wildfire event under (a) normal operation, (b) corrective strategy, (c) immediate proactive strategy given no components fail during wildfire, and (d) immediate proactive strategy given all potential components fail during wildfire

3.2.5.5 Impacts of Ramping Rates

The MDP solution relies on many factors including the dynamic characteristics of generators. Better resilience levels can be obtained through larger power capacity and faster ramping performance. In this case, the role of ramping rates is assessed. Three conditions are simulated: (a) nominal ramping rates, (b) 20% increase in ramping rates, and (c) 50% increase in ramping rates. The generator capacity is assumed fixed as provided in Table 3.2. For all simulated conditions, the initial generation levels are obtained from the scheduled generation dispatch solution under normal system operation, as shown in Fig. 3.11(a).

Fig. 3.14 shows the results for the two previously mentioned failure scenarios—S_1: no components fail, and S_2: all potential components fail. It is obvious that increasing the ramping rates results in a better performance represented in less load curtailments in both scenarios from 18:35 to 18:45. During the severe failure scenario (S_2), increasing the ramping rate by 50% enables the system to eliminate the avoidable curtailments of other cases and highlights the presence of non-avoidable load curtailments at 18:50. By comparing Fig. 3.14(c) and Fig. 3.14(e) with Fig. 3.14(a), it is noticeable that even with no failure occurrence, having a faster ramping provides the system with much faster response and proper immediate preparedness.

The generation profile of all generators varies based on ramping rates. Reliance on generators with low operation cost such as G_2 is noticed when the ramping capabilities increase. In Fig. 3.14(c) and Fig. 3.14(d), the generation profiles of G_3, G_4, and G_5 increase due to the need of high generation supply on the right side of the grid. Fig. 3.14(e) and Fig. 3.14(f) show that G_4 is utilized only when needed due to its high operational costs. In other words, G_4 ramps down at 18:40 to reduce operational costs. In most cases, G_1 ramps down due to its high cost compared to G_2—which is located in the same geographical vicinity—and transmission power limitation of line 4-12. In short, increasing the ramping rates creates more flexible system constraints achieving better resilient performance.

Table 3.5 shows the effect of various ramping rates on operational costs and curtailment costs. In S_1, the total costs with 20% ramp increase is almost half the total costs for nominal case. The total costs in S_1 with 50% ramp increase is $2600, which is very close to normal operation condition of $2562. During severe situations, when all potential components fail, increasing the ramping rates reduces the curtailment costs dramatically but increases the operational costs slightly resulting in overall to-

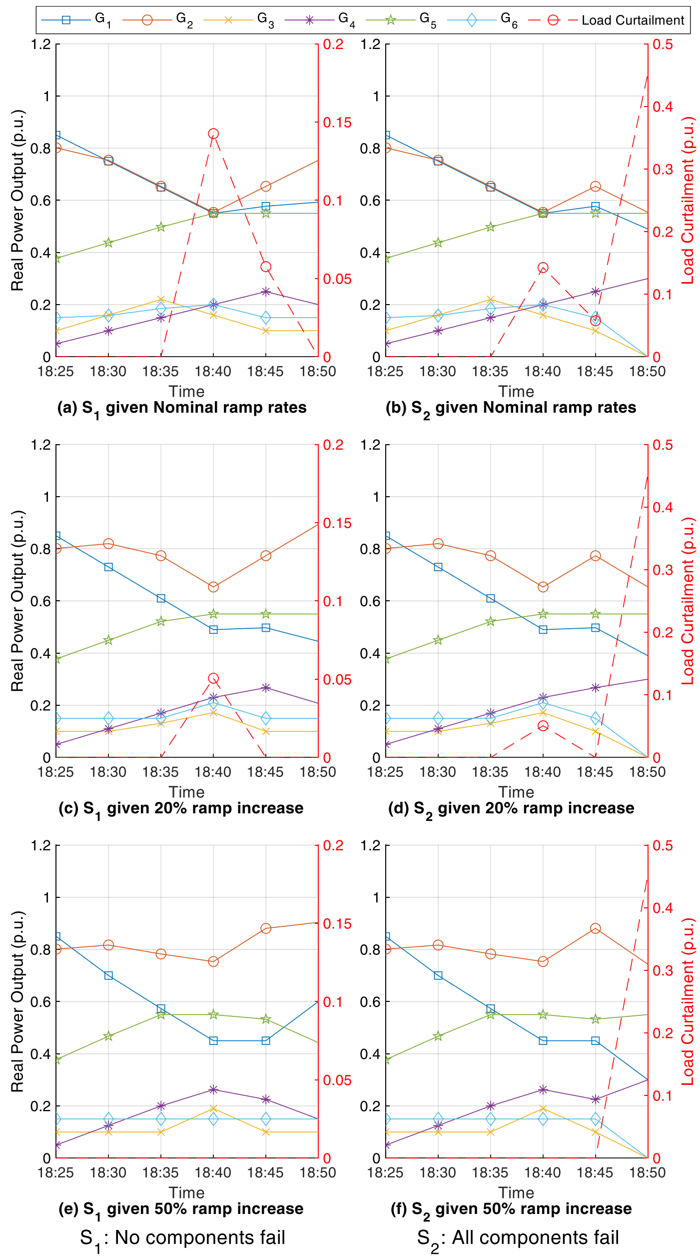

Figure 3.14: Optimal generation dispatch under varying ramping rates for S_1: (a), (c), and (e) and S_2:(b), (d), and (f)

tal costs reduction. In brief, increasing the ramping rates results in reducing the total costs between 25% to 67% among all scenarios.

Table 3.5: Cost Analysis under Various Ramping Rates

Cost ($)	S_1			S_2		
	Nominal	20%	50%	Nominal	20%	50%
Operat.	2573	2597	2600	2711	2735	2741
Curtail.	5347	1352	0	17454	13459	12107
Total	7920	3949	2600	20165	16193	14847

3.3 Defensive Islanding for CPPS

This section describes the proposed defensive islanding strategy to improve resilience of distribution systems against cyber-induced failures. First, it explains the concept of resilience-based islanding. Then, it illustrates the hierarchical spectral clustering approach to formulate the islanding scheme. Finally, it provides a few test cases for validation.

3.3.1 Cyber-induced Failure Model

CPPSs are usually decomposed of a physical layer representing the power grid and a cyber layer including communication and computation systems. According to complex network theory, both physical and cyber layers can be represented as graph networks [19]. A physical power system is represented by an undirected graph $G_P = (N_P, E_P)$, where N_P is a set of vertices corresponds to buses or nodes in the power system and E_P is a set of edges referring to transmission line segments or transformers. Following the same convention, the cyber layer can be represented as an undirected graph $G_C = (N_C, E_C)$, where N_C is a set of vertices that correspond to communication routers and control centers in the cyber system and E_C is a set of edges representing the communication channels between the information nodes.

The coupling between the information equipment and power system components shows the strong inter-dependency between the cyber and physical layers. In a conventional CPPS, the communication network is responsible for transferring measurements from power system sensors and sending decision control signals to power system actuators [19]. Various studies have been conducted to present a coupling model of the physical and cyber layers [30, 116, 121]; however, such coupling differs based on the system under study, the level of interaction among different layers, and the scope of the study. This study focuses on propagating the impact of cyber-induced failures into a power system. The presented coupling model between communication and physical layers is adopted from [122] and summarized as follows. A node-switch incidence matrix $A^{ns} \in \mathbb{R}^{N_P \times N_C}$ that represents the communication channel between a physical node and its terminal in the cyber layer can be constructed as follows.

$$a^{ns}_{i,j} = \begin{cases} 1, & \text{if node } i \text{ is connected to switch } j \\ 0, & \text{otherwise} \end{cases} \tag{3.17}$$

Also, a branch-switch incidence matrix $A^{bs} \in \mathbb{R}^{E_P \times N_C}$ describing the relationship between a physical edge and its assigned communication router can be formulated as follows.

$$a^{bs}_{i,j} = \begin{cases} 1, & \text{if branch } i \text{ is connected to switch } j \\ 0, & \text{otherwise} \end{cases} \tag{3.18}$$

Finally, a switch-switch incidence matrix $A^{ss} \in \mathbb{R}^{N_C \times N_C}$ can be used to describe the existing communication topology, such as star, ring, or meshed, and can be formed as follows.

$$a^{ss}_{i,j} = \begin{cases} 1, & \text{if switch } i \text{ is connected to switch } j \\ 0, & \text{otherwise} \end{cases} \tag{3.19}$$

3.3.2 Cyber Resilience-based Defensive Islanding

This section illustrates the proposed defensive islanding approach using graphical clustering. Also, a few weighting functions are proposed to capture both the physical and cyber features for proper clustering.

3.3.2.1 The Concept of Defensive Islanding

Defensive islanding aims to split a power system into smaller independent grids and isolate the vulnerable components based on constrained clustering. The defensive islanding approach provides a proactive strategy to exclude the vulnerable system components for enhanced resilience operation. Existing islanding approaches rely mainly on the topology and loading conditions of the physical electric power system [78, 123]. However, the integration of communication and cyber components introduces further challenges on clustering a CPPS [122]. For instance, during an extreme weather event, the communication channels connecting the power system components, such as circuit breakers, and tie-switches, to the main control center can be compromised. Though power components can still operate reliably, the vulnerabilities introduced in the cyber layer to measure, monitor, and control power systems will reduce the resilient operation.

Islanding is classified as a clustering problem within the context of graph theory [78]. Clustering a graph network is the process of identifying the list of edges (transmission lines) that can be disconnected to maintain minimal discrepancies among the connecting vertices (buses) [123]. This is usually achieved via assessing the correlation between vertices in a specific graph, and then, removing the edges having the least correlation values. Various methods have been used to evaluate the correlation within a graph network in terms of edge weights [103, 105, 124]. In electric power system studies, the following edge weight functions have been used:

1. Topology: $W_{i,j} = 1$, where $(i, j) \in E$

2. Admittance: $W_{i,j} = Y_{i,j} = 1/Z_{i,j}$ where $Z_{i,j}$ is the line impedance between buses i and j.

3. Power flow: $W_{i,j} = (|P_{i,j}| + |P_{j,i}|)/2$ where $P_{i,j}$ is the real power flow from bus i and bus j.

4. Optimal Power flow: $W_{i,j} = (|P^*_{i,j}| + |P^*_{j,i}|)/2$ where $P^*_{i,j}$ is the real power flow from bus i and bus j based on solving the optimal power flow problem.

3.3.2.2 Resilience-based Clustering

Different edge weight functions can be used to evaluate the characteristics and properties of a specific graph. In power system graphical representation, the topology weight function measures pure connectivity of a network whereas admittance weight matrix reveals the strength of graph edges (electrical distances). Also, power flow and optimal power flow weights are used to measure the loading level of transmission lines. However, these weight functions do not capture the fragility of system components during an extreme event [123]. In resilience-based studies, edge weights can be calculated based on the probability of failure of system components [84]. The weight matrix can be represented as $W_{i,j} = 1 - f_{i,j}$ where $f_{i,j}$ is the failure probability of an edge connecting buses i and j, which can be computed using fragility curve models [46]. Despite the capability to capture the vulnerability level of system components, the resilience-based weight function does not account for the loadability characteristics of system components.

A proper weight function that captures both the fragility and loadability features of graph edges will provide a better clustering against severe events. Four weight functions are proposed by integrating the steady-state solution of power flow and optimal power flow with the fragility behavior of power system components due to cyber-induced failures, which are explained as follows.

1. Integrated power flow and component availability: $W_{i,j} = ((|P_{i,j}| + |P_{j,i}|)/2)(1 - f_{i,j})$. Each element in the weight matrix corresponds to the multiplication of the average power flow and the probability of success for the corresponding edge.

2. Integrated optimal power flow and component availability: $W_{i,j} = ((|P^*_{i,j}| + |P^*_{j,i}|)/2)(1 - f_{i,j})$. Each element in the weight matrix corresponds to the multiplication of the optimal real power flow and the probability of success for the corresponding edge.

3. Integrated normalized power flow and component unavailability: $W_{i,j} = ((|\hat{P}_{i,j}| + |\hat{P}_{j,i}|)/2)(f_{i,j})$, where $\hat{P}$ is the normalized power flow between i and j.

4. Integrated normalized optimal power flow and component unavailability: $W_{i,j} = ((|\hat{P}^*_{i,j}| + |\hat{P}^*_{j,i}|)/2)(f_{i,j})$, where $\hat{P}^*$ is the normalized optimal power flow between i and j.

The normalized power flow values are selected to map the loadability level of transmission lines on a scale from zero to one—higher values imply higher loadability. Also, this ensures that same priority is given to both probability of failure (fragility feature) and power flow (loadability feature), since both reside within the same range. The probability of failure of a physical component can be computed using the probability of failure of the corresponding communication link as described in [122] and summarized as follows.

$$f_{i,j} = \begin{cases} f^{ns}_{i,j}, & \text{if node channel assigned to edge}(i,j) \text{ fails} \\ f^{s}_{i,j}, & \text{if switch connected to edge}(i,j) \text{ fails} \\ f^{bs}_{i,j}, & \text{if branch channel assigned to edge}(i,j) \text{ fails} \\ 0, & \text{otherwise} \end{cases} \tag{3.20}$$

3.3.3 Spectral Clustering for Defensive Islanding

This section explains hierarchical spectral clustering method to create defensive islands. Also, it provides a brief description of the clustering evaluation criteria including minimal amount of load curtailment and radiality constraints.

3.3.3.1 Hierarchical Spectral Clustering

The concept of hierarchical spectral clustering has been introduced in [123] for transmission power systems and in [124] for distribution systems. The general idea is to split a graph network into K sub-graphs. First, the normalized Laplacian matrix L_n representing a specific graph is evaluated using (3.21).

$$L_n = I - D^{-1/2} W D^{-1/2}, \tag{3.21}$$

where I is identity matrix, W is the edge weight matrix, and D is the diagonal degree matrix, which can be calculated as follows.

$$D_{j,j} = \sum_{i=1}^{N} W_{j,i}. \tag{3.22}$$

The formulated Laplacian matrix is used to determine the first K eigenvectors corresponding to the smallest eigenvalues. The extracted eigenvectors represent the coordinates of the graph vertices in $\mathbb{R}^K$. Once the K coordinate vectors are computed, the edge distance between each graph vertex, $i \in N$ and all $k \in K$ vertices is computed. A specific vertex i will be assigned to cluster k based on the minimum euclidean distance. In other words, the minimum distance over a path between i and k is used to allocate graph vertices into a specific cluster. Detailed illustration of the presented method can be found in [123].

3.3.3.2 Clustering Evaluation Criteria

Various methods have been used to assess the performance of the clustering techniques [125]. The evaluation criteria vary based on the system being assessed, the size of the graph, and the required objectives. In this study, two criteria are selected to evaluate the validity and efficiency of the calculated clusters, which are:

(1) The minimal amount of load curtailment: is an index that can be used to evaluate the level of resilience enhancement. The critical load curtailment can capture the severity of the multiple line outages due to a cyber-induced failure and is directly affected by the topology and locations of DERs in a distribution system. The total load curtailment in a distribution network can be expressed as follows.

$$LC_{tot} = \sum_{i=1}^{N} \Delta P_i, \tag{3.23}$$

where ΔP_i is the load curtailment at node i, and N is the total number of nodes in the system.

(2) Radiality requirements: should be satisfied in distribution systems to align with the existing protection coordination schemes and voltage regulation fundamentals. Each cluster (microgrid) is represented by sub-graph $G_k = (N_k, E_k)$, where N_k is a set of nodes (or vertices) and E_k is a set of edges (or branches) in the sub-graph or cluster. A node-branch incidence matrix A can be constructed using (3.24) for each cluster, such that $A \in \mathbb{R}^{n \times e}$, where $n = |N_k|$ denotes the number of nodes and $e = |E_k|$ denotes the number of edges of a particular cluster. Radiality constraint is

satisfied if matrix A is a full rank matrix.

$$a_{i,j} = \begin{cases} +1, & \text{if branch } j \text{ starts at node } i \\ -1, & \text{if branch } j \text{ ends at node } i \\ 0, & \text{otherwise} \end{cases} \tag{3.24}$$

3.3.3.3 Integrated Algorithm

Algorithm 1 provides the process of defensive islanding to split a distribution system into smaller microgrids considering the role of cyber-induced failures. First, the system physical and cyber graphs are defined. Then, a cyber-induced failure scenario is generated randomly and its impact on the physical power system is evaluated. Hierarchical clustering is used for each clustering strategy to determine list of new smaller microgrids. The amount of load curtailment and radiality rank are computed for comparison and validation.

Algorithm 1: Overview of Defensive Islanding Considering Cyber-induced Failures

Input: Define physical layer graph (G_P), cyber layer graph (G_C), number of clusters (K), and clustering strategies (S)

Generate a cyber failure scenario
Solve the power flow and optimal power flow
Propagate the cyber-induced failure to the physical layer using (3.17), (3.18), and (3.19)
Evaluate the probability of failure of power components using (3.20)
for $s \leftarrow 1$ **to** S **do**
    Compute the weight matrix W
    Calculate the Laplacian matrix L_n
    Evaluate the eigenvectors K
    Obtain clusters using hierarchical spectral methodology
    Remove lines (edges) to split the system into islands
    Calculate the minimal amount of load curtailment and radiality rank

Output: Defensive islands and their corresponding load curtailment and radiality rank

3.3.4 Implementation and Results

The proposed approach is applied on a modified version of the 33-node distribution feeder for validation. The defensive islanding framework is formulated using hierarchical spectral clustering integrated with resilience-based weighting functions.

A CPPS representing a modified version of the 33-node distribution feeder [126, 127] is formed as shown in Fig. 3.15. Each power system node and transmission line is assigned to a specific communication switch as provided in Table 3.6. Detailed explanation of the CPPS model has been provided in section 3.3.1. These routers are responsible for receiving measurement signals and sending control signals to the assigned physical components. All communication switches are connected to the main control center. A compromised router implies potential failure of all communication signals to the assigned physical components. Though the communication topology plays a vital role in addressing the correlation between cyber failures, this study focuses on the impact of cyber-induced failures on the performance of power system components. To create independent microgrids, eight DERs are connected to the distribution feeder at arbitrarily chosen locations as shown in Fig. 3.15. The maximum power capacity of each DER is 500 kW. The proposed algorithm takes into consideration the DER locations in assigning proper islands. In this work, it is required to determine proper islands based on predefined system resources and characteristics.

The proposed clustering approach relies mainly on the probability of failure of cyber failures during extreme events. Due to the lack of information regarding the failure behavior of cyber and communication components, studies have adopted a scaling approach to compensate for the elevated extreme fragility conditions during severe conditions [59, 128]. In this work, the failure rate and repair time of the cyber components are adopted from [121, 122]. The failure rate of the cyber components

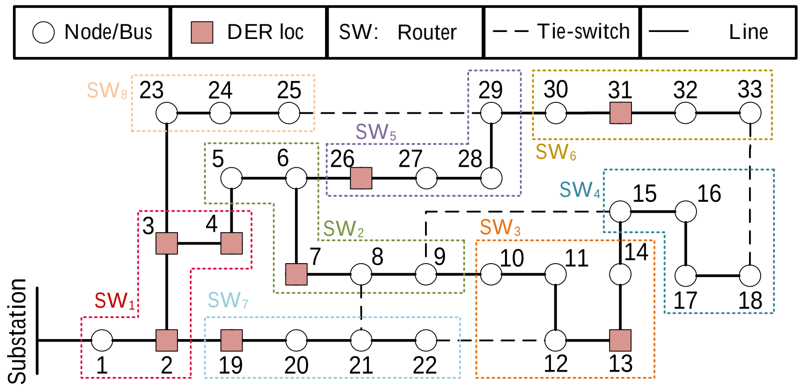

Figure 3.15: CPPS schematic diagram of a modified 33-node distribution feeder

Table 3.6: Assigned Physical Components to Communication Switches

Switch	Assigned nodes	Assigned lines
SW_1	1,2,3,4	1,2,3,14,18,22
SW_2	5,6,7,8,9	5,6,7,8,9,25,33,34
SW_3	10,11,12,13,14	10,11,12,13,14,35
SW_4	15,16,17,18	15,16,17,36
SW_5	26,27,28,29	26,27,28,29,37
SW_6	30,31,32,33	30,31,32
SW_7	19,20,21,22	19,20,21
SW_8	23,24,25	23,24

are scaled by a factor of four; whereas, the repair time is doubled from [59, 127].

Several test cases are conducted to validate the effectiveness of the proposed approach to provide defensive islanding for enhanced resilience. First, the proposed algorithm is tested for a predefined failure scenario to ensure the robustness of the obtained islands. In this case, we have used eight strategies for clustering the distribution system as shown in Table 3.7. Two criteria are used for comparison: the minimal amount of load curtailment and the radiality constraints. A clustering strategy resulting in small of amount of load curtailment and satisfied radiality constraints is preferred. In the second case, the robustness of the proposed algorithm against diverse cyber-related failure scenarios is validated. Finally, the third case provides a deeper analysis on the trade-off between sizes of clusters and efficiency of the proposed algorithm.

Table 3.7: Clustering Strategies

Index	Weight matrix
S_1	Admittance
S_2	Power flow
S_3	Optimal power flow
S_4	Resilience-based
S_5	Integrated power flow and component availability
S_6	Integrated optimal power flow and component availability
S_7	Integrated power flow and component unavailability
S_8	Integrated optimal power flow and component unavailability

3.3.4.1 Algorithm Validation

In this case, a predefined cyber-induced failure is simulated. The impact of the cyber failure is propagated to the physical system using the coupling matrices described in section 3.3.1. The communication router SW_7 is assumed to be compromised resulting in a severe potential physical failure of 3 line segments and 4 load nodes. The probability of failure of physical components is computed based on the conditional probability failure of a connected cyber link, as explained in section 3.3.3.1. For valid comparison, all clustering strategies are set to split the distribution feeder into four independent islands.

Fig. 3.16 shows the clusters obtained for each strategy represented by different colors. The number of nodes in each cluster varies from one strategy to another. For instance, S_2 and S_5 have two islands each composed of a single node (7 and 19) which undermines these strategies to provide less resilient microgrids. In other words, nodes 7 and 19 could have been connected to nearby nodes yielding enhanced resilient topology. Strategies S_7 and S_8 provide very similar clustering solutions; however, the difference relies in the capability of S_8 to capture the whole generation benefits of the existing DERs. In S_4, the clusters are formed based on the resilience level of system components. This results in islands that do not follow radiality constraints and ignore system operating conditions such as cluster C_1 including node 7 and 20.

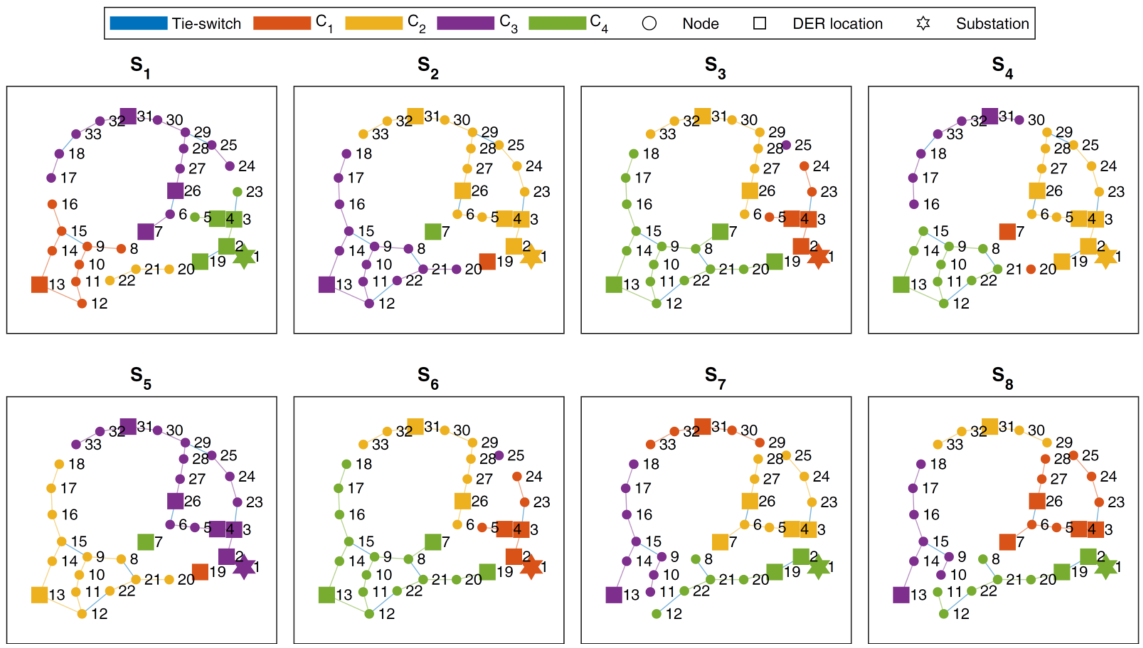

Figure 3.16: Clusters using different strategies

Table 3.8 shows the amount of load curtailment (LC) and degree of radiality (R) of all clusters obtained by different strategies. The R value reflects the number of clusters satisfying radiality constraints within a specific clustering strategy. It is obvious that the proposed strategies (S_7 and S_8) result in least amount of load curtailment relative to other clustering strategies with only 13% of the system nominal load to be curtailed. In general, using steady-state value of admittance matrix (S_1) and power flow solution (S_2) is not sufficient for proper clustering, specifically during severe conditions. Also, using resilience-based clustering (S_4) solely results in much higher curtailment as it ignores the loadability behavior of distribution line segments. Though S_3 provides acceptable results compared to S_5 and S_6, the obtained solution relies on the performance of the system prior to a cyber-induced failure ignoring the fragility behavior of each system component. On the other hand, the effectiveness of the proposed algorithm to provide clusters satisfying radiality constraints has been confirmed through values of R. Both S_7 and S_8 show that all obtained clusters satisfy the radial topology configuration of a distribution system. Also, it is noticeable that S_2, S_4, and S_5 do not usually maintain radial topology in the formed islands.

Table 3.8: Load Curtailment and Radiality Rank of Clustering Strategies

	S_1	S_2	S_3	S_4	S_5	S_6	S_7	S_8
LC (MW)	1.635	1.545	1.125	1.755	1.545	1.125	0.910	0.470
LC (%)	44	42	30	47	42	30	25	13
R	3	2	3	2	2	3	4	4

3.3.4.2 Assessing Stochastic Behavior of Cyber-induced Failures

The solution of the proposed strategy will vary based on the cyber-induced failure scenario. In this case, the efficiency of the proposed clustering approach is validated under different cyber failure scenarios. A total of 10,000 cyber failure scenarios, with diverse impact level, are randomly generated and simulated. The amount of load curtailment and radiality rank are computed for each failure scenario. All clustering strategies are required to split the system into four independent islands.

Table 3.9 summarizes the main statistical parameters including the average, the standard deviation, the minimum value, and the maximum value of the load curtailment and radiality rank for all the clustering strategies. Strategies S_1, S_2, and S_3 provide the same amount of load curtailment regardless the simulated cyber failure scenario because these strategies rely mainly on the steady-state constant system characteristics and power flow in the system. Based on the load curtailment, S_8 shows the least average load curtailments which confirms its effectiveness to cluster the distribution system into islands considering both the loadability of distribution lines and the vulnerability of system components. Also, S_6 and S_7 provide acceptable values compared to basic clustering strategies (S_1, S_2, and S_3). As previously noted, the resilience-based clustering does not usually provide the best solution given diverse system operational conditions. The wide spectrum of load curtailment value realized in S_7 and S_8 ensures the capability of the proposed algorithm to capture the stochastic behavior of cyber failures. From the radiality prospective, it is noticeable that the average value of radiality rank of S_7 and S_8 exceeds three implying the tendency of the proposed strategies to maintain radiality constraints. Though S_1, S_2, and S_3 provide more robust results, one out the four clusters will always fail to satisfy the radiality constraints. In S_8, 32% of the simulated cases satisfy the radiality constraints. In general, the proposed clustering strategies outperform other strategies providing a clustering methodology that reduces the impact of cyber-induced failures on the performance of the power system.

Table 3.9: Assessment of Clustering Strategies considering Cyber-failure Uncertainties

		S_1	S_2	S_3	S_4	S_5	S_6	S_7	S_8
LC(MW)	mean	1.635	1.545	1.125	1.468	1.492	1.106	1.025	0.863
	st. dev.	0.0	0.0	0.0	0.246	0.180	0.166	0.377	0.398
	min	1.635	1.545	1.125	0.175	0.210	0.060	0.0	0.0
	max	1.635	1.545	1.125	1.935	1.935	1.935	2.195	2.015
R	mean	3.0	3.0	3.0	2.988	3.001	3.000	3.189	3.303
	st. dev.	0.0	0.0	0.0	0.108	0.028	0.025	0.459	0.495
	min	3	3	3	2	3	2	2	2
	max	3	3	3	3	3	4	4	4

3.3.4.3 Trade-off between Efficiency and Number of Clusters

In this case, the effectiveness of the proposed clustering strategies to capture the impact of cyber-induced failures to create defensive islands is assessed based on the number of clusters. The same previously generated 10,000 cyber-induced failure scenarios are simulated for different number of clusters. The average load curtailment and the radiality rank are recorded for each specific number of clusters. Three strategies are selected for comparison including S_3, S_7, and S_8.

Fig. 3.17 shows the average value of both the load curtailment and the radiality rank. It is noticeable that the amount of load curtailment increases with the increase in the number of clusters. This reveals the importance of installing more DERs for better performance; however, the scope of this work is comparing the clustering strategies based on predefined energy resources. Strategy S_8 outperforms S_3 when having up to five clusters resulting in a better clustering strategy that encounters the cyber-induced failure. In case of six clusters formation, both S_3 and S_8 have very similar values of average load curtailment. Also, the performance of S_7 decreases as the number of cluster increases which can be inferred from the increase in amount of load curtailment relative to other strategies. Using the radiality rank criterion, the performance of the selected strategies is almost the same for small number of clusters. The higher the radiality rank is, the better the clustering strategy will be for a fixed number of clusters. Strategy S_8 outperforms S_3 and S_7 for the studied number of clusters. The performance of the proposed strategies is significantly impacted by the number DERs, the size of the system being analyzed, and the system physical characteristics. In general, the proposed strategies can be used to create defensive islands that capture the impact of cyber-induced failures into power systems.

3.4 Conclusion

In this chapter, two proactive strategies have been proposed; proactive generation redispatch strategy and resilience-based defensive islanding strategy. The generation redispatch strategy was implemented on a transmission system under both hurricane and wildfire events. The proposed method minimizes the amount of load curtailment

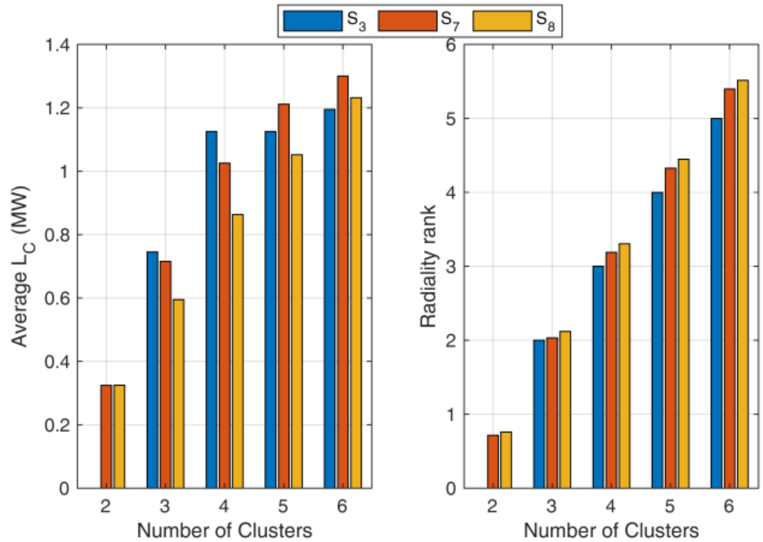

Figure 3.17: Efficiency vs. cluster sizes

as well as system operational costs. The optimization problem was formulated a MDP including generation and transmission constraints. The results showed that generation redispatch strategy enhances the operational resilience of power grids. It also showed the effectiveness of the algorithm to reduce the overall costs via proactive redispatch. The proposed method has shown the capability to consider current and potential failures of system components regardless the event type. The proposed approach provides a sequential decision process for system operators to improve resilience of power grids given specific available assets. On the other hand, the defensive islanding strategy was implemented and tested on a distribution CPPS to enhance the resilience against cyber-induced failures. The proposed framework reduces the amount of load curtailment by splitting the system into smaller microgrid taking into account the system operational conditions and the components vulnerabilities. The results showed the effectiveness of the proposed clustering strategies to provide a list of islands considering operating conditions of the system, the available generation resources, and the probability of failure of system components. Also, the robustness of the proposed framework against diverse cyber-induced failures was validated.

The proposed algorithm provides the system operators with a proactive resilience enhancement strategy to create defensive islands prior to an extreme or disruptive event.

Chapter 4

Corrective Strategies

Corrective resilience enhancement strategies aim to control power system components during an extreme event for improved performance. The negative impacts of extreme weather events can be mitigated, reduced, or even eliminated through corrective strategies. However, the high stochastic nature of resilience-based problem induces further complexities in modeling and providing feasible solutions. Also, it is required to provide fast and efficient decisions during a severe event for noticeable improvements. In this chapter, three corrective strategies are developed including network reconfiguration, sizing and locating of DERs, and dispatching shunt reactors. This chapter leverages reinforcement learning approaches to formulate the control-based decision process of each strategy. In the network reconfiguration, it is required to determine the set of tie-switches or lines to be reconnected based on occurring severe failure scenario. The second strategy focuses on determining the most convenient locations and sizes of DERs in an islanded distribution feeder upon multiple line failures. Finally, the shunt dispatching strategy provides a methodology to improve the voltage profile of transmission systems under severe events. The proposed strategies are tested and validated on standard distribution and transmission systems.

4.1 Introduction

Numerous corrective power system resilience enhancement methods have been proposed from different standpoints.Fast and efficient restoration of lost loads due to extreme events is one of the most important attributes to achieve resilient operation of power systems and reduce their economic and community impact [52, 53]. This can be achieved via microgrid formation [129], network reconfiguration [130], and utilization of DERs [105]. Also, existing resilience enhancement approaches give less attention to dispatch shunts to maintain voltage magnitudes within the standard limits during extreme weather events [131].

Resilience Enhancement through Network Reconfiguration. Resilience enhancement strategies have been proposed to provide emergency responses through switching topology [132], using energy storage devices [133], re-dispatching loads [134], and forming networked microgrid [135]. A spectral clustering algorithm has been employed to determine optimal network partitions under tight potential $N-k$ (i.e., $k>1$) contingencies [103]. A risk-based defensive islanding approach has been studied in [78] to reduce the impact of cascading failures on transmission systems due to extreme events. Resilience-based microgrid formation frameworks have been proposed to enhance the restoration of critical loads in both radial and meshed networks [106]. An evolutionary algorithm approach has been proposed in [136] to restore lost loads via dispatching tie-switches in distribution feeders. In [137], a heuristic approach integrated with a fuzzy multi-objective function has been proposed to determine the sequence of line energizing for enhanced restoration. A mixed-integer linear programming optimization-based formulation has been used to retain critical loads through microgrid formation after an extreme event [138]. Most of these studies have leveraged analytical and heuristic-based techniques for enhanced resilience. Despite the significant contributions of these methods, their efficacy depends mainly on the accuracy of the system models and degree of approximations.

Resilience Enhancement through Leveraging DERs. In [62], a mixed-integer linear programming (MILP)-based method has been proposed to enhance power system resilience through re-dispatching generators, re-configuring network topology, and shedding loads. Moreover, several preventive action-based strategies such as a multi-sensor prediction-based wide-area monitoring and control [139], a linear-programming-based optimal siting and sizing of energy storage devices [66], a Monte-Carlo simulation (MC)-based proactive unit commitment framework [140], and an MC-based crew preposition and network reconfiguration technique [141] have been proposed to enhance power system resilience. In [142], we have developed a proactive generation redispatch strategy to improve the resilience of distribution power systems against hurricanes. Also, a sequential proactive strategy has been studied in [32] for enhanced resilience. In [53], a proactive microgrid management strategy to control existing DGs has been provided. Additionally, an MILP-based generation re-dispatch strategy has been proposed in [67] to enhance power system resilience during ice storms. These methods rely mainly on analytical and optimization techniques, which impose scalability challenges due to the increased modeling and computational complexities. Also, the capabilities of RL-based approaches to overcome the aforementioned constraints are still under investigation.

Resilience Enhancement through Dispatching Reactive Shunt Compensators. An algorithm for enhancing the resilience of a multi-microgrid system via dispatching of unused capacitor banks has been proposed in [143]. A model free Q-learning-based voltage control algorithm has been introduced in [144] to provide optimal control settings for the constrained load flow problem. In [145], a Q-learning-based distributed voltage control method has been proposed to optimally dispatch reactive power. A two-time scale voltage control algorithm that uses deep Q-network to determine optimal capacitor configuration in slow time scale has been proposed in [146]. In [147], optimal tap setting policy for voltage regulation transformers has been determined using a DRL algorithm. These methods are effective to provide control actions without accurate system knowledge to maintain voltage constraints under $N-1$ contingency. Also, most of these RL models are trained to provide a single type of corrective control action.

Resilience Enhancement Leveraging RL-based Techniques. Reinforcement learning approaches have been used to provide a fast-acting control algorithm for high-dimension stochastic optimization problems [148]. Several deep reinforcement learning methods have been proposed to improve resilience of electric power systems [149]. A soft actor-critic algorithm could potentially improve voltage stability of transmission systems during a hurricane based on dispatching shunt resources [150]. In [151], a DRL-based protection scheme has been used to improve the operational efficiency of microgrids integrated with market participation constraints. An optimal rescheduling strategy has been used to train RL networks for improved resilience during hurricanes [152]. RL-based optimal control algorithms have been used to improve the operational performance of microgrids after a disaster [153]. Authors of [154] have developed a DRL method that provides real-time operation decisions to optimally dispatch DERs installed at specific locations for restoring power to customers after sudden outages. RL-based approaches provide a pathway to overcome some of the challenges of analytical and population-based search methods. In addition, learning-driven models have the capability to apply lessons from experiences during online operations [155]. Also, RL-based methods can be easily integrated into online decision making process once fully trained and implemented.

The main contributions of this chapter are summarized as follows:

1. Develop and validate the efficiency of distribution network reconfiguration (DNR) strategy for enhanced operational resilience.

2. Develop a multi-agent DRL algorithm to determine the optimal locations and sizes of DERs to improve distribution system resilience during an extreme event.

3. Develop a mitigation strategy to dispatch reactive power reactors for enhanced voltage profile of transmission systems due to extreme weather event.

4.2 Reinforcement Learning Approaches

RL-based approaches rely mainly on estimating optimal value functions and discovering the optimal policy for a given problem environment. Various methods have been used to estimate the value functions including dynamic programming and backward induction methods [117]. RL involves a repetitive sequential MDP from a sample of states, actions, and rewards. The Markov game comprises an uncertain *environment* where an agent makes an *action* to maximize cumulative *reward*. The *state* representing a specific condition of the environment changes based on the executed action. In some problems where the action space is significantly large or the problem environment is highly non-linear, temporal difference approaches have been used to overcome these challenges [156] including Q-learning, deep Q-networks, and actor-critic algorithms.

In Actor-Critic algorithms (ACAs), a single or multi-agent framework is formulated as a Markov game where it is required to maximize the discounted returns of the agents. The ACA is composed of an actor network and a critic network. The former is trained to determine the proper actions whereas the latter is trained to determine the optimal policy upon which the actor makes proper actions. A policy is defined to be the mapping process from the environment state to the action space.

The goal of each agent is to find a policy that maximizes its total rewards.

4.2.1 Single Agent Actor-Critic Algorithm

A single agent has one actor network to provide appropriate actions with a policy that can be expressed as follows.

$$\alpha_t \sim \pi_\xi(\alpha_t|O_t), \tag{4.1}$$

where O_t is the state vector at time t, α_t is the provided action by the actor-network, ξ is the parameter for policy, and $\pi_\xi(\alpha_t|O_t)$ is an unbounded Gaussian policy. In case of continuous action space, a squashing function needs to be applied on $\pi_\xi(\alpha_t|O_t)$ to bound actions of the agent to a finite value.

In each iteration, the policy is updated to maximize the expected return of an agent in the fundamental ACA model. A value function, $V_\psi(O_t)$, is used to measure the value for a policy and expressed as follows.

$$V_\psi(O_t) = \mathop{\mathbb{E}}_{\alpha_t \sim \pi_\xi} \left[Q_\theta(s_t, \alpha_t) \right], \tag{4.2}$$

where ψ represents parameter of the value function network, θ represents parameter for the Q value function, α_t is the action provided by an actor network, s_t is a set for system states, and $Q_\theta(s_t, \alpha_t)$ is a critic policy evaluation function, which can be calculated as follows.

$$Q_\theta(s_t, \alpha_t) = r(s_t, \alpha_t) + \beta \mathbb{E}_{s_{t+1} \sim p}[V_\psi(o_{t+1})], \tag{4.3}$$

with $\beta \in [0, 1]$ a discount factor and ψ an average of the weights for the value network.

The expression provided in (4.4) is used to minimize the residual squared error of a soft Bellman function to train value functions of the actor network.

$$J_v(\psi) = \mathbb{E}_{s_t} \left[\frac{1}{2} \left(V_\psi(O_t) - Q_\theta(s_t, \alpha_t) \right)^2 \right]. \tag{4.4}$$

The gradient of (4.4) to sample actions from the current policy is determined as follows.

$$\hat{\nabla}_{\psi} J_v(\psi) = \nabla_{\psi} V_{\psi}(O_t) \left[V_{\psi}(O_t) - Q_{\theta}(s_t, \alpha_t) \right]. \tag{4.5}$$

To update the Q-parameters of the basic actor, the following expression can be used.

$$J_{Q_\theta}(\theta) = \mathbb{E}_{(s_t,\alpha_t)} \left[\frac{1}{2} \left(Q_\theta(s_t, \alpha_t) - \hat{Q}(s_t, \alpha_t) \right)^2 \right]. \tag{4.6}$$

The value of Q-function (4.6) is optimized as follows:

$$\hat{\nabla}_{\theta} J_{Q_\theta}(\theta) = \nabla_{\theta} Q_{\theta}(s_t, \alpha_t) \left[Q_\theta(s_t, \alpha_t) - \hat{Q}(s_t, \alpha_t) \right]. \tag{4.7}$$

The policy needs to be updated in each iteration to maximize the rewards.

4.2.2 Multi-Agent Soft Actor-Critic Algorithm

Each agent in a multi-agent soft actor critic (MASAC) framework has one actor network to provide actions, which is developed using a squashed Gaussian distribution function [150]. The policy of the actor network to provide actions is expressed as follows:

$$\alpha_t^{ci} \sim \pi_{\xi^{ci}}(\alpha_t^{ci} | O_t^i), \tag{4.8}$$

where i represents the i^{th} agent of the multi-agent framework, O_t^i is the observation vector of the i^{th} agent at time t, α_t^{ci} is the provided action by the actor-network of the i^{th} agent, ξ^{ci} is the parameter for policy of the i^{th} agent, and $\pi_{\xi^{ci}}(\alpha_t^{ci}|o_t^i)$ is an unbounded Gaussian policy of the i^{th} agent. A squashing function needs to be applied on $\pi_{\xi^{ci}}(\alpha_t^{ci}|o_t^i)$ to bound actions of the i^{th} agent to a finite value.

In the fundamental MASAC, the policy is updated in each iteration to maximize the expected return and entropy (randomness measure of the policy). Following the same convention, policies of the proposed algorithm are also updated in each iteration. A value function, $V_{\psi^i}^{ci}(O_t^i)$, which is used to measure the soft value for policy of the i^{th} agent can be expressed as follows:

$$V^{ci}_{\psi^i}(O^i_t) = \mathop{\mathbb{E}}_{\alpha^{ci}_t \sim \pi_{\xi^{ci}}} \left[Q_\theta(s_t, \alpha^{ci}_t, \alpha^{-ci}_t) - \alpha^{ci} \log\left(\pi_{\xi^{ci}}(\alpha^{ci}_t | O^i_t)\right)\right], \tag{4.9}$$

where ψ^i represents parameter of the value function network for the i^{th} agent, θ represents parameter for the Q value function, $Q_\theta(s_t, \alpha^{ci}_t, \alpha^{-ci}_t)$ is a critic or centralized policy evaluation function for all the actors, α^{-ci}_t is the action provided by actors of agents except agent i, α^{ci} represents a parameter to determine the relative importance between reward and entropy of the i^{th} agent, and s_t is a set for system states.

The expression provided in (4.10) is used to minimize the residual squared error of a soft Bellman function to train value functions of the actors.

$$J^{ci}_v(\psi^i) = \mathbb{E}_{s^{ci}_t \sim \mathcal{D}} \left[\frac{1}{2} V^{ci}_{\psi^i}(O^i_t) - \left[Q_\theta(s_t, \alpha^{ci}_t, \alpha^{-ci}_t) \ - \alpha^{ci} \log\left(\pi_{\xi^{ci}}(\alpha^{ci}_t | O^i_t)\right)\right]^2 \right], \tag{4.10}$$

where $\mathcal{D}$ is a replay buffer to store experiences of the actors.

The gradient of (4.10) using an unbiased estimator is determined as follows to sample actions from the current policy:

$$\hat{\nabla}_{\psi^i} J^{ci}_v(\psi^i) = \nabla_{\psi^i} V^{ci}_{\psi^i}(O^i_t) \left(V^{ci}_{\psi^i}(O^i_t) - Q_\theta(s_t, \alpha^{ci}_t, \alpha^{-ci}_t) \ + \alpha^{ci} \log\left(\pi_{\xi^{ci}}(\alpha^{ci}_t | O^i_t)\right)\right). \tag{4.11}$$

In this work, we have modified the expression for training the soft-Q parameters of the basic actor given in [157], which can be expressed as follows:

$$J^{ci}_{Q_\theta}(\theta^i) = \mathbb{E}_{(s^{ci}_t, \alpha^{ci}_t) \sim \mathcal{D}} \left[\frac{1}{2} \left(Q_\theta(s_t, \alpha^{ci}_t, \alpha^{-ci}_t) \ - \hat{Q}(s_t, \alpha^{ci}_t, \alpha^{-ci}_t) \right)^2 \right], \tag{4.12}$$

where

$$\hat{Q}(s_t, \alpha^{ci}_t, \alpha^{-ci}_t) = r(s_t, \alpha^{ci}_t, \alpha^{-ci}_t) + \beta \mathbb{E}_{s_{t+1} \sim p}[V^{ci}_{\bar{\psi}^i}(o^i_{t+1})] \tag{4.13}$$

with $\beta \in [0, 1]$ a discount factor and $\bar{\psi}^i$ an average of the weights for the value network of i^{th} agent.

The value of Q-function (4.12) is optimized as follows:

$$\hat{\nabla}_{\theta^i} J^{ci}_{Q_\theta}(\theta^i) = \nabla_{\theta^i} Q_\theta(s_t, \alpha^{ci}_t, \alpha^{-ci}_t) \left(Q_\theta(s_t, \alpha^{ci}_t, \alpha^{-ci}_t) - r(s_t, \alpha^{ci}_t, \alpha^{-ci}_t) - \beta V^{ci}_{\bar{\psi}^i}(o^i_{t+1}) \right)^2 . \tag{4.14}$$

The policy needs to be updated in each iteration to maximize the rewards for improving the policy. The authors of [157] have directed the policy update toward exponential of new soft Q-function as they intended to track the policy update. Also, the potential policies are restricted to a parameterized distribution (i.e., Gaussian) family. Following the same convention, we have updated the expression for policy update of basic SAC algorithm for the proposed algorithm as follows:

$$\pi^{new}_{\xi^{ci}} = \arg\min D_{KL} \left(\pi_{\xi^{ci}}(.|O^i_t) \middle|\middle| \frac{Q_\theta(s_t, .)}{Z_\theta(s_t)} \right), \tag{4.15}$$

where $Z_\theta(s_t)$ is an intractable partition function that does not contribute to the gradient with respect to the new policy.

The policy $\pi_{\xi^{ci}}(.|O^i_t)$ is parameterized for action setting using the policy network of agent i with parameter ξ^{ci}. Finally, the expected KL-divergence of (4.15) is multiplied by α^{ci} and then minimized, ignoring $Z_\theta(s_t)$ to train the policy parameters of agent i as follows:

$$J^{ci}_{\pi_{\xi^{ci}}}(\xi^{ci}) = \mathbb{E}_{s^{ci}_t \sim \mathcal{D}} \left[\mathbb{E}_{\alpha^{ci}_t \sim \pi_{\xi^{ci}}} \left[\alpha^{ci} \log \left(\pi_{\xi^{ci}}(\alpha^{ci}_t | O^i_t) \right) \; - Q_\theta(s_t, \alpha^{ci}_t, \alpha^{-ci}_t) \right] \right] . \tag{4.16}$$

Although several options are available to minimize the objective function $J^{ci}_{\pi_{\xi^{ci}}}(\xi^{ci})$, the authors of [158] have applied the reparameterization trick to achieve target density (the Q-function). The modified expression to reparameterize the policy of agent i is as follows:

$$\alpha^{ci}_t = f_{\xi^{ci}}(\epsilon^{ci}_t; o^i_t), \tag{4.17}$$

where ϵ^{ci}_t is a noise vector that uses a spherical Gaussian distribution.

Thus, the new policy objective for agent i is as follows:

$$J^{ci}_{\pi_{\xi^{ci}}}(\xi^{ci}) = \mathbb{E}_{s^{ci}_t \sim \mathcal{D}}, \epsilon^{ci}_t \sim \mathcal{N}\left[\alpha^{ci} \log\left(\pi_{\xi^{ci}}(f_{\xi^{ci}}(\epsilon^{ci}_t; o^i_t)|O^i_t)\right)\right.$$
$$\left. -Q_\theta(s_t, f_{\xi^{ci}}(\epsilon^{ci}_t; o^i_t), f_{\phi^{-ci}}(\epsilon^{-ci}_t; s^{-i}_t))\right], \tag{4.18}$$

where $f^{-ci}_\phi(\epsilon^{-ci}_t; s^{-i}_t)$ is the parameterized policies of other actors.

In [159], the authors have provided a detailed formulation of an alternative approach to obtain the temperature parameter learning objective function, which is not strictly relevant to this work. However, we modify their temperature objective function for the actors of each agent of the proposed framework as follows:

$$J^{ci}(\alpha^{ci}) = \mathbb{E}_{\alpha^{ci}_t} \sim \pi_{\xi^{ci}}\left[-\alpha^{ci}\left(\log\left(\pi_{\xi^{ci}}(\alpha^{ci}_t|O^i_t\right) + \bar{H}\right)\right], \tag{4.19}$$

where $\bar{H}$ is an equivalent constant vector of the hyper-parameter to represent target entropy. Equation (4.19) cannot be minimized directly due to the expectation operator. Therefore, it is minimized using a MC estimator after sampling experiences from a replay buffer based on the procedure from [159]. In the proposed multi-agent algorithm, two soft Q-networks for all agents are trained and then the minimum value among the outputs of the two Q-networks is used in the objective function of (4.19) to combat state-value overestimation [160].

4.3 Distribution Network Reconfiguration

This section proposes a RL-based approach to control tie-switches of distribution circuits to enhance the operational resilience of power systems due to an extreme event. The proposed algorithm is developed leveraging distribution network reconfiguration strategy to reduce/eliminate the amount of load curtailment. A single-agent ACA is used to train a RL-based model under multiple line outages in a distribution system. An MDP is used to formulate the sequential iterative learning process for the agent. An action implies connecting tie-switches to modify the system topology, while a system state provides information about the system operating conditions and availability of system components. A reward function is used to assess the goodness of the executed action. A proper action should satisfy the traverse constraint and radiality constraint of the distribution system. The sequential MDP is repeated for numerous failure scenarios till the agent is fully-trained. The trained ACA provides a set of tie-switches to be reconnected for enhanced resilient operation after an extreme event. The proposed algorithm provides a corrective and restorative resilience enhancement strategy that can be adopted for real-time applications. The ACA is tested on the 33-node distribution feeder for validation.

A distribution power system can be represented as an undirected graph $G_P = (N_P, E_P)$, where N_P is a set of vertices corresponding to buses or nodes in the power system and E_P is a set of edges referring to distribution line segments, transformers, sectionalizing switches, and tie-switches [19]. Changing the status of sectionalizing switches and tie-switches provides different topologies of a distribution feeder. For enhanced resilience, minimal amount of load curtailment should be achieved. Also, node traversing constraint and radiality constraint should be fulfilled for feasible operation of distribution system.

- Traversing Constraint: In the absence of DERs, only the main substation can supply energy to load nodes. There should be at least one path from the source node to each load node. In other words, all system nodes should be connected together without the existence of islanded nodes.

- Radiality Constraint: Radiality requirements should be satisfied in distribution systems to align with the existing protection coordination schemes and voltage regulation fundamentals. A node-branch incidence matrix A can be constructed using (4.20) for a distribution network, such that $A \in \mathbb{R}^{n \times e}$, where $n = |N_k|$ denotes the number of nodes and $e = |E_k|$ denotes the number of edges. Radiality constraint is satisfied if matrix A is a full rank matrix.

$$a_{i,j} = \begin{cases} +1, & \text{if branch } j \text{ starts at node } i \\ -1, & \text{if branch } j \text{ ends at node } i \\ 0, & \text{otherwise} \end{cases} \tag{4.20}$$

4.3.1 Problem Environment

This section formulates the DNR problem as a MDP representing the ACA approach. The MDP is a sequential process where a reward value is calculated based on a specific action to change the problem environment from one state to another. The better the action, the higher the reward. The states, the actions, and the rewards are formulated as follows.

4.3.1.1 States

The state set describes the system conditions and the required information to fully observe the system characteristics. In this study, a vector of on/off status of network branches including both distribution lines and tie-switches is taken as the state. For a system with N_l distribution lines and N_s tie-switches, the state of length $(N_l{+}N_s)$ is formulated as follows.

$$s_i = \begin{cases} 1, & \text{if line is connected} \\ 0, & \text{if line is not connected} \end{cases} ,\forall i \in N_l + N_s \tag{4.21}$$

4.3.1.2 Action

In the proposed problem, a discrete action representing changing the status of a specific tie-switch is considered as an action. A vector of on/off status of network tie-switches is fed into the problem environment. The action vector is formulated as follows.

$$a_j = \begin{cases} 1, & \text{if tie-switch is connected} \\ 0, & \text{if tie-switch is not connected} \end{cases} ,\forall j \in N_s \tag{4.22}$$

4.3.1.3 Reward

A proper reward value, r_t, should be defined to assess the effectiveness of the actions. An agent is encouraged to determine the best set of tie-switches to be turned on for a specific failure scenario. A discrete reward function is formulated where a value of -1 is given for each wrong action and a value of 10 when reaching a feasible solution. The total reward at time step t is computed as follows.

$$R_t = \begin{cases} 10, & \text{if all constraints are satisfied} \\ -1, & \text{if any constraint is violated} \end{cases} \tag{4.23}$$

4.3.2 Training and Execution Algorithms

The proposed ACA agent is trained to determine the set of tie-switches to be connected for improved resilience. The agent is subjected to different failure scenarios from a list of potential failures. For each failure scenario, the agent takes an action and a reward is calculated. The process is repeated till the ACA converges. The training and testing procedure for the ACA are summarized in Algorithm 2 and Algorithm 3 as follows.

4.3.3 Implementation and Results

The proposed approach is applied on the 33-node distribution feeder for validation. The proposed ACA model is formulated to control tie-switches of the distribu-

Algorithm 2: Training of the ACA Framework

```
Define hyper-parameters of ACA
for episode = 1 to M_train do
    Create failure scenario
    Reset the environment to default settings
    while Constraints not fulfilled and step < N do
        Generate an action (set of connected tie-switches) using the actor network
        Evaluate the value of the current state using the critic network
        Execute the action on the environment
        Compute the reward value
        Observe the new state
        Check terminal condition, reset the environment if terminal reached
        Update the weights of the actor network
        Update the weights of the critic network
    end while
end for
```

Algorithm 3: Testing of the ACA Framework

```
for episode = 1 to M_test do
    Create failure scenario
    Reset the environment to default settings
    Generate an action using the actor network
    Execute the action on the environment
    Count success if terminal condition is fulfilled
end for
```

tion feeder for enhanced resilience leveraging DNR approach.

4.3.3.1 System under Study

The 33-node distribution test system is a radial distribution system with 33 nodes, 32 branches, and 5 tie-lines (37 branches) with total system load of 3.72 MW [161]. The proposed algorithm is implemented on the original system to validate the effectiveness of the proposed algorithm to adapt to existing system characteristics. A list of vulnerable lines and tie-switches is summarized in Table 4.1 and highlighted in Fig. 4.1.

The proposed ACA model is trained for three cases based on the number of failed

Table 4.1: List of Vulnerable Lines and Tie-switches

Tie-Switch	Connecting nodes	Vulnerable lines	Connecting nodes
SW_1	21-8	L_1	3-23
SW_2	9-15	L_2	5-6
SW_3	12-22	L_3	21-22
SW_4	18-33	L_4	10-11
SW_5	25-29	L_5	29-30

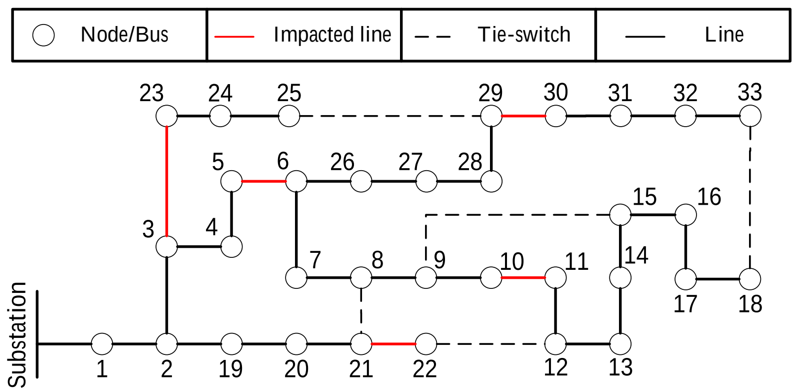

Figure 4.1: Schematic diagram of the 33-node distribution feeder with list of potential impact locations

lines, as follows: (a) Case C_1: single line failure, (b) Case C_2: two line failures, and (c) Case C_3: randomly selected failures between one and four. The training is performed for 30,000 episodes with a maximum of ten iterations per episode. Also, a stopping criterion is adopted to terminate the training process if the average reward value exceeds a specific threshold for 100 consecutive episodes. This is due to the high step impact from one episode to another causing potential instability in the ACA networks [150]. The hyper-parameter settings of the actor and critic networks of the proposed framework are shown in Table 4.2.

4.3.3.2 Training ACA-DNR Model

In each training episode, the system is initialized with a random state representing the status of all the system lines. A set of failed lines is selected randomly from

Table 4.2: Hyper-parameter Settings of the ACA-DNR Model

Hyper-parameters	Values
Number of hidden layers	3
No. of neurons in hidden layers	100, 100, 100
Learning rate	10^{-3}
Reward discount factor	0.99
Activation function of output layer	Sigmoid
Activation function of hidden layers	ReLU
Optimizer	Adam

the set of vulnerable lines. An action is generated using the actor network and a corresponding value is computed using the critic network for the given system state. A reward value is calculated based on the obtained new system state. The process is repeated for all aforementioned cases. For evaluation, the running mean of the episodic rewards and the number of iterations per episode are calculated using a window of 100 episodes.

Fig. 4.2 and Fig. 4.3 show the running mean and number of iterations per episode for cases C_1 and C_2. The average reward value increases as the number of training episodes increases, as anticipated. The average reward value reaches the saturation level in less than 1,500 episodes in C_1 yielding the effectiveness of the proposed algorithm to turn on a proper tie-switch to maintain system constraints. In C_2, the average reward reaches saturation around 5,000 episodes. This is due to the existence of more than one possible action for a specific failure scenario. For instance, failure of L_4 (nodes 10-11) and L_5 (nodes 29-30) can be mitigated by turning on either SW_4 and SW_2 (nodes 18-33 and 9-15) or SW_4 and SW_3 (nodes 18-33 and 12-22). On the other hand, the number of iterations per episode decreases as the ACA networks are trained. As the average value of iterations per episode reaches one, the trained ACA is capable of determining the set of tie-switches that maintain radiality constraints and eliminate the amount of load curtailments within one decision iteration.

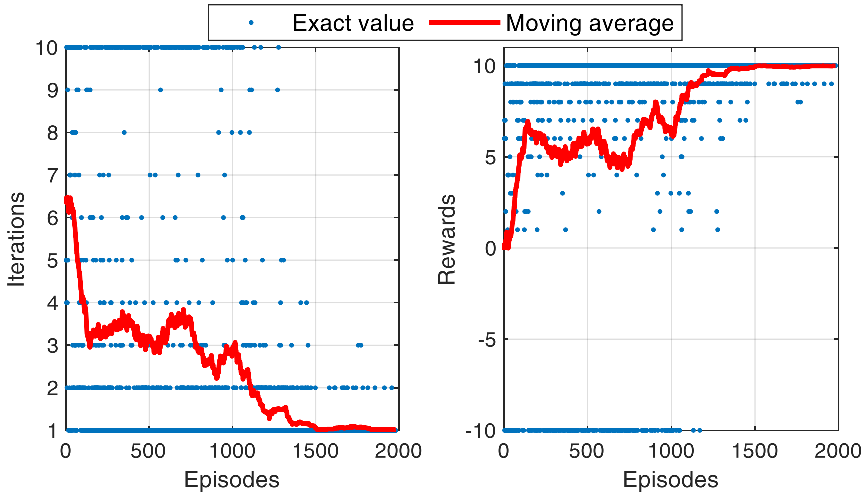

Figure 4.2: Reward and iterations per episode for C_1

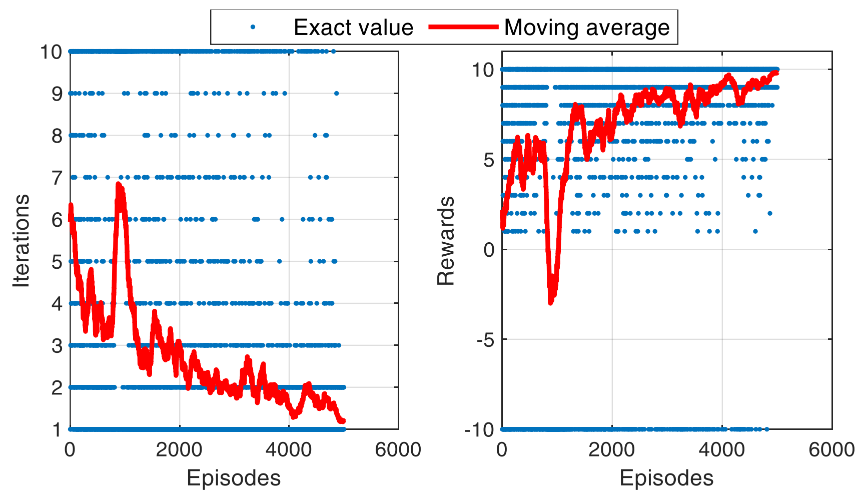

Figure 4.3: Reward and iterations per episode for C_2

Fig. 4.4 shows the running mean and number of iterations per episode for cases C_3. The average reward converges in around 12,000 episodes. The proposed ACA has the capability to learn and make proper decisions as more training episodes are executed. In C_3, the average reward converges in a much slower rate due to the high variability in the environment behavior. In other words, for a specific failure scenario, more than one set of tie-switches is considered a feasible solution. Also, the random failure scenario generation creates further challenges to train the ACA networks.

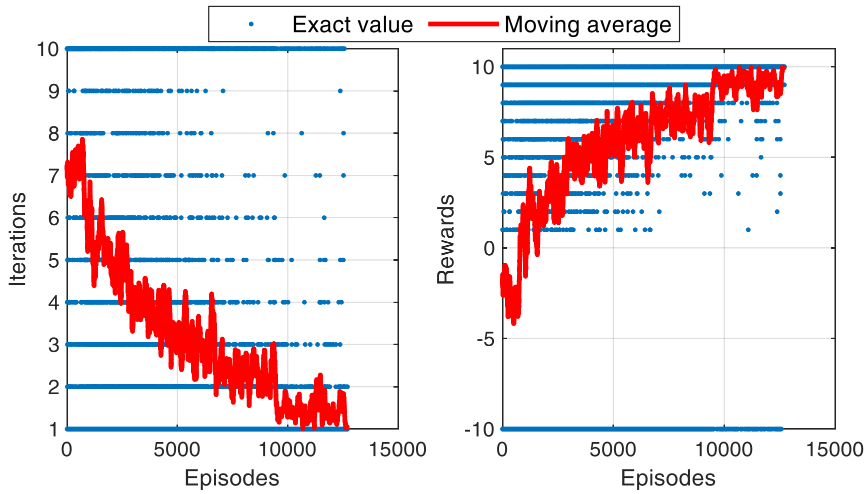

Figure 4.4: Reward and iterations per episode for C_3

4.3.3.3 Testing ACA-DNR Model

To validate the efficiency of the trained models, a total of 1000 failure scenarios are tested for each case. For each episode, the model is required to provide a feasible set of tie-switches to reconfigure the distribution feeder for enhanced resilience. A successful decision is counted if the provided decision is a proper solution. The success rate is shown for all cases as summarized in Table 4.3.

Table 4.3: Efficiency Percentage of Trained ACA models

Case	C_1	C_2	C_3
Success rate	99.7 %	96 %	93.5 %

The trained ACA models are capable of providing a proper reconfiguration of the 33-node feeder with relatively high success rate. Though the efficiency rate can be improved through various modifications of the ACA networks and hyper-parameters tuning procedure, this study focuses on the capability of the proposed ACA to reconfigure a given distribution system under a specific failure scenario. It is worth noting that all trained ACA models are able to achieve 100% accuracy when two iterations of decisions are allowed. In other words, if the maximum number of iterations per episode is two, a 100% success rate is achieved.

4.3.3.4 Validation of ACA-DNR Model

In this case, a failure scenario is provided to visualize the impact on network reconfiguration using the ACA model. Lines L_2 and L_4 are selected to fail resulting in two islands as shown in Fig. 4.5.

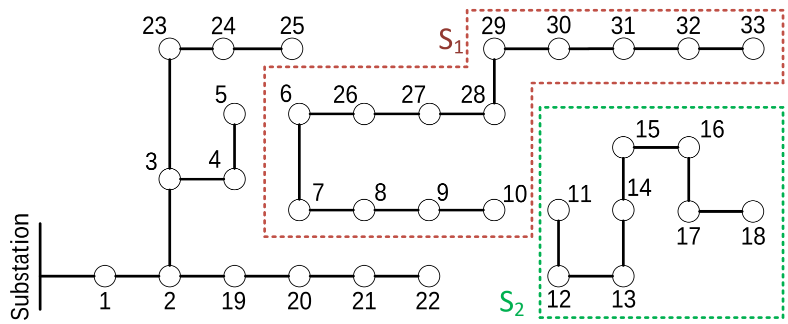

Figure 4.5: IEEE 33-node topology due to failure of L_3 and L_4

The trained ACA provides two possible network reconfigurations, as shown in Fig. 4.6 and Fig. 4.7, respectively. It is worth noting that both solutions satisfy the traversing constraint—no islands, and radiality constraint—no circulating loops. In Fig. 4.6, both SW_3 and SW_4 are connected, whereas switches SW_3 and SW_5 are connected in Fig. 4.7. Though other possible feasible reconfigurations might exist, the ACA selects the decision based on their corresponding probability of success. In other words, connecting SW_1 and SW_3 will result in feasible reconfiguration solutions. However, this decision is associated with less probability value within the trained ACA model.

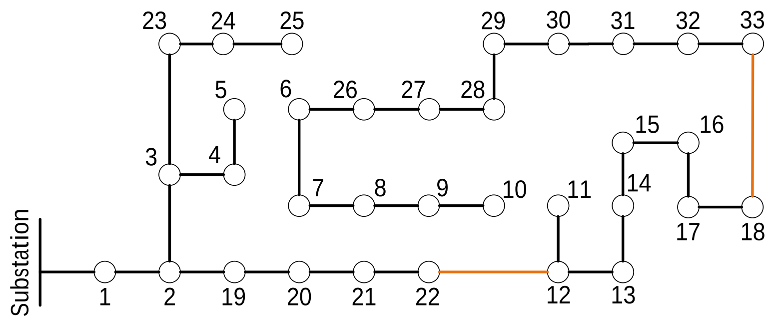

Figure 4.6: First possible network reconfiguration due to failure of L_3 and L_4

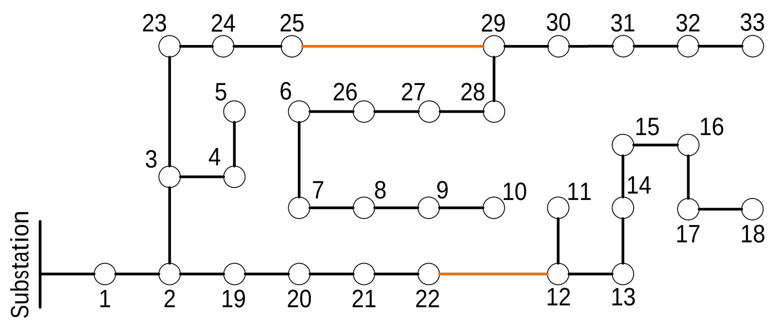

Figure 4.7: Second possible network reconfiguration due to failure of L_3 and L_4

4.4 Allocation and Sizing of Distributed Energy Resources

This section proposes RL-based approach to allocate DGs to enhance the operational resilience of distribution power systems. The proposed algorithm is developed based on dispatching movable DGs to reduce the amount of load curtailments. It also considers proper sizing of DGs to avoid additional operational costs. An MASAC model is formulated to control generation dispatch under single or multiple line outage conditions. In the proposed method, the power grid is split into various regions where each region is assigned to an agent. An MDP is formulated to train the MASAC model. A reward scheme is developed to learn the agent for better decision making. The algorithm is trained using a hurricane fragility model of transmission lines. The trained algorithm provides a set of corrective control actions to reduce the amount of load curtailments and to maintain sizes of DGs within a permissible range. The proposed algorithm is tested on the IEEE 33-node distribution feeder for validation.

4.4.1 Problem Environment

An MDP is used to formulate the problem where a system state represents specific system conditions. A transition to another state is due to taking certain actions yielding a reward that can be defined as a function of desired outcome. The components of the formulated MDP are defined below.

4.4.1.1 State

The state set describes the system conditions and the required information to fully observe the system characteristics. The state set is defined as:

$$s_t = \left\{G_i^l, G_i^s, G_i^r, L_n, Cu_n, u_j\right\}, \forall n \in \Omega^N,\ \forall i \in \Omega^G\ \forall j \in \Omega^B, \tag{4.24}$$

where G_i^l is the DG location, G_i^s the DG size, G_i^r the DG generation reserve, L_n the real power load, Cu_n the curtailed load, u_j the line status, Ω^N the set of system nodes, Ω^G the set of DGs, and Ω^B the set of lines.

4.4.1.2 Action

In the proposed problem, a discrete and a continuous action needs to be taken by each agent. The discrete action signifies the location of the DG whereas the continuous action represents the size of the DG. For each agent, the action is represented as follows:

$$\alpha_t^i = \left\{G_i^l, G_i^s\right\}, \tag{4.25}$$

where α_t^i represents the action specifying the size and location of DG for the i^{th} agents and G_i^l and G_i^s are the location and size of the i^{th} agent, respectively,

4.4.1.3 Reward

A proper reward value, r_t, should be defined to assess the effectiveness of the actions. Each agent is encouraged to reduce the amount of load curtailment and to maintain enough generation reserve during contingencies. Generally, the reward value increases as the amount of load curtailment decreases. Also, the reward value increases as the amount of generation reserve exceeds a specific threshold. The reward r_t for taking a specific action is calculated as:

$$r_t = -C_{cu} \ . \sum_{n \in \Omega^N} Cu_n - C_r \ . \sum_{i \in \Omega^G} G_i^r, \tag{4.26}$$

where C_{cu} is the cost of load curtailments, Cu_n the load curtailment at bus n, Ω^N the set of all buses, and C_r the cost of additional generation reserve.

To obtain the amount of load curtailment, an AC optimal power flow (OPF) is formulated and solved by setting the sizes and locations DGs equal to the action taken by each agent. The amount of generation reserve is the difference between the sizes of DGs as determined by the agents and the obtained sizes from solving the AC OPF problem after including 25% generation reserve.

4.4.2 Training and Execution Algorithms

The power grid is divided into several regions based on the electrical distance between components such that each region is controlled by one agent. Each agent is responsible for determining the location and size of a DG unit to supply loads within its region. To train all agents, a replay buffer is used as follows:

$$\mathcal{D} \leftarrow \left(s_t, o_t^i, \alpha_t^i, r_t, s_{t+1}, o_{t+1}^i, \alpha_{t+1}^i\right). \tag{4.27}$$

The training and testing steps for the multi-agent framework are summarized in Algorithm 4 and Algorithm 5. For a generated failure scenario, each agent determines location and size of DG. All DGs are integrated into the system topology and the optimal power flow is solved. The amount of load curtailment and generation reserve are computed for the reward function. If a terminal condition is not reached, new actions are taken by each agents till maximum number of iterations is reached. The process is repeated for diverse failure scenarios to trains the NN models.

Algorithm 4: Training of the Multi-agent Framework

for episode = 1 to M **do**
    Create failure scenario from list of potential components
    Reset the environment to default settings
    Solve AC OPF to determine o_i^t and s_t of each agent
    while load curtailed, additional reserve and step $< N$ **do**
        Evaluate actions, α_t^i for agent i
        Execute actions α_t^i using AC OPF environment (e.g., Pandapower)
        Observe s_{t+1}, r_t, and d to check terminal conditions.
        Store (state, action, and reward) in $\mathcal{D}_i$
        If s_{t+1} is terminal, reset the environment
        Update weights of the policies using (4.18)
        Update the Q-function parameters of local and target networks of each agent using (4.14)
        Update temperature of actor-networks using (4.19)
        Update target networks weights of each agent using $\bar{Q}_m \leftarrow \tau Q_m + (1-\tau)\bar{Q}, \text{where, } m \in \{1,2\} \text{ and } m \ll 1$
    end while
end for

4.4.3 Implementation and Results

The proposed approach is applied on the IEEE 33-bus distribution feeder. Several failure scenarios are created using the hurricane fragility model provided in section

Algorithm 5: Testing of the Multi-agent Framework

for episode = 1 to M **do**
  Create failure scenario using fragility curve
  Reset the environment to default settings
  while load curtailed, additional reserve and step $< N$ **do**
    Evaluate actions, α_t^i for each agent
    Execute actions α_t^i using power flow solver
    Observe s_{t+1}, r_t, and d to validate terminal conditions
  end while
end for

2.3.1. The vulnerable lines are (1-2), (2-3), (5-6), (9-10), (15-16), (21-22), (26-27), and (31-32), as shown in Fig. 4.1. To create a more severe condition, the connection to the main feeder is disconnected with the result being the system acting as an islanded microgrid. Also, the impact of load variation is considered by scaling the system nominal load using load demand profile obtained from [118]. The power grid is split into 6 regions. An agent is assigned to each region as shown in Table 4.4. Each DG is assumed to have maximum capacity of 2 MW.

Table 4.4: Assigned Nodes to each agent

Agent	Nodes
A_1	1, 2, 3, 4, 5, 6
A_2	7, 8, 9, 10, 11
A_3	12, 13, 14, 15, 16
A_4	17, 18, 19, 20, 21, 22
A_5	23, 24, 25, 26, 27, 28
A_6	29, 30, 31, 32, 33

The proposed algorithm is implemented for a fixed number of episodes (failure scenarios). A total of $10,000$ episodes are used for training. The cumulative reward for each episode is plotted as shown in Fig. 4.8. The learning rate of the agents is improved as more scenarios are simulated. Also, the algorithm explores more situations providing the agents with more experience. Reward values reaching zero

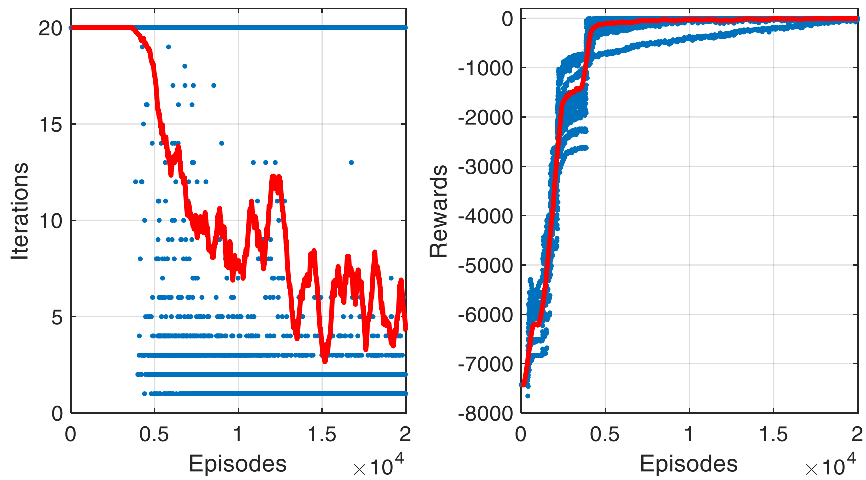

Figure 4.8: Reward and iterations per episode performance

value after 5,000 episodes implies significant amount of load curtailments and learning experience. As reward value approaches zero, the amount of load curtailment is reduced and the capacity of DGs is within permissible limits. On the other hand, the average number of iterations decreases dramatically after 5,000 episodes reaching a value of five iterations per episodes. This shows the capability of the proposed algorithm to determine an optimal solution in five trials.

To visualize the internal learning behavior, the actor and critic losses of all agents are plotted, as shown in Fig. 4.9. It is worth noting that training episode differs from running episodes since training the model is executed every ten episode after having enough scenarios in the memory buffer. The actor losses of A_3, A_4, and A_5 converge faster than A_1 and A_2. All agents converge to almost zero losses after 14,000 training episodes. On the other hand, the critic losses show much faster converging rate. All agents provide pre-mature convergence after 5,000 training episodes. The sudden improved learning behavior of A_1 at 5,000 training episode and A_2 at 8,000 training episode instant is reflected in the critic losses curve.

The results showed that the proposed approach could provide proper decisions to maintain reliable operation of an islanded distribution feeder during impacts of

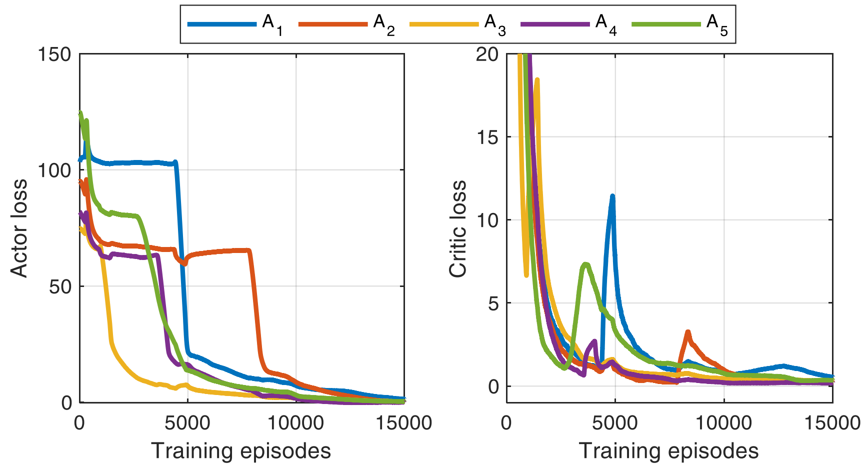

Figure 4.9: Actor and critic losses of each agent

hurricane. The trained algorithm is capable of determining feasible sizes and locations of DGs for enhanced resilience. The proposed algorithm can be extended to include other resources such as load shedding, network reconfiguration, and energy storage for further improvements.

4.5 Dispatching Reactive Power Compensators

This section proposes a DRL-based approach to enhance power system resilience against hurricanes. The proposed method is developed based on dispatching of reactive power compensators, and thereby preserving bus voltages within the acceptable limits in case of single or multiple line outages. A MASAC algorithm is used to develop a DRL-based framework to control the reactive power output of shunt compensators. In the proposed method, power systems are divided into regions, where each region represents an agent. The algorithm is trained using historical data and fragility curves of transmission lines against windstorms. The trained algorithm is then used to provide corrective control actions when a power system is impacted by a hurricane. The proposed algorithm is tested on the IEEE 30-bus system.

4.5.1 Problem Environment

Various parameters can be used to represent system states [162, 163, 164]; however, for reactive power control studies, voltage magnitudes have been widely used. In this study, voltage states are divided into three zones as shown in Table 4.5.

Table 4.5: Reward Value based on Voltage Levels

Operation Zone	V_k^t	r_k^t
Normal	$[V_{ref}, V^{ub}]$	$\dfrac{V^{ub} - V_k^t}{V^{ub} - V_{ref}}$
Normal	$[V^{lb}, V_{ref}]$	$\dfrac{V_k^t - V^{lb}}{V_{ref} - V^{lb}}$
Violation	$[V^{ub}, 1.25]$	$\dfrac{V_k^t - V_{ref}}{V_{ref} - 1.25}$
Violation	$[0.8, V^{lb}]$	$\dfrac{V_{ref} - V_k^t}{0.8 - V_{ref}}$
Diverge	$[0.0, 0.8]$	-5
Diverge	$[1.25, \infty]$	-5

Each agent is assumed to observe and control voltage profile of the assigned region. Voltage magnitudes are readjusted based on the reactive power output of shunt compensators as well as their locations. The two control variables are continuously updated within their predefined range limits.

A proper reward value, R_k^t, should be defined to assess the effectiveness of the actions. Each agent is encouraged to reduce the deviation of voltage magnitudes during contingencies from a predefined reference value, $V_{ref} = 1.0$ p.u. Rewards could be classified based on voltage operating limits as described in Table 4.5. Generally, the reward value increases as the voltage deviation decreases. If the value of all bus voltages remain in normal or violation zones after dispatching shunts, then the total reward is calculated using (4.28); otherwise, a relatively large penalty is assigned.

$$r^t = \sum_{k=1}^{N^b} R_k^t / N^b. \tag{4.28}$$

4.5.2 Training and Execution Algorithms

The power grid is divided into several regions based on the electrical distance between components such that each region is controlled by one agent. The number of regions (agents) varies according to system sizes. The set of bus voltages in each region during a contingency is regulated within the acceptable voltage limits. The set of control actions for each agent, i, can be expressed as follows.

$$\alpha_t^{ci} = \begin{cases} \pi_{\phi^{ci}}(\alpha_t^{ci} | o_t^i), & \text{if } \mid \Lambda_t^i \mid > 0 \\ a_{t-1}^{ci}, & \text{if } \mid \Lambda_t^i \mid = 0 \end{cases} \tag{4.29}$$

where $\mid \Lambda_t^i \mid$ represents the number of violated bus voltages in the i^{th} region; and α_t^{ci} represents the action specifying the amount and locations of dispatch shunts for the i^{th} agent.

To train all agents, a replay buffer is used as follows.

$$\mathcal{D} \leftarrow \left(s_t, o_t^i, \alpha_t^{ci}, \alpha_t^{-ci}, r^t, s_{t+1}, o_{t+1}^i, \alpha_{t+1}^{ci}, \alpha_{t+1}^{-ci}\right). \tag{4.30}$$

The training and testing steps for the multi-agent framework are summarized in Algorithm 4 and Algorithm 5.

4.5.3 Implementation and Results

The proposed approach is applied on a modified IEEE 30-bus system [165]. A windstorm is assumed to pass through the system as shown in Fig. 4.10. For assessment purpose, we assume that five shunt compensators are located at buses 3, 7, 11, 18, and 27 of the IEEE-30 bus system. Each shunt has a reactive power capacity of 13 MVAr. To validate the accuracy and effectiveness of the proposed method, the

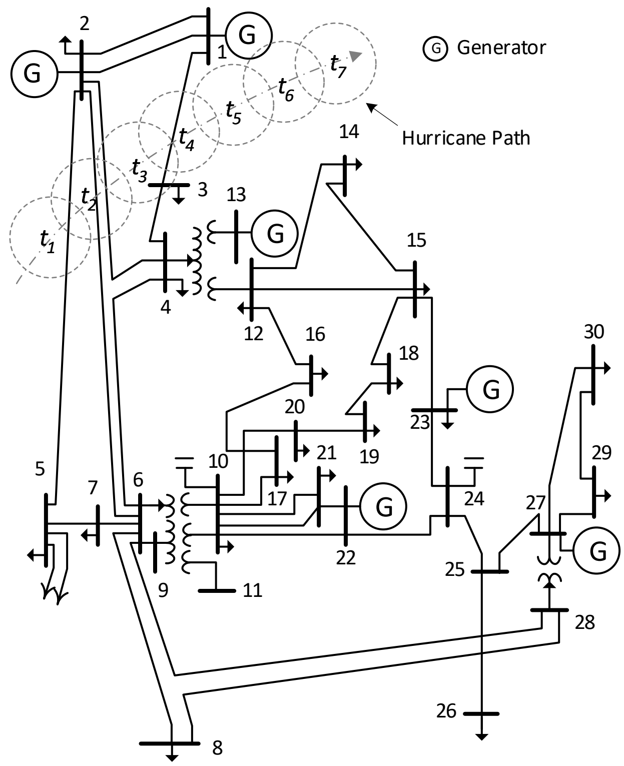

Figure 4.10: IEEE 30-bus system under hurricane impact

following procedures are implemented sequentially. First, several failure scenarios are created using windstorm modeling approach provided in section 2.3.1 for the defined windstorm in Fig. 4.10. To capture wide range of failure scenarios, wind speed is assumed to be within 15–51 m/s. For each failure scenario, power flow solution is obtained. Algorithm 4 is used for training the multi-agent framework. In this case, action represents size of shunt compensators.

4.5.3.1 Training

The proposed algorithm is implemented for a fixed number of episodes (failure scenarios). The number of iterations and corresponding rewards for each episode are plotted as shown in Fig. 4.11a and Fig. 4.11b, respectively. It is obvious that as the algorithm explores more scenarios, the action time decreases and the reward value increases. The learning rate of agents is enhanced based on previous experiences to

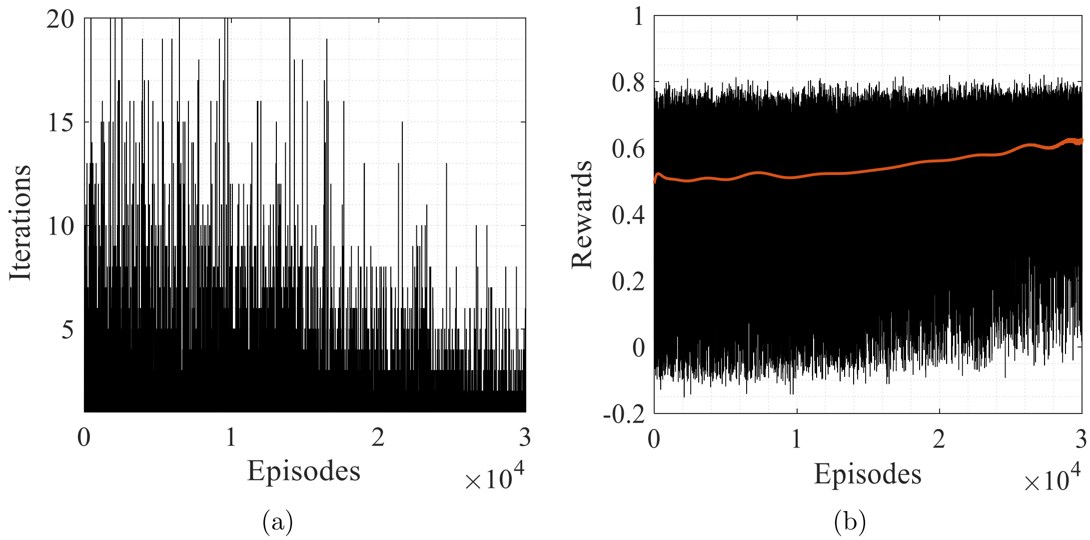

Figure 4.11: (a) Required number of iterations (b) Amount of rewards of training episodes for the IEEE-30 bus system

avoid bad actions. From Fig. 4.11a and Fig. 4.11b, we can see that the ability of agents to resolve the impacts of windstorms on voltage constraints advances very quickly after 15000 episodes and noticeable increase happens in the reward values. For further details, Fig. 4.12a shows the losses for the critics that fluctuate at the beginning of episodes' period, and finally converge to equilibrium solutions. For accuracy validation, the trained agents are tested using a set of failure scenarios included in testing data. Fig. 4.12b shows the number of iterations and reward values, respectively, for testing data. The trained agents are able to determine proper actions to control shunt compensators within one iteration with maximum reward value for testing scenarios. Thus, the proposed multi-agent framework is trained to provide actions to control shunts reactive power output.

4.5.3.2 Testing and Validation

Finally, the trained agent is used to check its effectiveness on improving power system resilience against several windstorms. The performance of the agent for 9 unique

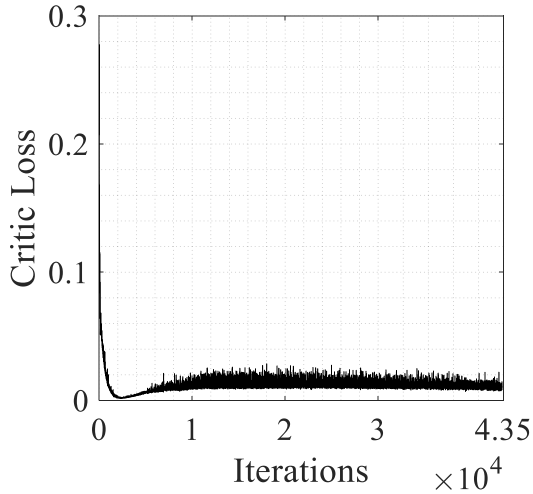

(a)

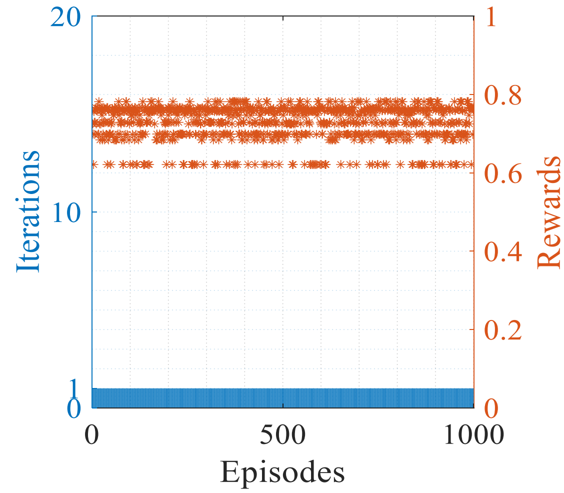

(b)

Figure 4.12: (a) Losses of critics during training and (b) Number of iterations and amount of rewards for testing episodes

line failure scenarios among these windstorms is given in Table 4.6. It can be seen that the trained agent can maintain voltage stability with and without the trained agent violates for 2 and 6 scenarios, respectively. Thus, the proposed algorithm can enhance the resilience of the power system through controlling shunt reactive power output. Also, from Table 4.6, we can see that the trained agent cannot maintain the voltage stability for scenarios 9 and 10. This happens due to the fact that the shunts alone cannot maintain voltage magnitudes within limits.

4.6 Conclusion

In this chapter, three corrective strategies have been studied: distribution network reconfiguration, allocation and sizing of DERs, and dispatching reactive power compensators. RL approaches have been leveraged to train the proposed control-based corrective enhancement models. Single-agent and multi-agent frameworks were developed based on the problem under study. In the DNR strategy, the results showed

Table 4.6: Resilience Enhancement using the Trained Agents

S/L No.	Tripped Lines	Voltage Violations (Bus No.)	
		Without Agent	With Agent
1	2–5	None	None
2	1–3, 2–6, 2–5	5, 6, 7, 8	None
3	2–6, 2–5, 2–4	5, 6, 7, 8, 28	None
4	2–5, 2–4	7	None
5	2–5, 1–3, 2–4	7, 8	None
6	2–6, 2–5, 1–3, 2–4	None	None
7	2–4, 3–4, 2–5, 1–3	None	None
8	1–3, 2–5, 3–4, 2–6	All	All
9	2–6, 3–4, 2–5, 2–4, 1–3	All	All

the effectiveness of the proposed ACA to determine the set of tie-switches that allow feasible network reconfiguration maintaining traverse and radiality constraints. The trained ACA was tested against single, double, and multiple line failure scenarios and showed accuracy of almost 97%. The proposed algorithm provides the system operators with a fast-acting algorithm to restore curtailed loads in distribution networks during and after an extreme event. The results of the allocation and sizing DERs strategy showed its capability to determine feasible sizes and locations of DGs for enhanced resilience of an islanded distribution feeder during extreme events. The proposed MASAC was trained against multiple line outages and showed accuracy of almost 95%. Moreover, a MASAC framework has been studied to dispatch reactive power compensators for enhanced voltage profile due to extreme events. The results showed that the proposed approach could maintain voltage magnitudes at system buses within the standard limits for most of the cases. Voltage magnitudes in some cases could not be maintained within the limits, which is not surprising. Since shunts alone cannot maintain voltage magnitudes within limits in some cases, the proposed approach can be extended (or integrated with existing algorithms) to include other resources such as generation dispatch, load shedding, and reconfiguration. Also, the scalability of the proposed methods to large-scale problems still require further investigation.

Chapter 5

Restorative Strategies

The main goal of restorative resilience enhancement strategies is to retain the power service to curtailed loads in a fast and efficient means. This chapter provides a preliminary analysis on improving the restoration behavior of distribution power systems via DER dispatching. Though restoration of curtailed loads can take place during or after an extreme event, this work aims to study restoration techniques regardless their execution time. In this chapter, a multi-agent DRL framework is developed such that each agent controls a specific DG. Deep Deterministic Policy Gradient (DDPG) approach is adopted to create and train the developed DRL model. The proposed algorithm is tested on a modified version of the IEEE 33-node distribution feeder with arbitrarily allocated DGs.

5.1 Introduction

Several studies have been conducted to develop fast and efficient resilience-based restorative strategy. Authors of [154] have developed a RL-based controller to make fast real-time decisions to dispatch DERs during a hurricane. The proposed framework has shown promising results to outperform classic optimization approaches in terms of operation costs and computation time. A multi-agent DRL approach has been developed in [153] to optimize the control operation of a microgrid after a disaster. In [166], a priority-weighted optimal load restoration technique has been developed to improve restoration resilience of distribution systems. A DRL-based model-free method has been leveraged to improve load restoration with high penetration of wind energy in [167]. Authors of [168] has provided a two-stage restoration strategy of islanded microgrids using DRL methods. Also, a Q-learning algorithm has been used to generate the sequential order of repairing damaged components and update the network topology for enhanced restoration [169]. Since RL-based methods can be easily integrated into online decision-making process, they can learn from experiences during online operations [155]. The diverse learning methods have pushed toward deeper investigation of DRL methods in controlling and dispatching DERs for enhanced resilience after an extreme event.

The main contribution of this chapter is:

1. Develop and validate the efficiency of a multi-agent DRL framework to dispatch DGs due to extreme failure scenario in distribution power systems.

5.2 Multi-Agent Deep Deterministic Policy Gradient Approach

Multi-Agent Deep Deterministic Policy Gradient (MADDPG) algorithm is an improved version of the DDPG algorithm for multi-task applications. In a multi-agent system, the agents are not only affected by the environment, but also by other agents where the critic is augmented with extra information about the policies of other agents. The return of a single agent in the multi-agent system is related to both its own actions and the actions of other agents. Markov games are often used to describe multi-agent systems. In MADDPG, a Markov game for N agents is defined by a set of states (S) describing the possible configurations of all agents, actions (a), and observations (o) for each agent. The control law for each agent with a Gaussian noise $\mathcal{N}$ can be expressed as follows.

$$a_i^t = \pi_i\big(o_i^t|\theta_i^\pi\big) \; + \; \mathcal{N}(0\,,\,\sigma_i^t)\;, \tag{5.1}$$

where $\theta_i^{(\pi)}$ is the weights of actor for agent i, and σ_i^t is a parameter for exploration. The discount accumulate reward of the ith Actor is as follows.

$$J_i = E_{\mu_i}\, R_i\;, \quad R_i = \Big[\,\sum_{t=1}^{T}(\gamma^{t-1}\; r_i^t)\,\Big], \tag{5.2}$$

where μ_i is the policy network of the ith Actor, γ is a discount factor, r_i^t is the reward obtained time step t in an episode, T is the time horizon. Updating actor using the sampled policy gradient of the (5.2) is given by

$$\nabla_{\theta_i^\mu} J_i \;\approx\; \frac{1}{S}\sum_{j=1}^{S}\nabla_{\theta_i^\mu}\;\mu_i\;(o_i^j)\nabla_{a_i}\;\; Q_i^\mu(x^j,\,a^j)\,|_{a_i^j=\mu_i(o_i^j)}, \tag{5.3}$$

where Q is the action-value function, x^j is state, and S is the sample number of a random mini-batch. o_i^j and a_i^j are the observation and action of the ith Actor, $\nabla i = 1,\, 2,\, \ldots,\, N$, respectively. A Critic's primary task is to predict the discount accumulate reward based on the current observations and actions of all Actors. The i critic can be updated minimizing the following loss function

$$L(\theta_i^Q) = \frac{1}{S}\;\sum_j (y^j - Q_i^\mu(x^j,\,a^j))^2, \tag{5.4}$$

$$\begin{aligned} y^j = r_i^j + \gamma\; Q_i^{\mu'}(x'^j, a'^j)|_{a'_k=\mu'_k(o'^j_k)}\;, \\ a'^j_i \in a'^j, o'^j_i \in x'^j, \end{aligned} \tag{5.5}$$

$$x^j = \big[o_1^j,\, o_2^j,\, \ldots,\, o_N^j\big]\;,\;\; a^j = \big[a_1^j,\, a_2^j,\, \ldots,\, a_N^j\big], \tag{5.6}$$

$$x'^j = \big[o'^j_1,\, o'^j_2,\, \ldots,\, o'^j_N\big]\;,\;\; a'^j = \big[a'^j_1,\, a'^j_2,\, \ldots,\, a'^j_N\big], \tag{5.7}$$

$$\theta'_i \;\leftarrow\; \tau\theta_i + \,(1-\tau)\theta'_i, \tag{5.8}$$

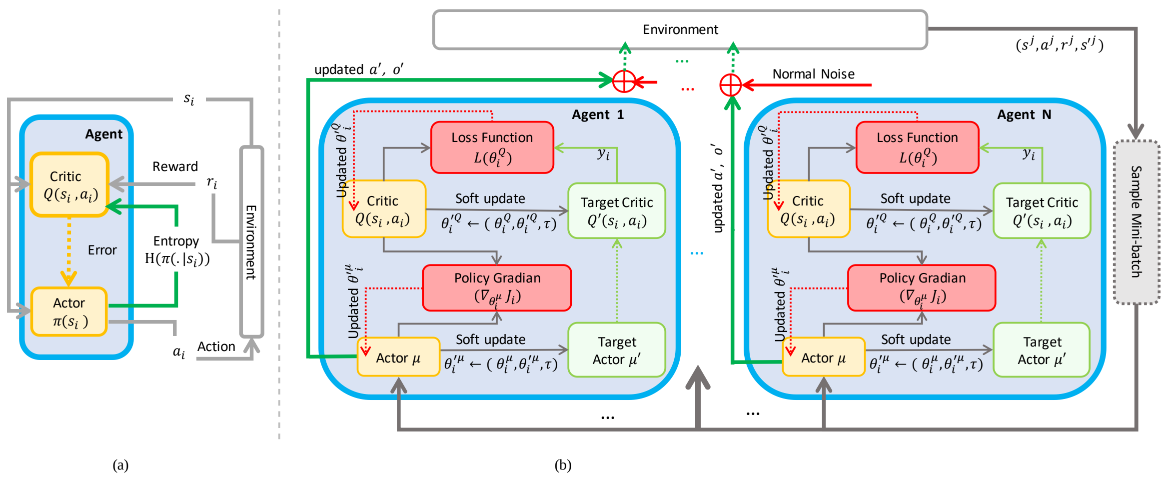

Figure 5.1: (a) A general actor critic framework (the green path shows the difference of soft actor critic framework with entropy term) and (b) The proposed MADDPG framework.

where $(.)'$ donates to the target for Q' and μ' and next for a' and o'. $\theta_i^{(.)}$ shows the weight of parameter. (5.8) can be used to softly update target network parameters (Q' and μ') for each agent i that τ is a control parameter for updating the target networks.

The SAC algorithm is an off-policy maximum entropy actor-critic algorithm. The main difference of SAC and AC is the introduction of the entropy of the actor outputs during the training phase that is showed in Fig. 5.1.b.

Fig. 5.1.a shows the complete MADDPG framework with soft update and random noise.

To train all agents, a replay buffer is used as follows:

$$\mathcal{D} \leftarrow \left(s_t, o_t^i, \alpha_t, r_t, s_{t+1}, o_{t+1}, \alpha_{t+1}, d\right). \tag{5.9}$$

5.3 The Proposed MADDPG Dispatch Algorithm

This section describes the proposed RL-based approach to dispatch DERs for resilience enhancement of distribution systems. First, it describes the MADDPG-dispatch environment and then it explains the algorithm training the testing procedure.

5.3.1 MADDPG Dispatch Environment

An MDP is used to formulate the problem where a system state represents specific system conditions. A transition to another state is due to taking certain actions yielding a reward that can be defined as a function of desired outcome. For a multi-agent framework, a system state is decomposed into observations equal to the number of agents. The components of the formulated MDP are defined below.

5.3.1.1 States

A system state is defined to be the set of parameters that can be used to describe the system conditions and it includes required information to observe the system characteristics under specific circumstances. The state set is defined as:

$$s_t = \{G_i^s, \Delta G_i^m, u_j, o_i^n\} \ \forall n \in \Omega^N, \ \forall i \in \Omega^G \ \forall j \in \Omega^B, \tag{5.10}$$

where G_i^s is the DG power, ΔG_i^m is the DG power mismatch, u_j is the line status, o_i is the set of connected nodes to the i^{th} agent, Ω^N the set of system nodes, Ω^G the set of DGs, and Ω^B the set of lines.

5.3.1.2 Actions

It is required to determine the power supply of each DG to minimize the amount of power balance mismatch. In other words, the amount of power supplied by DGs shall be equal to the load demand within a specific grid. In the proposed problem, a continuous action representing the DG real power needs to be taken by each agent, which is represented as follows,

$$\alpha_t^i = \{G_i^s\}, \tag{5.11}$$

where α_t^i represents the action taken by the i^{th} agent.

5.3.1.3 Rewards

A proper reward value, r_t^i, should be defined to assess the effectiveness of the taken actions. Each agent is responsible for controlling the power supply of a specific DG through reducing/eliminating the amount of load curtailment after an extreme event. This can be achieved by minimizing the amount of power balance mismatch—given enough generation resources are available. The reward value increases as the absolute power mismatch approaches zero value. Due to multiple line failures, a system can split into one or more microgrids, M. Therefore, the set of DGs in a specific microgrid should supply enough generation for minimal power mismatch. The reward r_t^i for taking a specific action is calculated as:

$$r_t^i = G_i^s - \big[\sum_{n\in\Omega_m^N} L_n\big]/N_G^m, \tag{5.12}$$

where L_n is the load demand of n^{th} node, N_G^m is the number of DGs in the m^{th} microgrid, and Ω_m^N is the set of all connected nodes in the m^{th} microgrid.

5.3.2 Training and Execution Algorithms

The training and testing/execution steps for the multi-agent framework are summarized in Algorithm 6 and Algorithm 7. Each agent is assigned to a a specific DG unit. A failure scenario is generated using multiple line outages. An action is determined by each agent representing the amount of power generation by the corresponding DG. Power mismatch is calculated as reward for each agent. The process is repeated for diverse failure scenarios till the MADDPG converges.

Algorithm 6: Training of the MADDPG-dispatch Framework

```
for Episode = 1 to E_train do
    Create failure scenario
    Reset the environment to default settings
    Extract observations of all agents (o_t) using current state (s_t)
    while Constraints not fulfilled and step < N do
        for i = 1 to N_agents do
            Generate an action (α_t^i) using (5.1)
        end for
        Append all actions
        Execute action (α_t) on the environment
        Obtain new state (s_{t+1}), new observations (o_{t+1}), reward (r_t), and terminal
        conditions (d).
        Store (s_t, o_t, α_t, r_t, s_{t+1}, o_{t+1}, d) in D_i using (5.9)
        if size(Memory) ≥ batch size then
            Randomly select minibatch
            Update weights of the policies using (5.3)
            Update the Q-function parameters of each agent using (5.4)
            Update temperature of networks using (5.8)
            Update target network weights of each agent using (5.8)
        else if d is true then
            Reset the environment
        end if
    end while
end for
```

5.4 Implementation and Results

The proposed approach is applied on the 33-node distribution feeder for validation. The proposed MADDPG model is formulated to dispatch DERs connected to distribution feeder for enhanced resilience after an extreme weather events.

Algorithm 7: Testing of the MADDPG-dispatch Framework

for episode = 1 to E_{test} **do**
  Create failure scenario
  Reset the environment to default settings
  for i = 1 to N_{agents} **do**
    Generate an action (α_t^i) using actor network
  end for
  Execute action (α_t) on the environment
  Observe s_{t+1}, r_t, and d.
end for

5.4.1 System under Study

The 33-node distribution test system is a radial distribution system with 33 nodes and 32 branches with a total system load of 3.72 MW [161]. Five DGs are connected to the feeder at arbitrarily chosen locations as shown in Fig. 5.2, where each DG is represented by a single agent. Although the locations of DGs play a vital role to improve the resilience of the system, this work focuses on leveraging RL-based approaches to control predefined DERs after an extreme event. The list of vulnerable lines include (2-19), (3-23), (6-26), (29-30), and (10-11), as shown in Fig. 5.2. To induce further operating conditions, the connection to the main feeder is disconnected with the result being the system acting as an islanded microgrid. The failure of any vulnerable line results in splitting the main feeder into smaller microgrids operating. The list of all possible microgrids is summarized in Table 5.1 with their corresponding load demand.

5.4.2 Training

The proposed MADDPG algorithm is implemented for a fixed number of episodes (failure scenarios). A total of 20,000 episodes are used for training with a maximum of 20 iterations per episode. In each failure scenario, single or multiple lines are

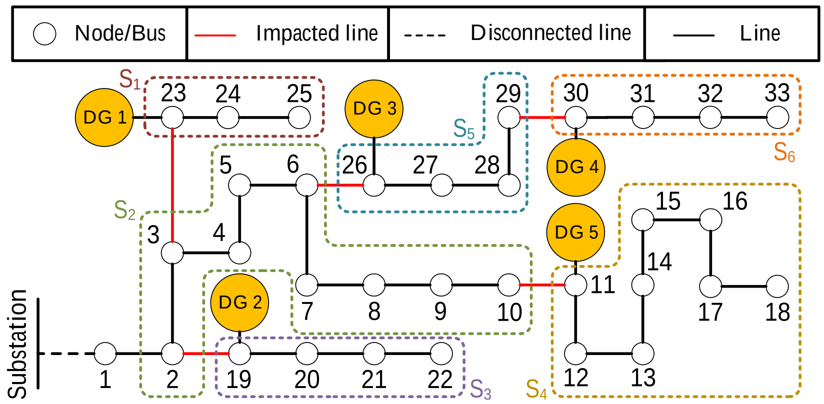

Figure 5.2: IEEE 33-bus distribution feeder

Table 5.1: List of Potential Microgrids

Index	Connecting nodes	Power (KW)
S_1	23, 24, 25	930
S_2	1, 2, 3, 4, 5, 6, 7, 8, 9, 10	855
S_3	19, 20, 21, 22	360
S_4	11, 12, 13, 14, 15, 16, 17, 18	555
S_5	26, 27, 28, 28, 29	400
S_6	30, 31, 32, 33	620

selected from the vulnerable lines to be disconnected. The hyper-parameter settings of the actor and critic networks of the proposed framework for the modeled 33-node system are shown in Table 5.2. The recursive MDP process provided in algorithm 6 is used to train the MADDPG model. For evaluation, the running mean of the episodic rewards and the number of iterations per episode are calculated using a window of 100 episodes.

Fig. 5.3 shows the running mean and number of iterations per episode for the MADDPG model. The average reward value increases as the number of training episodes increases, as anticipated. The average reward value reaches a saturation level in less than 8,000 episodes. At 5,000 episodes, a rapid increase in the reward value is noticed. This is due the decentralized structure of the MADDPG where

Table 5.2: Hyper-parameter Settings of the MADDPG Model

Hyper-parameter	Value
Number of hidden layers	3
No. of neurons in hidden layers	64
Learning rate	10^{-3}
Learning episodes	every 10
Temperature rate (τ)	0.01
Reward discount factor	0.99
Batch size	512
Activation function of output layer	Sigmoid
Activation function of hidden layers	ReLU
Optimizer	Adam

each agent is trained independently. Also, the random selection of mini-batch plays a vital role to provide a set of scenarios where exploratory feature is achieved. On the other hand, the average number of iterations decreases dramatically after 5,000 episodes reaching a value of five iterations per episodes. This shows the capability of the proposed algorithm to determine an optimal solution in five trials.

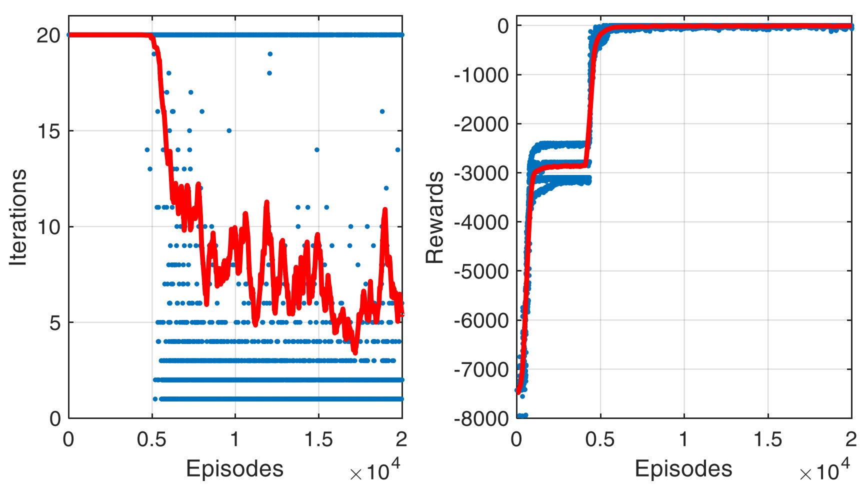

Figure 5.3: Rewards and iterations per episode

To visualize the internal learning behavior the MADDPG, the actor and critic losses of all agents are plotted, as shown in Fig. 5.4. It is worth noting that training episode differs from running episodes since training the model is executed every ten episode after having enough scenarios in the memory buffer. The actor losses of A_1, A_4, and A_5 converge faster than A_2 and A_3. Also, A_3 takes more time to learn due to the unique location of DER_3 in the middle of distribution feeder where it has more possible island connections. For instance, DER_3 is responsible to supply S_5 only in case lines (29-30) and (6-26) fail; however, DER_3 and DER_4 will supply S_5 and S_6 if only line (6-26) fails. All agents converge to almost zero losses after 14,000 training episodes. On the other hand, the critic losses show much faster converging rate. All agents provide pre-mature convergence after 5,000 training episodes. The sudden improved learning behavior of A_2 and A_3 at 9,000 training episode instant is reflected in the critic losses curve.

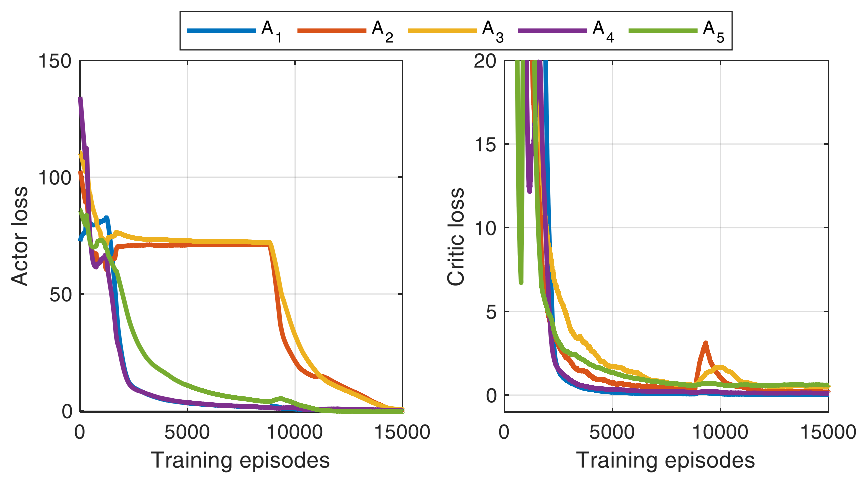

Figure 5.4: Actor and critic losses for each agent

5.4.3 Testing and Validation

To validate the efficiency of the trained models, a total of 1,000 failure scenarios are tested. Algorithm 7 is used to test the proposed dispatch algorithm. For each episode, the model is required to provide the required power supply by each available DER in the system. The trained model achieves 99.1% success rate of all the simulated cases. A successful decision is counted if the power supply mismatch of each DER does not exceed 15 KW. To validate the accuracy of the calculated DER powers for the successful cases, the average power mismatch is 8.5 KW. For non-successful cases, the average power mismatch is 22 KW. This implies that the non-successful cases have relatively close values to the predefined threshold. Further tuning of MADDPG hyper-parameters can results in enhanced accuracy.

The MADDPG is trained to determine the power supply of each DG to avoid load shedding. Table 5.3 provides the resulting outcome of the trained MADDPG model for ten failure scenarios. It is worth nothing that the proposed algorithm computes the power supply based on the number of connected DGs in each microgrid. In other words, the required load demand of each microgrid is divided equally on the connected DGs within the same grid. In F_1, two microgrids are formed such that the first one includes S_5 and S_6 with total demand of 915 KW and the second one includes the rest of the feeder with total demand of 2805 KW. The total supplied power by DG_3 and DG_4 for the first microgrid is 922 KW; whereas, other DGs have total supply of 2784 KW. This shows the capability of the trained algorithm to provide relatively close values from the first trial. The same behavior is observed in F_2, F_3, F_4, and F_5. In case of two line fail, the distribution feeder is split into three smaller microgrids. Each set of DGs have a total power supply equals to the load demand of their corresponding microgrid. For instance, F_8 shows that DG_1 and DG_5 supply S_1, S_2 and S_4; DG_2 supplies S_3; and DG_3 and DG_4 supply S_5 and S_6; respectively. With three line failures, the operating conditions become more severe and higher power supply might be required from each independent DG. For example, DG_1 and DG_3 have supply higher power compared to DG_2 in F_{10} since they are connected to S_1, S_2, and S_5 forming the majority of the distribution feeder load. In general, the proposed algorithm shows the capability to dispatch DGs against very severe situations under single and multiple line failures.

Table 5.3: DG Dispatch for Selected Failure Scenarios

	Index	Impacted lines	DER power (KW)				
			1	2	3	4	5
One	F_1	6-26	919	933	459	463	932
	F_2	2-19	832	358	831	848	840
	F_3	3-23	922	698	689	702	699
	F_4	29-30	764	774	771	625	772
	F_5	10-11	791	795	783	799	558
Two	F_6	2-19, 10-11	935	358	941	928	555
	F_7	3-23, 29-30	930	722	720	613	724
	F_8	2-19, 6-26	1218	364	460	453	1222
Three	F_9	3-23, 29-30, 10-11	931	809	807	615	554
	F_{10}	29-30, 2-19, 10-11	1092	358	1088	615	552

5.5 Conclusion

This chapter has studied a multi-agent reinforcement learning approach to enhance the operational resilience of islanded distribution systems after an extreme event. The proposed method computes the required power supply of DGs to maintain a minimal amount of load curtailments. The results showed that the trained MADDPG model could provide proper decisions to maintain reliable operation of an islanded power grid under additional multiple line failures. The trained model showed an accuracy exceeding 99%. The proposed method provides a corrective and restorative strategy to enhance resilience of distribution systems leveraging the capabilities of reinforcement learning techniques. An extension of this work will include the integration of network reconfiguration strategies and role of energy storage systems for further improvements.

Chapter 6

Resilience Assessment Approaches considering Uncertainties

Uncertainty quantification for resilience-based studies has become a key factor for proper system modeling and solution efficiency. Uncertainties in extreme weather events can be classified into spatiotemporal uncertainties and fragility uncertainties, which capture the impacts of extreme events on failure of system components. Also, the deployment of RESs and their stochastic behavior during extreme weather events alleviates several concerns regarding induced variability on power system performance. This chapter focuses on uncertainties of extreme weather events and RESs in resilience assessment studies. First, an evaluation framework is developed to assess the resilience of transmission systems against ice storms. Also, the uncertainties of hurricanes on transmission system components are assessed for improved resilience performance. Finally, the role of unavailability of RESs during extreme events is evaluated taking into account system operational constraints. The proposed frameworks are studied on IEEE 30-bus transmission system.

6.1 Introduction

Resilience assessment methods focus on quantifying the severe impacts of extreme events on the performance of power systems [2, 170, 171, 172]. Uncertainties in operational resilience-based studies include weather and load forecast errors, and system components monitoring errors [173]. Risk-based security assessment frameworks have been studied for malicious attacks [174], market prices [175], and RESs [176]. Resilience assessment approaches vary based on the type of extreme weather events due to the difference in the spatiotemporal characteristics of these events.

Resilience Assessment considering Uncertainties of Ice Storms. The impact of freezing ice storms on operational performance of power grids has gained significant interest. In [177], a model based on geographically moving winds and freezing precipitation has been developed to assess the reliability of transmission networks during ice storms. A numerical model to forecast icing precipitation accretion on overhead line conductors considering wind speed, ambient temperature, and ice precipitation rate has been developed in [178]. The probability of failure of transmission lines and towers has been calculated using the copula functions integrated with the extreme value theory in [179]. In [180], a radial ice thickness model has been used to estimate the ice thickness using a modified Ramer precipitation-type algorithm and weather research and forecasting model. A probabilistic assessment model for weather induced loads on overhead transmission lines has been developed in [181]. In [182], a socioeconomic and ecological impact assessment approach has been conducted for the great Chinese 2008 ice storm. In [183], a reliability evaluation method to study the communication network of power systems during ice storms has been formulated. Although these methods highlight the importance of considering the impacts of ice storms on system operation, quantifying uncertainties of ice storms is an important factor for long-term planning purposes.

Resilience Assessment considering Uncertainties of Hurricanes. A statistical evaluation framework has been developed in [184] to assess flooding impact on power system restoration after a hurricane event. In [89], a probabilistic resilience assessment method has been used to evaluate the long-term impact of typhoons from the system and the component perspectives. A data-driven approach has been studied in [59] assessing the uncertainties in loads, renewable generation, and market prices during extreme events. In [185], a probabilistic hurricane resiliency assessment framework has been provided of an active distribution system. Also, a non-simulation based method has been developed to assess resilience uncertainties of distribution systems [186]. Most of these methods have considered either the spatiotemporal uncertainties or the fragility uncertainties independently without comprehensively considering both uncertainties due to the complicated modeling. Although other methods have considered spatiotemporal assessment, the role of these uncertainties on resilience enhancement strategy adopting fragility uncertainties has not been deeply investigated.

Resilience Assessment considering Uncertainties RESs. The high penetration level of RESs has introduced significant uncertainties in the operation and control of power systems especially during extreme weather events. Assessing the impacts RESs on power system response to extreme events has become a key factor for modern power operation especially for resilience-based studies. Authors of [65] have proposed a stochastic programming approach to determine the optimal utilization of RESs when the main feeder in a distribution system is impacted by a wildfire. In [143], a two stage optimization function has been solved to minimize the costs for both dispatchable and non-dispatchable renewable generating units, and load curtailment of microgrids. The role of RESs to provide voltage support for resilience-based autonomous microgrid formation after disturbances has been studied in [9, 135]. The time-varying demand and renewable energy levels have been integrated into a probabilistic extreme event model to quantify the resilience level for planning purpose in [187]. Although several studies have focused on the role of RESs to improve resilience in distribution systems, only a few studies have focused on transmission systems [2]. Also, the 2021 Texas ice storm has raised concerns about the capability and availability of RESs during extreme events [35]; and hence, the impacts of RESs on resilience of transmission systems require further investigation.

The main contributions of this chapter are summarized as follows:

1. Develop an uncertainty quantification approach to quantify the stochasticity of ice storms on transmission system resilience.

2. Conduct statistical analysis of uncertainties of hurricane behaviors (long-term) and impacts (short-term) on system components for enhanced resilience.

3. Assess the role of unavailability of RESs during hurricane events for resilience enhancement.

6.2 Resilience of Power Systems to Ice storms

This section proposes a resilience assessment method to quantify impacts of ice storms on the overall performance of transmission power systems. First, an ice storm spatiotemporal model is developed to determine the propagation behavior and severity of ice storms. A fragility model is implemented to calculate the probability of failure of each component in the path of an ice storm at sequential time instants. Then, an extensive statistical analysis is conducted to determine the weather-related characteristics of the geographical location under study such as wind speed, wind direction, and ice precipitation rate. A combinatorial enumeration method is used to simulate various ice storm scenarios with diverse spatiotemporal characteristics. During each simulated ice storm, the worst failure scenario is obtained and used to calculate the total amount of load curtailment at each time instant. The resilience level of the system is evaluated based on the total amount of load curtailment and the probability of occurrence of ice storms. The proposed method is validated through a mapped IEEE 30-bus system on the Northeastern region of USA.

6.2.1 Resilience Quantification Framework

This section illustrates the resilience quantification framework of transmission systems during ice storms. First, it describes a resilience index based on system degradation performance. Then, it explains a statistical approach to assess the resilience due to uncertainties of ice storms.

6.2.1.1 Resilience Index

A quantitative index, R, is used to quantify the resilience level of the system, specifically in the planning phase. Previous studies have used the resilience triangle and the resilience trapezoidal curves for evaluation [2], where the resilience level of system, denoted by Q, is defined to be the normalized area of the performance degradation index during the period of an event [89]. As the performance of system degrades, the resilience of the system also degrades resulting in a high resilience index. Such method captures the resilience of the system for one event scenario; however, the transmission system may be impacted by various events that have diverse behavior and severity. A modified resilience index can be evaluated as follows,

$$R = \sum_{s \in S} P_s Q_s, \tag{6.1}$$

where S is the set of all possible ice storms, P_s is the probability of the s^{th} ice storm, and Q_s is the worst amount of degradation in system performance. In this work, the value of Q_s is represented by the total amount of load curtailment during an ice storm.

6.2.1.2 Combinatorial Enumeration Method

The combinatorial enumeration method has been widely used to quantify uncertainties of various random variables on a certain process given predefined PDF for each random variable [89]. The combinatorial enumeration method is implemented in the probabilistic ice storm model to simulate various potential ice storms. For a given scenario, the failure probability of transmission corridors can be calculated using the spatiotemporal fragility model presented in section 2.3.2 and section 2.4.

Each ice storm parameter is governed by a well-known PDF. In the combinatorial enumeration method, each PDF is divided into several equal portions. An ice storm scenario can be generated by enumerating a selection of specific segmented interval. For example, the original PDF of wind speed is divided into C equal portions and a segmented interval C_i. For a specific ice storm scenario s, the wind speed probability can be obtained as follows,

$$P_r(V_{w,s}) = \int_{V_{w,s}-C_i/2}^{V_{w,s}+C_i/2} f(V_w)dV_w, \tag{6.2}$$

where $P_r()$ is the probability of each parameter and C is the length of each portion.

By following the same convention, the probability of each parameter can be calculated. Thus, for a specific ice storm scenario s, its occurrence probability can be evaluated as follows,

$$P_s = P_r(H_{0,s})P_r(P_s)P_r(V_{T,s})P_r(V_{w,s})P_r(\delta_s)P_r(x_{0,s}, y_{0,s}), \tag{6.3}$$

Under a simulated ice storm, the cumulative failure probability of each corridor can be evaluated using the spatiotemporal fragility model. The sequential failure of system components is injected into a DC optimal power flow to determine the amount of load curtailment. The detailed algorithm to evaluate the resilience of transmission system against ice storms is provided in Algorithm 8.

Algorithm 8: Resilience Assessment Methodology Considering Ice Storm Uncertainties

Input: Weather-related data for key parameters including, wind speed, wind direction, precipitation rate, central pressure difference, translational speed, and landing location

Compute the PDF for each key parameter
Divide the the PDFs into fixed number of segments
Define the total number of ice storm scenarios S
for $s \leftarrow 1$ **to** S **do**
    Generate random value for each key parameter
    Calculate probability of each parameter using their PDF
    Evaluate the probability of occurrence of the ice storm scenario P_s
    Inject the random values into the ice storm model to simulate its propagation behavior
    for $t \leftarrow 1$ **to** T **do**
        Determine set of potential components to fail
        Use fragility model to evaluate the probability of failure for each component
        Determine the failed components
        Run DC optimal power flow
        Calculate amount of load curtailment
    Sum up total energy not supplied for the whole ice storm duration Q_s
Evaluate the system resilience index using the obtained P_s and Q_s for each s

Output: System resilience index

6.2.2 Implementation and Results

The resilience assessment framework is formulated using the proposed ice storm model and fragility model. The proposed approach is applied on the IEEE 30-bus system mapped on the Northeastern region of USA as shown in Fig. 6.1. The distance between two consecutive transmission towers is assumed to be 500 meters. The Northeastern side of USA is selected since it is one of the most impacted regions by ice storms [188].

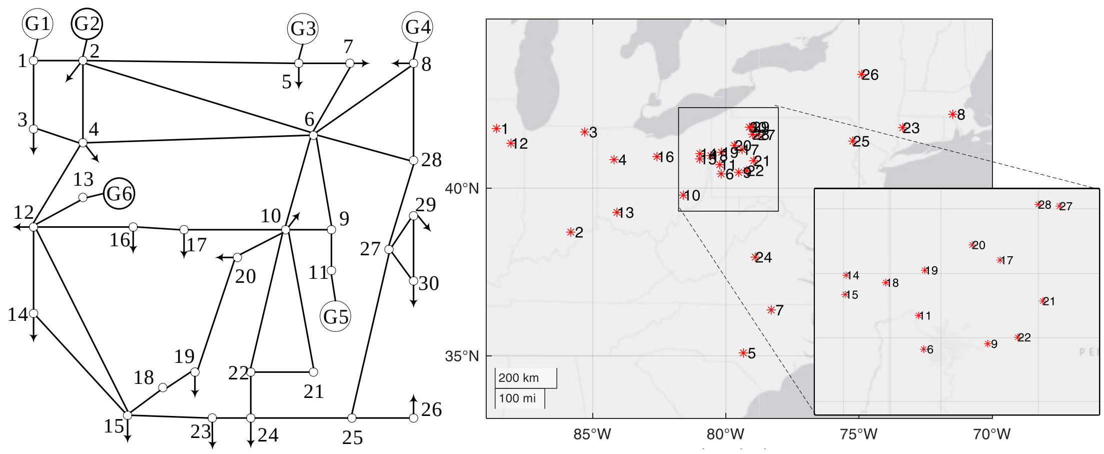

Figure 6.1: The mapped IEEE 30-bus system on Northeastern region of the USA

6.2.2.1 Ice Storm Parameters

Since weather parameters vary based on geographical location, statistical analysis is conducted on the Northeastern region of USA to determine the proper PDF for each parameter. Ice storm events in the Northeastern region can be found in [189]. Wind speed and direction data are extracted from [190] and ice precipitation rate data is extracted from [191]. Other parameters are assumed to have predefined PDFs. Landing location is assumed to follow a uniform distribution function, latitude, $y \in [34°, 45°]N$ and longitude, $x \in [90°, 70°]W$, central pressure difference is assumed to have a uniform distribution function, $H_0 \in [1.5, 3]$ hPa, and translational speed is assumed to follow a uniform distribution function, $V_T \in [0, 15]$ m/s. Although these parameters may have different distribution functions, the main scope of this work is the resilience evaluation rather than the statistical behavior of such parameters. Also, the scarcity and accessibility of data play a vital role to determine PDFs. A summary of PDF for wind speed, wind direction, and ice precipitation rate is summarized in Table 6.1.

Table 6.1: Parameters of Distributions for Ice Storm Parameters

Key parameter	PDF Type	Parameters
Ice precipitation	Lognormal	μ= 3.66 inc/hour, σ = 20.78
Wind speed	Lognormal	μ= 2.668 m/sec, σ = 0.5185
Wind direction	Binormal	μ_1= -73.3, μ_2= -7.2 σ = 22.6, σ = 70.35, α = 0.5

6.2.2.2 Single Ice Storm Scenario

A single ice storm scenario is simulated on the mapped system as shown in Fig. 6.2 to visualize the propagation of an ice storm through system corridors. The simulated ice storm propagates from South East to North West of the system where multiple transmission corridors are expected to fail. The central pressure difference is 1.5 hPa, the wind speed is 15 m/s, the translational speed is 1 m/s, the precipitation rate is 35 mm/hour, the landing site is 37°N/72°W, and the ice storm duration is 48 hours.

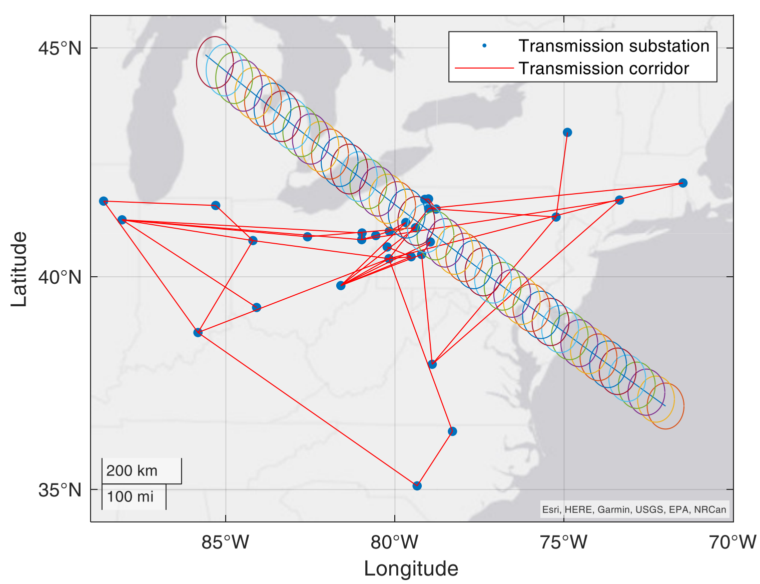

Figure 6.2: Ice storm scenario mapped on the IEEE 30-bus system

The list of impacted corridors and their time of failure is provided in Table 6.2. The total amount of energy not supplied during the whole ice storm is 1136 MWh with maximum load curtailment of 48.4 MW. Although some components may fail earlier in time, load curtailment does not take place till the third failure. Also, ice accumulation is larger at the center of the ice storm, and hence, components closer to the center are more vulnerable.

Table 6.2: Impact of Single Ice Storm Scenario

Time (Hour)	17	18	23	24		25	26		27		28	
Curt. (MW)	0	0	0	16.5		19.7	37.2		46.2		48.4	
From bus	23	24	6	4	6	15	10	21	16	12	19	10
To bus	24	25	8	6	28	23	21	22	17	13	20	20

6.2.2.3 System Resilience Level

The obtained and predefined PDF of each key parameter are integrated into the probabilistic ice storm model to calculate the probability of occurrence of each simulated scenario using the combinatorial enumeration method. The PDF of each key parameter is divided into 100 equal segments and a total number of simulation cases are set to 10,000. Each ice storm scenario is assumed to last for 24 hours period. For validation, the process is repeated twice with different ice storm scenarios.

Out of all the simulated scenarios, 2,021 scenarios result in load curtailment in the first case compared to 2,015 in the second case. The calculated resilience index for the two cases are 81.454 MWh/event and 81.44 MWh/event. The obtained values are relatively close assuring the effectiveness of the proposed approach to capture uncertainties of ice storms. For further assessment, the frequency of failure and total outage duration of each transmission corridor is obtained as shown in Table 6.3.

The results of both cases are relatively close which confirms the effectiveness of the proposed algorithm to quantify the stochastic behavior of ice storms on system resilience. Although the frequency of impact and duration of outage vary from one corridor to another, the outage duration per outage occurrence is almost the same

Table 6.3: Outage Analysis of Transmission Corridors

Corridor		Case 1			Case 2		
From	To	Freq.	Duration	Hour/occ	Freq.	Duration	Hour/occ
1	2	347	6642	19.141	349	6661	19.086
1	3	298	5742	19.268	300	5775	19.250
2	4	485	9857	20.324	488	9883	20.252
3	4	285	5757	20.200	286	5761	20.143
2	5	976	20185	20.681	979	20171	20.604
2	6	897	18862	21.028	899	18868	20.988
4	6	673	14169	21.053	679	14138	20.822
5	7	299	6116	20.455	296	6104	20.622
6	7	762	15867	20.823	764	15811	20.695
6	8	1366	28484	20.852	1366	28523	20.881
6	9	218	4558	20.908	218	4548	20.862
6	10	355	7410	20.873	355	7438	20.952
9	11	234	4775	20.406	234	4771	20.389
9	10	460	9680	21.043	461	9660	20.954
4	12	431	8533	19.798	425	8491	19.979
12	13	445	9178	20.625	444	9156	20.622
12	14	839	17195	20.495	840	17208	20.486
12	15	861	17578	20.416	859	17561	20.444
12	16	639	12967	20.293	640	12963	20.255
14	15	137	2765	20.182	137	2786	20.336
16	17	581	12192	20.985	581	12202	21.002
15	18	186	3748	20.151	186	3764	20.237
18	19	179	3624	20.246	182	3659	20.104
19	20	207	4261	20.585	208	4266	20.510
10	20	496	10234	20.633	497	10248	20.620
10	17	528	10864	20.576	526	10855	20.637
10	21	566	11765	20.786	564	11807	20.934
10	22	507	10566	20.840	509	10612	20.849
21	22	191	3894	20.387	190	3868	20.358
15	23	1226	25622	20.899	1230	25694	20.889
22	24	527	10970	20.816	531	10940	20.603
23	24	1091	22715	20.820	1090	22708	20.833
24	25	883	18377	20.812	880	18375	20.881
25	26	337	6620	19.644	328	6624	20.195
25	27	684	14299	20.905	682	14242	20.883
28	27	155	3120	20.129	155	3104	20.026
27	29	165	3395	20.576	165	3359	20.358
27	30	183	3684	20.131	180	3691	20.506
29	30	130	2640	20.308	130	2656	20.431
8	28	1145	23729	20.724	1140	23651	20.746
6	28	382	7902	20.686	384	7888	20.542

for many components. Some corridors are impacted more than 10% of ice storm scenarios such as 6-8, 23-24, 15-23, and 8-28, yielding longer outage duration. Such corridors should have a higher priority in resilience planning enhancements.

6.3 Quantifying Spatiotemporal and Fragility Uncertainties of Hurricanes

This section proposes a framework for resilience assessment to quantify uncertainties of hurricanes on the resilience of transmission systems. The previously described proactive generation redispatch strategy has been adopted for enhanced operational resilience against hurricanes. Fragility curve models are applied to determine probabilities of system component failures based on the wind speed value along the path of a hurricane. The optimal generation dispatch is obtained for a predefined hurricane scenario taking into consideration current and future potential failures. Then, various hurricane scenarios are generated based on varying weather parameters including central pressure difference, wind speed, wind direction, and landing site. Each parameter is represented by a PDF that can be calculated using historical weather data. A robustness factor is introduced and used to determine the list of failed components for each hurricane. Finally, a shortened set of hurricanes is extracted based on the number of failed components. For each selected hurricane, the proactive generation redispatch strategy is applied and the amount, location, and instant of load curtailment are recorded. The overall system performance is evaluated and the resilience level is quantified. The proposed approach is demonstrated on the IEEE 30-bus system. Fig. 6.3 shows an illustrative framework of the proposed methodology.

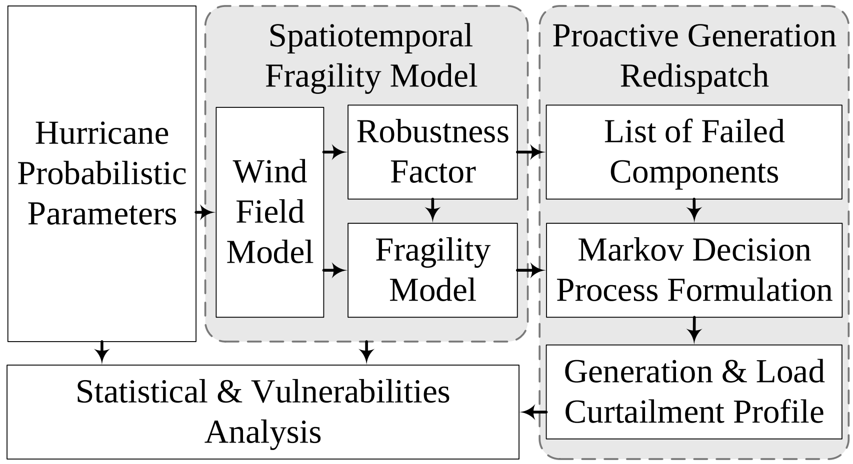

Figure 6.3: Uncertainty quantification research framework of hurricanes

6.3.1 Implementation Procedure

This section describes the combinatorial enumeration method to simulate various hurricanes. It also introduces the robustness factor approach to discretize the output of the fragility model. Then, it shows the overall integration algorithm.

6.3.1.1 Quantifying Uncertainties

Combinatorial enumeration methods can be used to enumerate values based on predefined PDFs. They have been utilized to quantify uncertainties associated with random variables on a given process [89]. In order to simulate many potential hurricane, the probabilistic wind field model applies the combinatorial enumeration method. A PDF defining each geographical- and weather-related parameter is divided into several equal portion. To generate a hurricane scenario, combinatorial enumeration method is applied to enumerate through selection of specific segmented interval. Once a hurricane is simulated, failure probabilities of transmission corridors are computed using the fragility model discussed in section 2.3.1.

6.3.1.2 Robustness Factor

The output of a fragility model is a probability of failure which is a continuous value between 0 and 1. These values are important to calculate the transition probability from one state to another in the MDP. However, many components will have infinitesimal failure probabilities that can be neglected. In this work, a robustness factor, α, is introduced to act as a threshold such that any component with failure probability exceeding this threshold will be considered in shutdown/failure status. In other words, the robustness factor is used as a filtration phase to select components with higher probability of failures and will have a value between 0 and 1. On the other hand, the robustness factor can be used as an assessment threshold to quantify the resilience level of a system. For instance, a system with robustness value of 0.1 implies very weak resilient system; whereas, a robustness factor of 0.9 reveals high resilience level.

6.3.1.3 Integrated Algorithm

Algorithm 9 provides the quantification process of hurricane uncertainties on the proactive generation redispatch strategy.

6.3.2 Case Studies and Results

This section provides accuracy validation of the proposed framework to quantify spatiotemporal and fragility uncertainties of hurricanes on transmission system. First, the stochastic impact of hurricanes on system components is assessed. Then, the impact of hurricane uncertainties on the proactive generation redispatch is evaluated.

Algorithm 9: Overview of Resilience Enhancement Strategy Considering Hurricane Uncertainties

Input: Total number of hurricane scenarios (H) and PDF for key parameters including central pressure difference, hurricane translational speed, hurricane direction, and landing-site coordinates

Determine the total number of hurricane scenarios H

for $h \leftarrow 1$ **to** H **do**

- Generate random numbers for key parameters using their PDFs
- Use the generated values to create a hurricane scenario h
- Simulate the generated hurricane using the wind field model
- **for** $t \leftarrow 1$ **to** T **do**
  - Calculate failure probabilities of transmission corridors using the fragility model
  - Determine the failed components based on robustness factor
  - Update the list of Markov states
  - Calculate the transition probabilities
- Solve MDP proactive generation redispatch
- Compute the amount of load curtailment and operational costs
- Calculate the average amount of load curtailments for all Markov states

Evaluate the overall system resilience level

Output: System resilience assessment level

6.3.2.1 Data Description

The proposed approach is applied on the IEEE 30-bus system [119]. Generator and other system data can be found in [192]. The behavior of load demand is integrated into system operating conditions by scaling nominal load using the load profile obtained from [118].

Weather parameters are different for each geographical location. In this work, the Northeastern region of USA is considered. Statistical analysis is conducted on data obtained from [188, 189, 190] to determine proper PDFs for the central pressure, wind speed, and hurricane directions (Table 6.4). The landing location of a hurricane is assumed to follow a uniform PDF, latitude, $y \in [34°, 45°]N$ and longitude, $x \in [90°, 70°]W$. Although PDFs representing these parameters may change based on diverse factors, this work focuses on evaluating the stochastic impacts of hurricanes on the proposed proactive generation redispatch algorithm and the overall system resilience. In other words, the proposed algorithm can be utilized given any defined PDFs.

Table 6.4: Parameters of Distributions for Windstorm Parameters

Key parameter	PDF Type	Parameters
Central pressure	Lognormal	μ= 2.901 hPa, σ = 0.6274
Translational speed	Lognormal	μ= 2.668 m/s, σ = 0.5185
Hurricane direction	Binormal	μ_1= -73.3, μ_2= -7.2 σ = 22.6, σ = 70.35, α = 0.5

Although hurricanes can take place at any time during the day, in this study, it is assumed to happen during peak load demand period to impose very tight operational conditions of the power system. The total duration of a hurricane varies based on weather parameters governing its spatiotemporal behavior and boundaries of geographical area under study. The hurricane is assumed to cross the system under study in 25 minutes sampled in a set of 5 minutes [33, 193]. Components may fail at any instant due to their fragility to spatiotemporal properties of hurricanes.

6.3.2.2 Assessing Stochastic Behavior of Hurricanes

In this case, the stochastic behavior of hurricanes on the power grid is quantified on a mapped version of the IEEE 30-bus system on the Northeastern region of the USA. A total of 10,000 hurricanes are simulated by randomly selecting a defined set of key parameters, which are given in Table 6.4. PDFs of key parameters are divided into 10 equal segments. The robustness factor approach is used to determine the failed components from the list of potential impacts during a hurricane. The process is repeated for varying robustness factors.

The stochastic behavior of hurricanes and accompanied potential failures on system components are analyzed. A failure scenario is defined to be a scenario where at least one component fails. Since transmission systems are designed to operate reliably on $N-1$ or even $N-2$ contingency, the number of failure scenarios with less than three failed components are filtered out. For the system under study, having more than 10 failed components will probably result in blackout of the whole system; and hence, such failure scenarios are excluded. In brief, the failure scenarios are classified into three main categories based on the number of failed components as follows: (1) at least one component fails; (2) at least 3 components fail; and (3) between 3 and 10 components fail.

Fig. 6.4 (a) shows the frequency of failure scenarios based on varying robustness factor. As the robustness factor increases, the number of failure scenarios decreases. Although the $N-2$ contingency provides the system with better preparedness characteristics, this might not be sufficient during extreme weather events. The number of failure scenarios can be easily determined given a defined robustness level. It is obvious that even with robustness level of 0.5, there is almost 150 failure scenarios with three to nine failed components, which implies the severity of hurricane events on power grids.

Fig. 6.4 (b) shows the conditional probability of occurrence of failure scenarios. The conditional probability of category 2 and category 3 is computed given a failure scenario takes place. On average, 75% of failure scenarios will encounter at least three failed components, of which almost 40% will encounter less than 10 failed components. The probability of having failure scenarios with more than three failed components decreases with increasing robustness level; however, the probability of a failure scenario having three to nine failed components increases with the robustness level. In other words, even with a very robust system, significant number of system components will be impacted during a hurricane event.

Table 6.5 shows the outage frequency of the most impacted transmission lines in

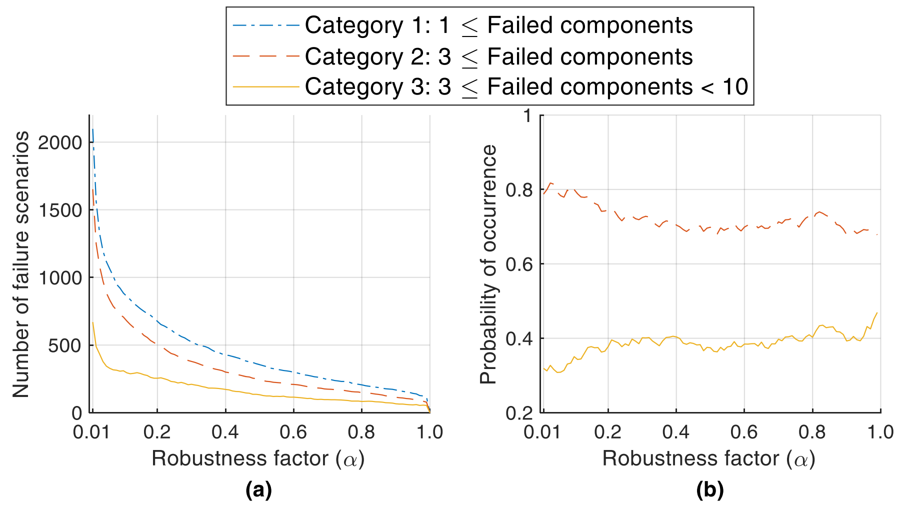

Figure 6.4: Relationship between robustness factor and (a) number of failure scenarios; and (b) probability of occurrence

the IEEE 30-bus system at different robustness levels. It is obvious that at higher robustness levels, less number of outages is noticed. Higher robustness levels imply higher strength of system components to withstand failure against severe weather events. This helps system planners to identify components of potential upgrades and improvements.

Table 6.5: Outage Frequency of Transmission lines at different Robustness Factor

Corridor		Robustness Factor							
From	To	0.01	0.05	0.1	0.2	0.4	0.6	0.8	0.95
2	5	5529	2845	2167	1508	964	646	443	262
2	6	4517	2368	1797	1211	732	471	336	223
6	8	4091	2159	1623	1175	697	468	333	236
12	14	4436	2361	1803	1193	709	513	347	213
12	15	4441	2384	1792	1205	724	513	347	214
15	23	3988	2116	1618	1111	668	444	303	222
23	24	3844	2029	1527	1031	605	456	321	232
24	25	3459	1828	1355	884	490	371	285	204
8	28	3353	1758	1325	921	563	392	274	210

To show the sequential failure impact of a hurricane event of system components, the average number of failed components at each time instant is computed for all simulated hurricanes resulting in component failures. Fig. 6.5 shows the average number of failed components at each time instant for a varying robustness factor. The failure rate of system components decreases as the event propagates in time. This might change from one geographical location to another or from one hurricane event to another; however, the spatiotemporal characteristics of hurricane events impose a unique timely-bounded sequential failure behavior that require rapid and dynamic resilience enhancement strategy.

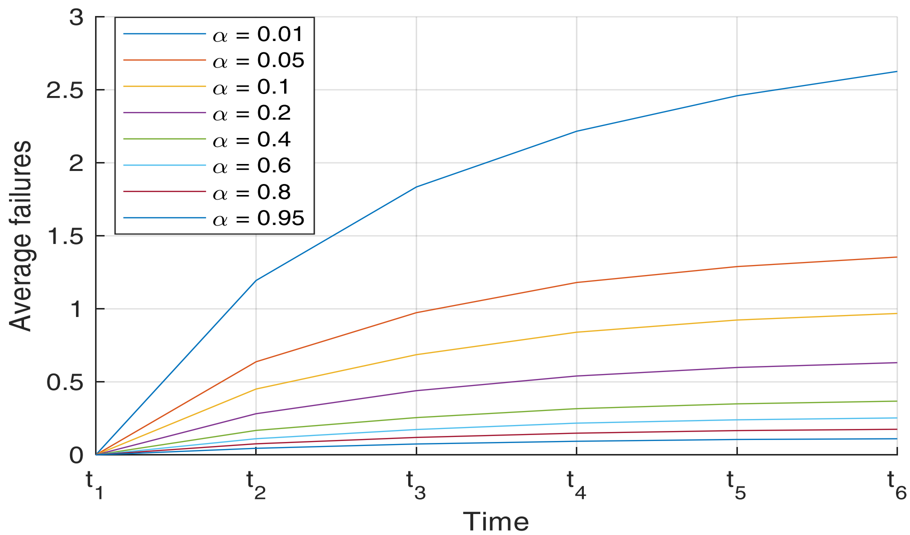

Figure 6.5: Average failures per time instant at different robustness factor

6.3.2.3 Impacts of Hurricanes' Stochasticity on Proactive Redispatch

The performance of the proposed proactive generation redispatch strategy will change based on the hurricane event. In this case, the overall performance of the proposed proactive generation algorithm is assessed based on different hurricanes. A robustness factor of 0.5 is selected yielding 126 hurricanes with 3-9 failed components. The attack time is the same for all hurricanes to ensure that the system is subjected to the same operating conditions and constraints.

The MDP is formulated for the 126 hurricanes resulting in 29 solved scenarios and 97 non-solved scenarios. Table 6.6 shows the relationship between the number of solved scenarios and the number of failed components. The reasons behind having a large number of non-solved scenarios are the very-tight operational constraints and large number of failed components causing dimensionality problem. It is clear that the MDP is capable of providing solutions for scenarios with less than 5 failed components. As the number of failed components increases, the search space increases dramatically yielding a dimensionality problem. Some cases with less than 5 failed components were not solved because of the very tight operational constraints used in the problem formulation. Since the hurricane is assumed to take place at the peak load, this creates more stressed operating conditions.

Table 6.6: Scenario Solution Status Vs Number of Failed Components

No. Failed Comp.	3	4	5	6	7	8	9
Solved	10	8	3	2	5	1	0
Non-solved	12	18	16	15	22	7	7

Fig. 6.6 shows relationship between the cumulative amounts of load curtailments for each scenario. Except for five scenarios, the total amount of load curtailment is less than 20 MW. Most of the scenarios encounter load curtailments during t_3 and t_4, based on the length of the yellow and purple colors in Fig. 6.6, implying higher withstand resilience index. Scenarios 26 and 27 have very high load curtailment at t_6 due to either islanding some parts of the power grid or occurrence of large number of failed components at same time. For instance, six components are subjected to failure at t_5 in scenario 26. Additionally, a reduction in the amount of load curtailment between two consecutive instants implies the capability of the proposed MDP to rapidly recover curtailed load. For instance, scenario 16 has large load curtailments at t_4 relative to t_5 and t_6. Same behavior is noticed in scenarios 2, 6, 13, 14, 20, 24, and 25.

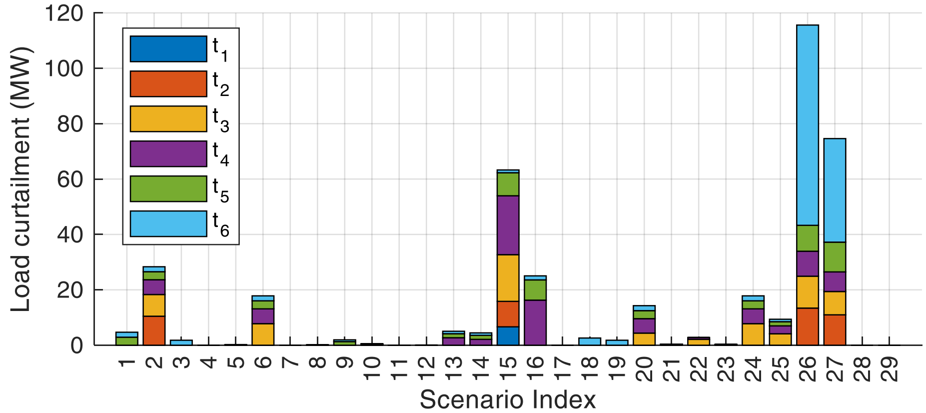

Figure 6.6: Load curtailment for solved scenarios

To summarize, Table 6.7 shows the load curtailment behavior of the solved cases at each time instant. On average, the amount of load curtailment is relatively small compared to the total system nominal load of 189.2 MW. Since the hurricane events take place during peak load during which the load demand is approximately 1.5 times the nominal load, it can be implied that the average load curtailment is significantly small. It is difficult to determine the trend behavior of the load curtailment due to the uncertain impact of each hurricane scenario on the system performance. The load curtailment shows reduction from t_4 to t_5 implying the efficiency of the proactive generation redispatch to compensate for the lost lines and retain some curtailed loads.

Table 6.7: Load Curtailment Analysis

	t_1	t_2	t_3	t_4	t_5	t_6
Min	0.0	0.0	0.0	0.0	0.0	0.0
Max	6.64	13.41	16.87	21.26	10.74	72.32
Sum	6.64	44.25	71.13	83.77	56.47	130.76
Avg	0.23	1.53	2.45	2.89	1.95	4.51

Fig. 6.7 visualizes the relationship between the amount of load curtailments and location of curtailments. Buses 8, 18, 19, 21, and 30 show higher load curtailment profile at most of the time instants compared to other buses. In particular, bus 8

shows the highest load curtailment for a few reasons such as: it is connected to the largest load spot, there isn't enough generation resources connected to that bus in case of islanding, and flow limits of the transmission lines connecting that bus with the rest of the system are low. Although buses 18, 19, 21, and 30 have not been impacted frequently as shown in Table 6.5, load curtailments occur due to tight transmission constraints. This analysis can be used to assess the level of vulnerability of system buses to hurricane impacts and direct specific planning-based resilience enhancement approaches towards these vulnerable buses.

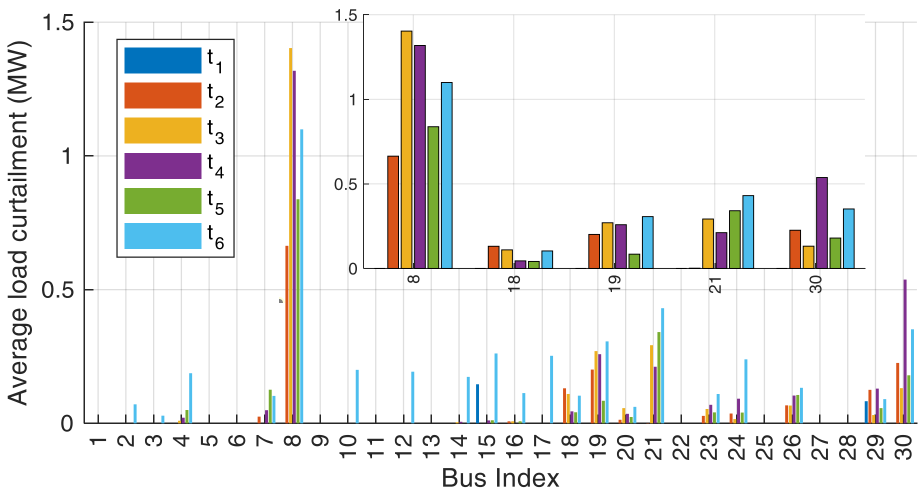

Figure 6.7: Average load curtailment for each bus

6.4 Role of RESs in Generation Redispatch

This section proposes a proactive generation redispatch strategy to enhance the operational resilience of power grids during hurricanes considering the role of RESs. Due to the spatiotemporal propagation characteristics of hurricanes, the status of each component in the power grid might vary, which can be classified into three main stages: prior, during, and after the event. The proposed strategy takes into consideration varying conditions of system components as well as the variability and intermittency of RESs. A mixed integer linear programming optimization problem is formulated to minimize the overall operating cost and amount of load curtailments. System generation and transmission constraints have been considered including power balance, transmission limits, load curtailment limits, generation limits (e.g., power output limits, ramping rates, and up/down times), and generator statuses. The proposed approach leverages the proactive generation redispatch strategy explained in section 3.2.2. However, the probabilistic transition behavior of system components has not been considered. This work focuses mainly on the unavailability of RESs during an extreme events. The proposed strategy provides a mitigation strategy to reduce the negative impacts of RESs on system resilience during a hurricane. The proposed method is tested on a modified version of the IEEE 30-bus system for validation.

6.4.1 Problem Settings

The proposed approach is applied on modified versions of the IEEE 30-bus system. The CPLEX solver is integrated with MATLAB environment to solve the MILP optimization problem. This section describes the system under study and simulated hurricane scenarios.

6.4.1.1 Modified IEEE 30-bus System

To accommodate the role of RESs in the proposed strategy, solar and wind energy sources are added to the IEEE 30-bus system. G_5 is replaced by a solar power plant with total power capacity of 25 MW, whereas G_6 is replaced by a wind power plant with maximum capacity of 30 MW. The parameters of both solar and wind energy are obtained from [89]. The curves of solar and wind power, shown in Fig. 6.8, are calculated based on historical data from [194]. Generators data are provided in Table

6.8. The generators ramping rate (MW/hour) is assumed to be 10% of the maximum power capacity. All generators are assumed to have minimum up/down time of 15 minutes. The impact of load variation is considered using 5 minute intervals load demand obtained from [118] as shown in Fig. 6.9.

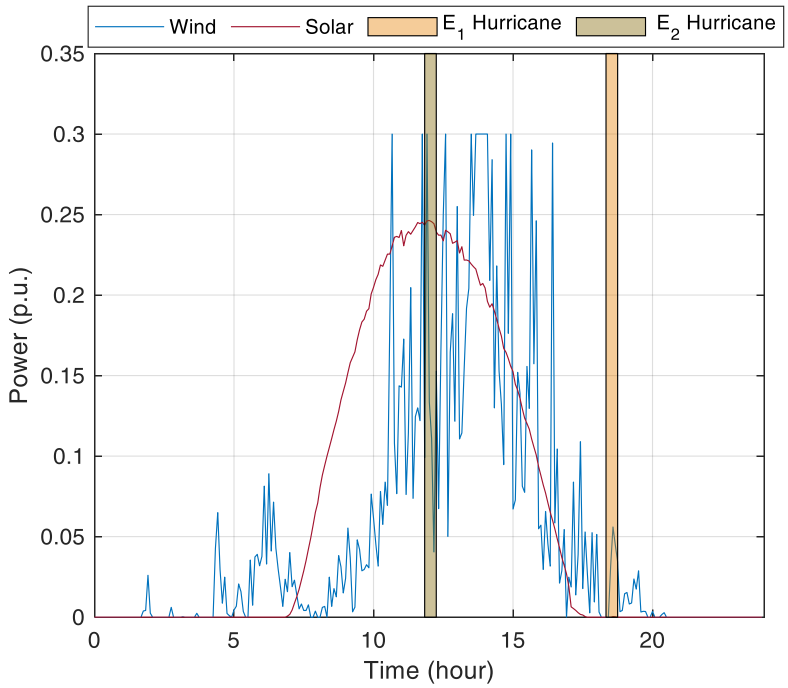

Figure 6.8: Solar and wind real power output

Table 6.8: Generator Parameters of IEEE 30-bus System

Unit	Cost ($)			Power (MW)	
	b	C_{su}	C_{sd}	P_{min}	P_{max}
G_1	1.75	70	176	30	120
G_2	2	70	176	35	140
G_3	2	70	176	10	50
G_4	2.25	70	176	5	30
G_5	0.75	0	0	10	25
G_6	0.75	0	0	15	30

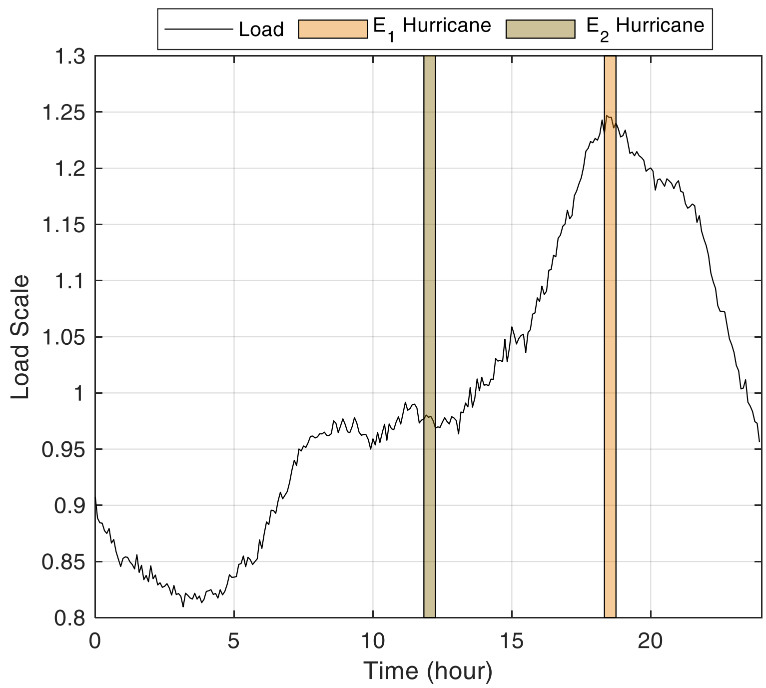

Figure 6.9: Load scaling profile

6.4.1.2 Hurricane Scenario

In this work, a hurricane scenario is assumed to propagate across the IEEE 30-bus system as shown in Fig. 6.10. The total duration of the hurricane is assumed to be 25 minutes. The hurricane period is sampled in sets of 5 minutes to discretize their propagation behavior. The set of failed components at each time instant is provided in Table 6.9 based on the trajectory of the hurricane using the approach proposed in [32, 89].

6.4.2 Validation of the Proposed Algorithm

The performance of the redispatch strategy relies on numerous factors such as the hurricane impact time, the severity of the hurricane, the preparedness strategy execution time, the duration of the event, and the scale of the system. In this work, two factors are considered: the hurricane impact time and the strategy execution time.

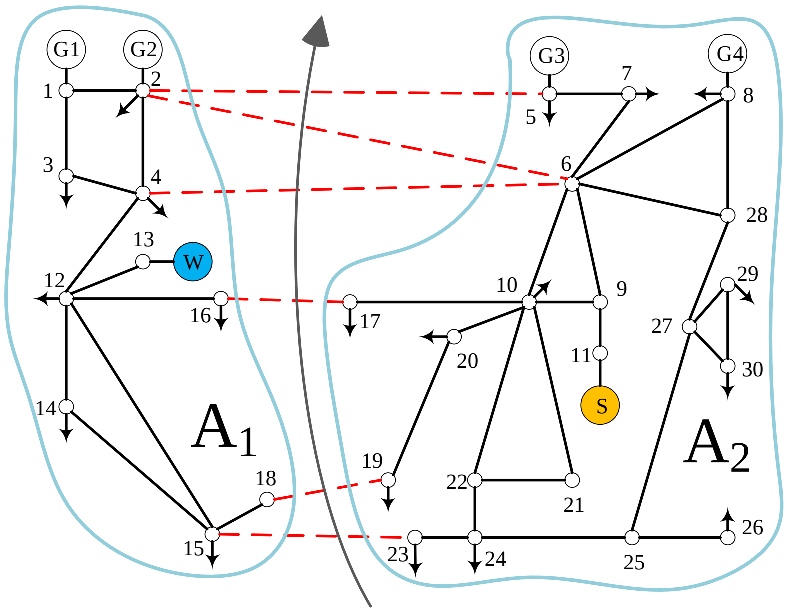

Figure 6.10: Hurricane propagation across IEEE 30-bus system

Table 6.9: List of Failure Components

Time Instant	Component No.	Component Description
t_1	–	–
t_2	C_1	Line 15-23
	C_2	Line 18-19
t_3	C_3	Line 16-17
t_4	C_4	Line 4-6
t_5	C_5	Line 2-6
	C_6	Line 2-5

Also, it is assumed that all failed components will be fully restored after one-hour period from the hurricane end instant. All test cases are validated through comparisons between the proposed proactive redispatch strategy and corrective redispatch strategy. In the corrective strategy, no prior redispatching is applied before the hurricane impact time; however, dispatching is readjusted at each time instant to encounter the failed components and fulfill the current system operational constraints.

6.4.2.1 Hurricane Impact Time

Within the context of this study, a hurricane impact time is the instant when a hurricane lands and its impacts are being realized on power grid components. Since a hurricane can occur at different times during a day, the realization of its impact will vary based on system operational conditions at the impact time. Two hurricane events are simulated: E_1–hurricane occurs during peak load demand and E_2–hurricane occurs during peak solar generation. Table 6.10 summarizes the two simulated hurricane events.

Table 6.10: Simulated Hurricane Events

	Impact period	Start time	End time
E_1	During peak load demand	18:25	18:50
E_2	During peak solar generation	11:55	12:20

(a) During peak load period

During normal operation, generators and RESs supply the full load demand; but, during a hurricane, RESs are forced to shut down due to their uncertain generation behavior. In this case, E_1–hurricane lands at 18:25 during which neither solar nor wind will have noticeable input, as shown in Fig. 6.8. Therefore, the dependency on conventional generators will increase significantly.

Fig. 6.11 shows the real power output of all four conventional generators for 24 hours. In a normal day, all generators are utilized at almost 50% of their capacities. The occurrence of hurricane imposes a corrective redispatch to adjust the generation based on the new system state. This is noticed at G_1 and G_2 where a ramp down behavior is realized to maintain operational constraints. The generation profiles have changed completely due to applying the proposed proactive generation redispatch. Prior to the hurricane, higher utilization of G_1 is noticed to compensate for the less utilization of G_3 and G_4. During the hurricane, G_3 and G_4 ramp up to match the

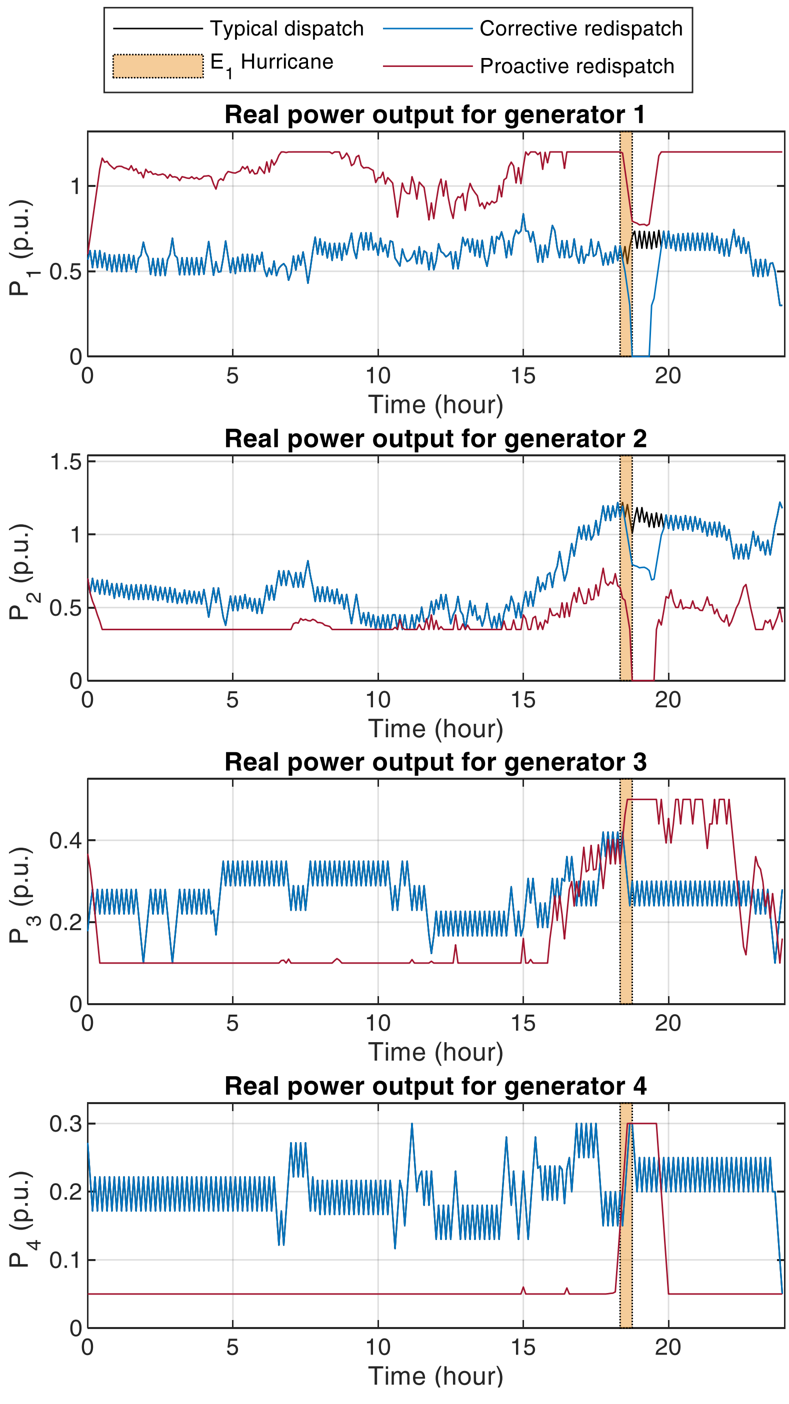

Figure 6.11: Real power output of all conventional generators with and without proactive redispatch strategy during E_1 hurricane (case 1(a))

required load demand and compensate the ramping down of G_1 and G_2. Also, G_2 comes to a complete shutdown at 18:50. After the restoration of system components

(1 hour post hurricane end time), G_1 and G_2 ramp up to benefit from their low operational costs. G_3 operates at almost the full capacity to maintain high load demand; whereas G_4 ramps down to reduce overall operational costs. Generally, the proactive redispatch provides a better preparedness of the system.

The failure of system components on the hurricane trajectory results in splitting the power system into two islands. Most of the load spots exist in A_2; while the two largest generators exist in A_1. Insufficient generation resources at a specific area yields non-avoidable load curtailments. Fig. 6.12 shows the amount of load curtailments with and without the proactive redispatch strategy. The proactive redispatch shows less load curtailments compared to the corrective redispatch. At the first few instants during hurricane, the proactive redispatch has avoided any load curtailments. Afterwards, the proposed algorithm has shown at least 30% reduction in load curtailments. At 18:50, the amount of load curtailments is still growing momentarily under the corrective strategy. After the restoration of failed components, the proactive redispatch provides faster recovery of curtailed load.

(b) During peak solar generation period

Since RESs are forced to shut down during the hurricane because of their uncertain behavior, this case assess the proactive redispatch algorithm when the hurricane lands during high generation supply from RESs. E_2–hurricane lands at 11:55 during which RESs have high generation, as shown in Fig. 6.8. The capabilities of the proactive redispatch strategy can be realized due to high reliance on conventional generators.

Fig. 6.13 compares the real power output of all conventional generators with and without proactive redispatch. Although the proposed algorithm is applied for a whole day, Fig. 6.13 shows a view for two–hour period starting at the hurricane impact time. Overall, the generation profiles varies based on the applied redispatch strategy.

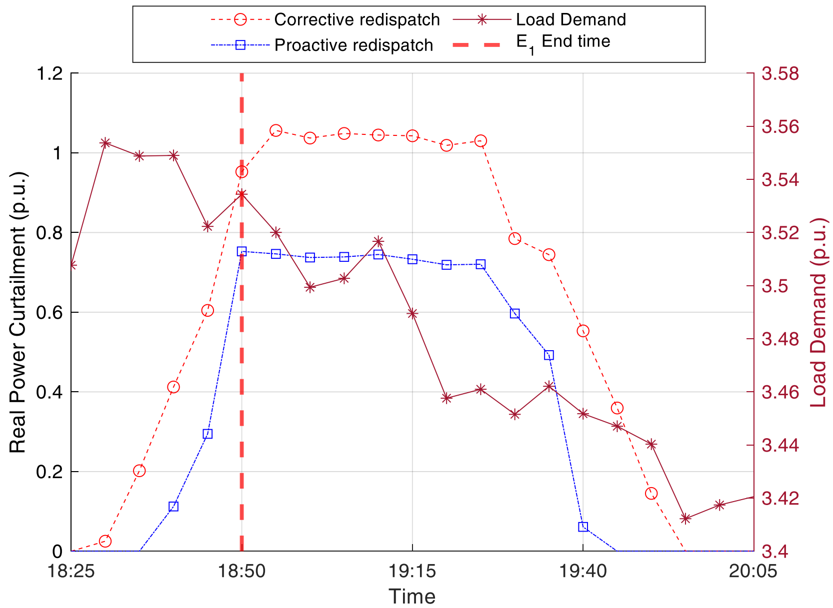

Figure 6.12: Load curtailments with and without proactive redispatch strategy during E_1 hurricane (case 1 (a))

In a typical day with normal operating conditions, the power supplied from RESs will yield less utilization of conventional generators. This is clearly noticed in the corrective strategy results of Fig. 6.13. Applying the proactive redispatch strategy encourages the system to rely on G_1 due to its high capacity and low operational costs. Also, G_3 and G_4 ramp up during the hurricane to match the required load demand. On the other hand, G_1 ramps down very fast to maintain all dynamic constraints post islanding behavior.

The significant impact of the redispatch strategy is the capability to minimize load curtailments even with unavailability of RESs as shown in Fig. 6.14. It is worth noting that the proactive redispatch resulted in no curtailments during hurricane period and prior to islanding. At 12:20, the proactive redispatch has much lower load curtailments compared to corrective redispatch by almost 60%. After the hurricane, the curtailed load under proactive redispatch is due to islanding behavior and insufficient generation in A_2. The increase in load demand starting at 12:30

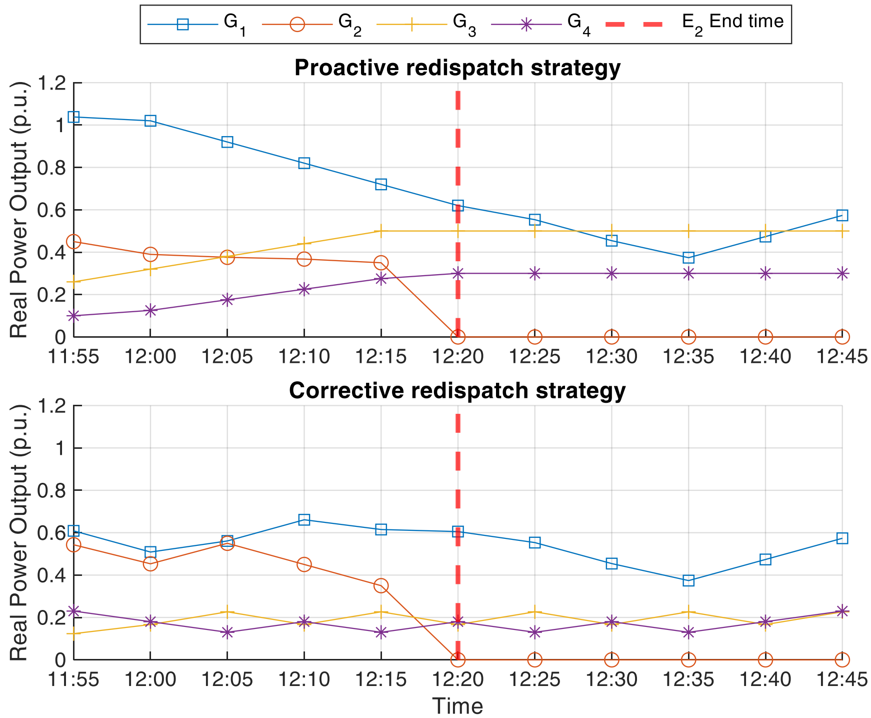

Figure 6.13: Real power output of all conventional generators with and without proactive redispatch strategy during E_2 hurricane (case 1(b))

does not impose further stress conditions on the proactive redispatch strategy. On average, proactive redispatch reduced the amount of load curtailment by 70% post the hurricane period.

6.4.2.2 Strategy Execution Time

Due to high uncertainties in hurricane's temporal and geographical progression and high possibility of changing its trajectory, it may not be essential to apply the redispatch strategy for the whole day resulting in overall high operational costs. The proposed algorithm can be executed at any instant prior to hurricane; however, diverse generation levels and costs are encountered. In this case, the impact of execution time of the proposed strategy is tested by comparing two scenarios: (i) 60-minute interval, and (ii) 120-minute interval prior to the hurricane.

Fig. 6.15 shows the real power output of all conventional generators for the

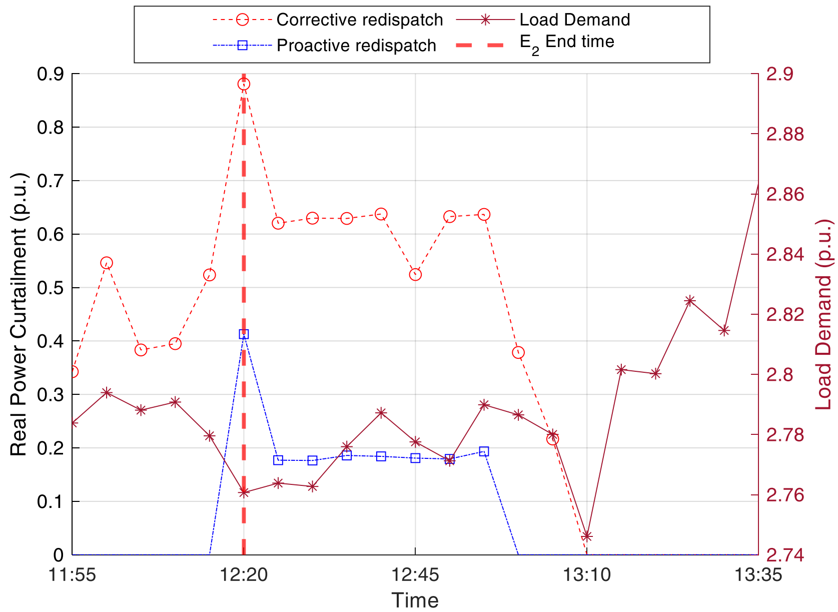

Figure 6.14: Load curtailments with and without proactive redispatch strategy during E_2 hurricane (case 1 (b))

two scenarios during E_2–hurricane. When the proactive redispatch strategy is executed earlier, operational costs are reduced and the utilization of reliable generators is achieved. For instance, G_1 ramps up as soon as the proactive strategy is being implemented while G_2 ramps down to complete shutdown. This implies the capability of the proactive redispatch strategy to prioritize low-operational cost generators over high-operational cost generators. Also, G_4 is pushed to maintain low generation level prior to the hurricane for further cost reduction. Although same load curtailment level is observed for both scenarios, different costs are encountered. The total operational costs for scenario (i) and (ii) are \$940,297.7 and \$937,629.7, respectively.

6.4.3 Effects of RES Sizes on the Resilience Level

In this case, further analysis is conducted to assess the impacts of varying penetration levels of RESs on the resilience of power systems and overall operational costs. The standard IEEE 30-bus system is modified to include solar power plants at buses

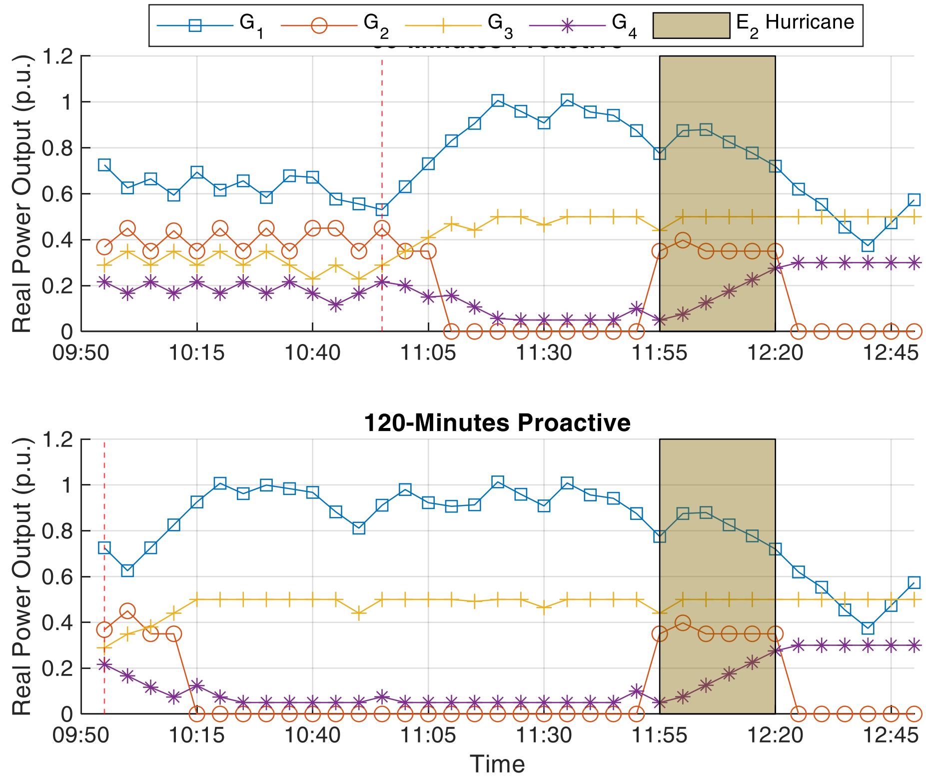

Figure 6.15: Generation profile under different implementation time

3, 6, and 10, and wind power plants at buses 12, 15, and 25. The generation cost coefficients for all units are modified to create a diverse cost profile as summarized in Table 6.11. All conventional generators are assumed to have 15 minutes minimum up/down time. E_2–hurricane is considered in this case. Simulations are run on the system with varying RESs levels under proactive redispatch and corrective redispatch strategies. For validation purpose, the initial generation level of all units is obtained from optimal power flow solution for a normal day—no hurricane is expected.

Fig. 6.16 shows that the operational cost decreases smoothly as the size of RESs increases when using the proposed proactive redispatch algorithm. Ignoring the proactive redispatch results in less operational costs due to the low utilization of conventional generators. Also, increasing the size of RESs without retiring conventional generators can reduce the total amount of load curtailments, which highlights

Table 6.11: Modified Generator Parameters of IEEE 30-bus System

Unit	G_1	G_2	G_3	G_4	G_5	G_6
b	1.8	2	1.8	2.2	1.9	1.6
C_{su}	70	75	80	65	60	70
C_{sd}	30	40	35	25	30	40
Unit	S_1	S_2	S_3	W_1	W_2	W_3
b	0.9	1	0.9	1.1	1	0.8

the importance of integrating RESs to resilience enhancement of power systems. At the beginning of the day, higher load curtailments may be observed compared to the end of the day due to the very tight operating conditions. Even with high generation capacities, the power flow for some transmission lines hits the maximum threshold yielding further burdens on system operation.

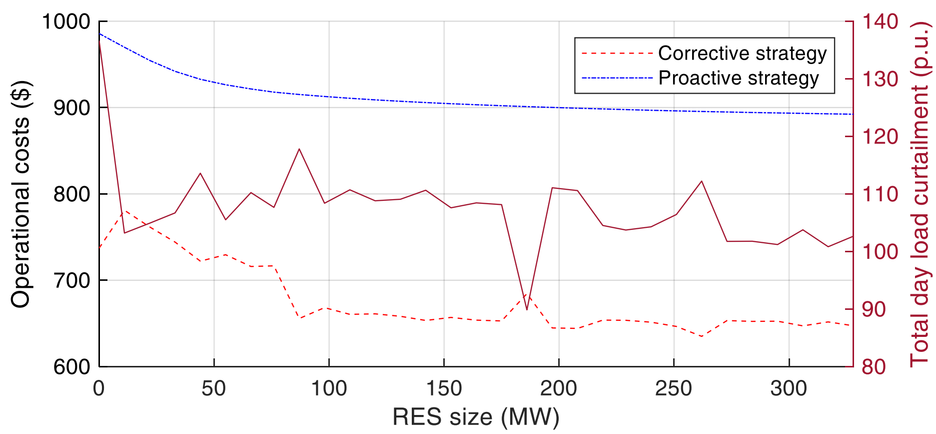

Figure 6.16: Variation between RES size and operational costs and total load curtailments

Fig. 6.17 shows the relationship between load curtailment and time under various RESs penetration levels. For each penetration level, the generation redispatch is solved with and without proactive strategy. It is noticeable that for all RESs penetration level, the proactive redispatch has avoided load curtailments. Without employing proactive generation dispatch similar to the proposed approach, load curtailments cannot be avoided regardless of RES sizes. As the RES sizes increase, the load curtailment profile changes based on the weather data and the total amount of load curtailments decreases. Due to the very tight operating conditions, load is curtailed even with zero penetration level of RESs.

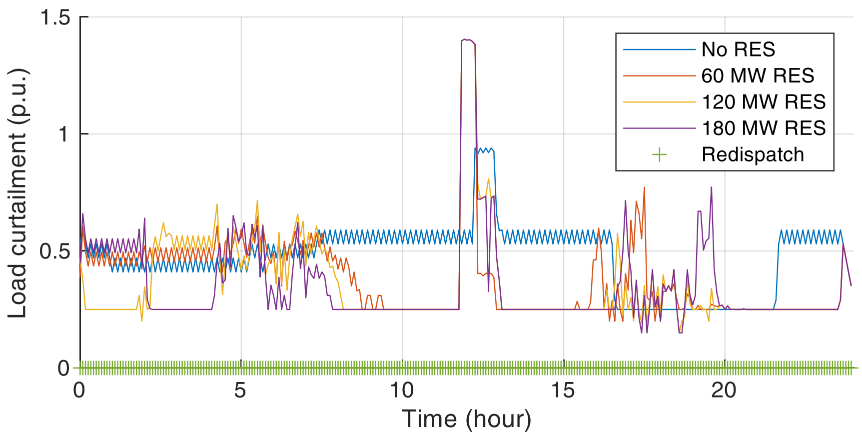

Figure 6.17: Variation between RES size and load curtailments

6.5 Conclusion

In this chapter, three assessment frameworks have been studied considering the impacts of uncertainties in extreme weather events and RESs. Ice storm events as well as hurricane events have been considered in this study. First, uncertainties of ice storms on transmission system resilience was quantified. The results showed the effectiveness of the proposed method quantify the impact of ice storms in a particular geographical location. The proposed algorithm provides a list of vulnerable components to ice storms. Also, the proposed algorithm provides a benchmark resilience metric to evaluate diverse resilience enhancement strategies. On the other hand, a resilience assessment evaluation method was developed and used to quantify the long-term spatiotemporal uncertainties and short-term impacts of hurricanes on power systems. The proposed framework leveraged proactive generation redispatch for enhanced resilience. The results showed the effectiveness of the proposed framework to quantify both the spatiotemporal uncertainties and the fragility uncertainties of hurricanes on power grid. Also, a list of the most vulnerable components to hurricanes was provided. The proposed framework paves the way to system planners to determine future resilience enhancement requirements. Finally, the impacts of unavailability of RESs during hurricane events on transmission power systems was evaluated. The assessment framework leveraged proactive generation redispatch to mitigate the negative impacts of RESs during an extreme event for enhanced resilience. The results showed that the proactive generation redispatch strategy is able to reduce the total amount of load curtailment by 60% in many cases and avoided load curtailments for hurricane taking place at high RESs generation period. Also, the role of execution time of the proposed proactive redispatch has been assessed providing deeper analysis on system resilience performance curve. Also, it paves a framework for system planners to determine proper upgrade and hardening requirements for resilient power grids. In the future, the role of large-scale energy storage systems integrated into proactive generation redispatch shall be considered. Also, the scalability of the proposed algorithm to larger systems will be studied.

Chapter 7

Conclusion and Future Work

This dissertation has studied resilience enhancement strategies including proactive, corrective, and restorative techniques. Also, the role of uncertainties in extreme weather events has been evaluated through various probabilistic methods for enhanced resilience performance. This chapter provides concluding remarks and discusses future directions.

Proactive resilience enhancement strategies. We have developed two proactive strategies to improve resilience of power grids against weather-related and cyber-related events. First, a proactive generation redispatch enhancement strategy was formulated using MDP for minimal load curtailment and operational costs. The proposed algorithm considered probabilistic failure behavior of system components and generation and transmission operational constraints. The generation redispatch strategy was tested against hurricane and wildfire events to measure their adaptability to different event types. Several test cases were performed on IEEE 30-bus system. Results showed that the proposed approach outperforms current corrective strategies for enhanced resilience. The second strategy provided a defensive resilience enhancement strategy through islanding of CPPSs into smaller microgrid for enhanced robustness. The proposed algorithm reduces the negative impacts of cyber-induced failures to power layer by isolating vulnerable components. Results showed the capability of the proposed defensive islanding to create smaller microgrids satisfying radiality constraint and minimal load curtailment.

Corrective resilience enhancement strategies. We have developed three corrective strategies to improve resilience of power grids against severe failure scenarios. Reinforcement learning approaches were leveraged to formulate the proposed control-based enhancement strategies. First, a distribution network reconfiguration strategy was developed to reroute the flow of energy to islanded load spots due to multiple line outages in a distribution feeder. An actor-critic algorithm was trained to determine the set of tie-switches to be turned on maintaining traversing and radiality constraints. The results showed the capability to determine new distribution system topology for enhanced resilience. The second strategy focused on allocating and sizing distributed generators in islanded distribution feeder due to diverse events. A multi-agent actor-critic algorithm was developed and trained considering system operational constraints. Results showed that the proposed RL-based framework is capable of determining locations and sizes of DGs on the IEEE 33-node system against multiple line outages. Finally, a reactive shunt dispatching strategy was formulated and modeled to maintain the voltage regulation of the transmission system within the permissible range after a severe event. A multi-agent soft actor-critic model was developed and tested on the IEEE 30-bus system. Results showed that the proposed shunt dispatching strategy can improve the voltage profile in many cases.

Restorative resilience enhancement strategies. We have developed a restorative strategy to retain curtailed loads of islanded distribution systems after extreme outage. The proposed algorithm was formulated using multi-agent reinforcement learning model to dispatch DGs for minimal load curtailment. Test cases were simulated to validate the efficiency of the proposed framework against single, double, and multiple line outages. The results showed that reinforcement learning methods can provide fast and efficient control actions for enhanced restorative resilience.

Uncertainty Quantification. We have modeled uncertainties of extreme events and unavailability of RESs in resilience assessment methods. First, a resilience evaluation framework was developed to measure the resilience of transmission system against freezing ice storms. Various ice storm scenarios were simulated using PDFs governing the behavior of weather-related parameters. The proposed algorithm was able to determine the list of most vulnerable components against ice storms. The second method quantified the spatiotemporal (long-term) and impact (short-term) uncertainties of hurricanes for enhanced power system. The proposed framework was tested on the IEEE 30-bus system mapped on the Northeastern region of the USA. A list of vulnerable components against hurricanes was extracted for future hardening and improvement upgrades. In the last strategy, the role of RESs during extreme events was assessed taking into account an integrated-proactive generation redispatch approach for enhanced resilience. The proposed framework highlighted the importance of generation redispatch to overcome tight generation challenges due to unavailability of solar and wind sources during hurricanes. The proposed method was tested on the IEEE 30-bus system. Detailed analysis was conducted to evaluate the importance of strategy execution time. Also, the correlation between size of RESs and resilience performance was quantified.

Future Work. The future directions of the proposed work can be stated as follows:

1. Developing a resilience enhancement strategy that fulfill all resilience attributes including resourcefulness, robustness, adaptability, and rapid recovery is a sophisticated problem. Integrating several strategies such as proactive generation redispatch and network reconfiguration can improve overall resilience. However, deeper investigation is still required to assess the interoperability of diverse

strategies within the cyber-physical power system domain.

2. Assessing vulnerabilities in CPPS has become important. Also, the developed CPPS models should take into account recent technological advancement in resilience, big data, cloud computing, and DER market participation.

3. Adopting existing standards such as IEC-61850 and IEEE-1547 to power systems has become essential to cope with the rapidly integration of information and communication technologies. Studying the formulated models from a resilience perspective is a sophisticated and challenging problem.

4. The capabilities of reinforcement learning methods are showing a promising pathway in the field of resilience enhancement strategies. Deeper analysis on scalability of proposed methods to larger problems with increased constraints and complexities will help in achieving the concept of smart grids.

5. Integrating the dynamic behavior of power system in resilience enhancement strategies will create comprehensive assessment models that achieve robustness of system performance.

Acknowledgment

The work in this dissertation was supported by the U.S. National Science Foundation (NSF) under Grant NSF 1847578.

References

[1] (2013) Presidential policy directive-21 critical infrastructure security and resilience. The White House, Office of the Press Secretary. [Online]. Available: https://obamawhitehouse.archives.gov/the-press-office/2013/02/12/presidential-policy-directive-critical-infrastructure-security-and-resil i, 3

[2] N. Bhusal, M. Abdelmalak, M. Kamruzzaman, and M. Benidris, "Power system resilience: Current practices, challenges, and future directions," *IEEE Access*, vol. 8, pp. 18 064–18 086, 2020. 1, 21, 113, 116, 117

[3] R. J. Campbell, "Weather-related power outages and electric system resiliency," Congressional Research Service, Tech. Rep., 2012. 1

[4] M. Panteli and P. Mancarella, "Modeling and evaluating the resilience of critical electrical power infrastructure to extreme weather events," *IEEE Systems Journal*, vol. 11, no. 3, pp. 1733–1742, Sep. 2017. 1, 9, 10, 12, 21

[5] S. Frueh, "Improving power system resilience in the 21st century," *The National Academics of Science, Engineering, and Medicine*, July 2014. 1, 9

[6] F. H. Jufri, V. Widiputra, and J. Jung, "State-of-the-art review on power grid resilience to extreme weather events: Definitions, frameworks, quantitative assessment methodologies, and enhancement strategies," *Applied Energy*, vol. 239, pp. 1049 – 1065, 2019. 1, 4, 9

[7] M. Finster, J. Phillips, and K. Wallace, "Front-line resilience perspectives: The electric grid," Argonne National Laboratory, Global Security Sciences Division. U.S. Department of Energy, Tech. Rep. ANL/GSS-16/2, 2016. 1, 9

[8] B. Preston, S. Backhaus, M.Ewers, J. Phillips, C. A. Silva–Monroy, J. Dagle, A. Tarditi, J. Looney, and T. King Jr., "Resilience of the u.s. electricity system: A multi-hazard perspective," US DOE, Tech. Rep., 2015. 1, 9

[9] A. Hussain, V. H. Bui, and H. M. Kim, "Microgrids as a resilience resource and strategies used by microgrids for enhancing resilience," *Applied Energy*, vol. 240, pp. 56–72, 2019. 1, 9, 115

[10] D. M. Ward, "The effect of weather on grid systems and the reliability of electricity supply," *Climatic Change*, vol. 121, no. 1, pp. 103–113, Nov 2013. 1, 9

[11] W. House, "Economic benefits of increasing electric grid resilience to weather outages," Executive office of the president, Washington, DC, USA, Tech. Rep., Aug 2013. 1

[12] Billion-dollar weather and climate disasters. [Online]. Available: https://www.ncdc.noaa.gov/billions/events/US/2013-2021 1

[13] L. Dale, M. Carnall, M. Wei, G. Fitts, and S. L. McDonald, "Assessing the impact of wildfires on the california electricity grid," *California Energy Commission. CCCA4-CEC-2018-002*, 2018. 1

[14] J. W. Muhs, M. Parvania, and M. Shahidehpour, "Wildfire risk mitigation: A paradigm shift in power systems planning and operation," *IEEE Open Access, Power and Energy*, vol. 7, pp. 366–375, 2020. 1

[15] C. King, J. D. Rhodes, J. Zarnikau, N. Lin, E. Kutanoglu, B. Leibowicz, D. Niyogi, V. Rai, S. Santoso, D. Spence *et al.*, "The timeline and events of the february 2021 texas electric grid blackouts," *The University of Texas Energy Institute*, 2021. 2

[16] (2021) Nevada wildfire map. [Online]. Available: https://www.fireweatheravalanche.org/fire/state/nevada 2

[17] Summary of january 2022 winter storm. [Online]. Available: https://www.weather.gov/akq/Jan22-2022Snow 2

[18] R. V. Yohanandhan, R. M. Elavarasan, P. Manoharan, and L. Mihet-Popa, "Cyber-physical power system (CPPS): A review on modeling, simulation, and analysis with cyber security applications," *IEEE Access*, vol. 8, pp. 151 019–151 064, 2020. 2

[19] B. Ti, G. Li, M. Zhou, and J. Wang, "Resilience assessment and improvement for cyber-physical power systems under typhoon disasters," *IEEE Transactions on Smart Grid*, vol. 13, no. 1, pp. 783–794, 2022. 2, 50, 51, 77

[20] G. Cao, W. Gu, P. Li, W. Sheng, K. Liu, L. Sun, Z. Cao, and J. Pan, "Operational risk evaluation of active distribution networks considering cyber contingencies," *IEEE Transactions on Industrial Informatics*, vol. 16, no. 6, pp. 3849–3861, 2020. 2

[21] E. L. Hotchkiss and A. Dane, "Resilience roadmap: a collaborative approach to multi-jurisdictional resilience planning," National Renewable Energy Lab.(NREL), Golden, CO (United States), Tech. Rep., 2019. 2

[22] H. H. Alhelou, M. E. Hamedain-Golshan, T. C. Njenda, and P. Siano, "A survey on power system blackout and cascading events: Research motivations and challenges," *Energies*, vol. 12, no. 4, pp. 1–28, 2019. 2

[23] S. Paul, F. Ding, K. Utkarsh, W. Liu, M. J. O'Malley, and J. Barnett, "On vulnerability and resilience of cyber-physical power systems: A review," *IEEE Systems Journal*, pp. 1–12, 2021. 2

[24] L. M. Robert, M. Assante, and T. Conway, "Analysis of the cyber attack on the ukrainian power grid," Electricity Information Sharing and Analysis Center, Washington, DC, Tech. Rep., 2016. [Online]. Available: https://ics.sans.org/media/E-ISAC_SANS_Ukraine_DUC_5.pdf 2

[25] D. U. Case, "Analysis of the cyber attack on the ukrainian power grid," *Electricity Information Sharing and Analysis Center (E-ISAC)*, vol. 388, pp. 1–29, 2016. 2

[26] B. AIRES. (2019, June) Massive blackout hits tens of millions in south america. Argentina. [Online]. Available: https://www.apnews.com/a29b1da1a91542faa91d68cf8e97a34d 2

[27] A. B. D. Costa and G.Suroyo. (2019, Aug) Power restored to some areas in indonesia capital, parts of java after 9 hours. [Online]. Available: https://www.reuters.com/article/us-indonesia-power-idUSKCN1UU060 2

[28] A. Fitzsimmons, "Securing us critical infrastructure against cyberattacks," in *Harvard Model Congress, Boston*, 2022. 2

[29] S. Slaughter. (2022) Cybersecurity considerations impacting the us critical infrastructure: An overview. [Online]. Available: https://americanctri.org/wp-content/uploads/2022/02/Cybersecurity-Considerations.pdf 2

[30] R. He, H. Xie, J. Deng, T. Feng, L. L. Lai, and M. Shahidehpour, "Reliability modeling and assessment of cyber space in cyber-physical power systems," *IEEE Transactions on Smart Grid*, vol. 11, no. 5, pp. 3763–3773, 2020. 2, 51

[31] J. Kim and Y. Dvorkin, "Enhancing distribution system resilience with mobile energy storage and microgrids," *IEEE Transactions on Smart Grid*, vol. 10, no. 5, pp. 4996–5006, 2019. 3, 12, 21, 22

[32] C. Wang, Y. Hou, F. Qiu, S. Lei, and K. Liu, "Resilience enhancement with sequentially proactive operation strategies," *IEEE Transactions on Power Systems*, vol. 32, no. 4, pp. 2847–2857, 2017. 3, 12, 13, 21, 22, 25, 28, 30, 34, 69, 137

[33] M. Abdelmalak and M. Benidris, "Proactive generation redispatch to enhance power system operation resilience during hurricanes," in *2020* 52^{nd} *North American Power Symposium (NAPS)*, 2021, pp. 1–6. 3, 21, 22, 128

[34] F. Qiu, J. Wang, C. Chen, and J. Tong, "Optimal black start resource allocation," *IEEE Trans. on Power Syst.*, vol. 31, no. 3, pp. 2493–2494, 2016. 3, 21

[35] H. Nazir, “Lessons learned from the february 2021 Texas power outage,” Canadian Energy Research Institute, Tech. Rep., 2021. 3, 116

[36] C. Field, V. Barros, T. Stocker, D. Qin, D. Dokken, K. Ebi, M. Mastrandrea, K. Mach, G.-K. Plattner, M. T. S.K. Allen, , and P. Midgley, Eds., *Managing the risks of extreme events and disasters to advance climate change adaptation. A Special Report of Working Groups I and II of the Intergovernmental Panel on Climate Change*. Cambridge University Press Cambridge, UK, and New York, NY, USA, 2012. 3

[37] EPRI, “Enhancing distribution resiliency: opportunities for applying innovative technologies,” Palo Alto, CA, USA, Tech. Rep. 1026889, Jan 2013. 4

[38] “Critical infrastructure resilience final report and recommendations,” National Infrastructure Advisory Council, Washington, D.C, 2009. 4

[39] Severe Impact Resilience Task Force, “Severe impact resilience: Considerations and recommendations,” NERC, May 2012. 4

[40] Y. Li, K. Xie, L. Wang, and Y. Xiang, “Exploiting network topology optimization and demand side management to improve bulk power system resilience under windstorms,” *Electric Power Systems Research*, vol. 171, pp. 127–140, 2019. 4, 12

[41] A. Gholami, T. Shekari, M. H. Amirioun, F. Aminifar, M. H. Amini, and A. Sargolzaei, “Toward a consensus on the definition and taxonomy of power system resilience,” *IEEE Access*, vol. 6, pp. 32 035–32 053, 2018. 4, 12

[42] H. H. Willis and K. Loa, “Measuring the resilience of energy distribution systems,” RAND corporation, 2015. 4

[43] M. Panteli and P. Mancarella, “Influence of extreme weather and climate change on the resilience of power systems: Impacts and possible mitigation strategies,” *Electric Power Systems Research*, vol. 127, pp. 259 – 270, 2015. 4, 12

[44] L. M. F. Stevens, C. G. Rieger, and W. C. Phoenix, “HTGR resilience control system strategy,” Idaho Falls, ID, United States, Tech. Rep. INL/EXT-10-19645, 2010. 4

[45] C. G. Rieger, “Resilient control systems practical metrics basis for defining mission impact,” in *2014 7th International Symposium on Resilient Control Systems (ISRCS)*, Denver, CO, USA, Aug 2014, pp. 1–10. 4

[46] M. Panteli and P. Mancarella, “The grid: Stronger, bigger, smarter?: Presenting a conceptual framework of power system resilience,” *IEEE Power and Energy Magazine*, vol. 13, no. 3, pp. 58–66, May 2015. 4, 12, 53

[47] M. Panteli, D. N. Trakas, P. Mancarella, and N. D. Hatziargyriou, "Power systems resilience assessment: Hardening and smart operational enhancement strategies," *Proceedings of the IEEE*, vol. 105, no. 7, pp. 1202–1213, July 2017. 5

[48] M. Panteli, P. Mancarella, D. N. Trakas, E. Kyriakides, and N. D. Hatziargyriou, "Metrics and quantification of operational and infrastructure resilience in power systems," *IEEE Transactions on Power Systems*, vol. 32, no. 6, pp. 4732–4742, Nov. 2017. 5, 12

[49] (2019) NOAA national centers for environmental information (NCEI) U. S. Billion-Dollar Weather and Climate Disasters. [Online]. Available: https://www.ncdc.noaa.gov/billions/ 9

[50] E. Smith, S. Corzine, D. Racey, P. Dunne, C. Hassett, and J. Weiss, "Going beyond cybersecurity compliance: What power and utility companies really need to consider," *IEEE Power and Energy Magazine*, vol. 14, no. 5, pp. 48–56, Sep. 2016. 9, 11

[51] S. Chanda, A. K. Srivastava, M. U. Mohanpurkar, and R. Hovsapian, "Quantifying power distribution system resiliency using code-based metric," *IEEE Transactions on Industry Applications*, vol. 54, no. 4, pp. 3676–3686, July 2018. 10, 25

[52] A. Kavousi-Fard, M. Wang, and W. Su, "Stochastic resilient post-hurricane power system recovery based on mobile emergency resources and reconfigurable networked microgrids," *IEEE Access*, vol. 6, pp. 72 311–72 326, 2018. 10, 21, 68

[53] A. Gholami, T. Shekari, and S. Grijalva, "Proactive management of microgrids for resiliency enhancement: An adaptive robust approach," *IEEE Trans. on Sust. Energy*, vol. 10, no. 1, pp. 470–480, Jan 2019. 10, 21, 68, 69

[54] Z. Li, M. Shahidehpour, and F. Aminifar, "Cybersecurity in distributed power systems," *Proceedings of the IEEE*, vol. 105, no. 7, pp. 1367–1388, July 2017. 10, 11

[55] S. Abbasi, M. Barati, and G. J. Lim, "A parallel sectionalized restoration scheme for resilient smart grid systems," *IEEE Transactions on Smart Grid*, vol. 10, no. 2, pp. 1660–1670, March 2019. 10

[56] Y. Yang, W. Tang, Y. Liu, Y. Xin, and Q. Wu, "Quantitative resilience assessment for power transmission systems under typhoon weather," *IEEE Access*, vol. 6, pp. 40 747–40 756, 2018. 10, 12

[57] M. Kaâniche, "Resilience assessment of critical infrastructures: From accidental to malicious threats," in *2011 Fifth Latin-American Symposium on Dependable Computing Workshops*, April 2011, pp. 35–36. 10

[58] M. Panteli, C. Pickering, S. Wilkinson, R. Dawson, and P. Mancarella, "Power system resilience to extreme weather: Fragility modeling, probabilistic impact assessment, and adaptation measures," *IEEE Transactions on Power Systems*, vol. 32, no. 5, pp. 3747–3757, Sep. 2017. 10

[59] A. Hussain, A. Oulis Rousis, I. Konstantelos, G. Strbac, J. Jeon, and H. Kim, "Impact of uncertainties on resilient operation of microgrids: A data-driven approach," *IEEE Access*, vol. 7, pp. 14 924–14 937, Jan. 2019. 10, 12, 58, 59, 115

[60] P. J. Vickery, J. Lin, P. F. Skerlj, L. A. Twisdale Jr, and K. Huang, "Hazus-mh hurricane model methodology. i: Hurricane hazard, terrain, and wind load modeling," *Natural Hazards Review*, vol. 7, no. 2, pp. 82–93, 2006. 10

[61] M. H. Amirioun, F. Aminifar, and H. Lesani, "Towards proactive scheduling of microgrids against extreme floods," *IEEE Transactions on Smart Grid*, vol. 9, no. 4, pp. 3900–3902, July 2018. 10, 11, 12

[62] G. Huang, J. Wang, C. Chen, J. Qi, and C. Guo, "Integration of preventive and emergency responses for power grid resilience enhancement," *IEEE Transactions on Power Systems*, vol. 32, no. 6, pp. 4451–4463, Nov. 2017. 10, 69

[63] C. Chen, J. Wang, and D. Ton, "Modernizing distribution system restoration to achieve grid resiliency against extreme weather events: An integrated solution," *Proceedings of the IEEE*, vol. 105, no. 7, pp. 1267–1288, July 2017. 10

[64] C. Scawthorn, P. Flores, N. Blais, H. Seligson, E. Tate, S. Chang, E. Mifflin, W. Thomas, J. Murphy, C. Jones *et al.*, "Hazus-mh flood loss estimation methodology. ii. damage and loss assessment," *Natural Hazards Review*, vol. 7, no. 2, pp. 72–81, 2006. 10

[65] D. N. Trakas and N. D. Hatziargyriou, "Optimal distribution system operation for enhancing resilience against wildfires," *IEEE Transactions on Power Systems*, vol. 33, no. 2, pp. 2260–2271, March 2018. 10, 23, 26, 115

[66] M. Nazemi, M. Moeini-Aghtaie, M. Fotuhi-Firuzabad, and P. Dehghanian, "Energy storage planning for enhanced resilience of power distribution networks against earthquakes," *IEEE Transactions on Sustainable Energy*, DOI: 10.1109/TSTE.2019.2907613, 2019. 11, 12, 21, 69

[67] M. Shahidehpour, M. Yan, X. Ai, J. Wen, Z. Li, S. Bahramirad, and A. Paaso, "Enhancing the transmission grid resilience in ice storms by optimal coordination of power system schedule with pre-positioning and routing of mobile dc de-icing devices," *IEEE Transactions on Power Systems*, 2019. 11, 69

[68] J. Lu, J. Guo, Z. Jian, Y. Yang, and W. Tang, "Dynamic assessment of resilience of power transmission systems in ice disasters," in *International Conference on Power System Technology (POWERCON)*, Guangzhou, China, Nov. 2018, pp. 7–13. 11, 13, 18

[69] Y. Xu, C. Liu, Z. Wang, K. Mo, K. P. Schneider, F. K. Tuffner, and D. T. Ton, "DGs for service restoration to critical loads in a secondary network," *IEEE Transactions on Smart Grid*, vol. 10, no. 1, pp. 435–447, Jan. 2019. 12

[70] X. Liu, M. Shahidehpour, Z. Li, X. Liu, Y. Cao, and Z. Bie, "Microgrids for enhancing the power grid resilience in extreme conditions," *IEEE Transactions on Smart Grid*, vol. 8, no. 2, pp. 589–597, March 2017. 12

[71] B. J. Pierre, B. Arguello, A. Staid, and R. T. Guttromson, "Investment optimization to improve power system resilience," in *IEEE International Conference on Probabilistic Methods Applied to Power Systems (PMAPS)*, Boise, ID, USA, June 2018, pp. 1–6. 12

[72] M. Panwar, S. Chanda, M. Mohanpurkar, Y. Luo, F. Dias, R. Hovsapian, and A. K. Srivastava, "Integration of flow battery for resilience enhancement of advanced distribution grids," *International Journal of Electrical Power & Energy Systems*, vol. 109, pp. 314–324, July 2019. 12

[73] A. Hussain, V. Bui, and H. Kim, "Optimal operation of hybrid microgrids for enhancing resiliency considering feasible islanding and survivability," *IET Renewable Power Generation*, vol. 11, no. 6, pp. 846–857, 2017. 12, 21

[74] S. Lei, C. Chen, Y. Li, and Y. Hou, "Resilient disaster recovery logistics of distribution systems: Co-optimize service restoration with repair crew and mobile power source dispatch," *IEEE Transactions on Smart Grid*, 2019. 12

[75] S. Espinoza, M. Panteli, P. Mancarella, and H. Rudnick, "Multi-phase assessment and adaptation of power systems resilience to natural hazards," *Electric Power Systems Research*, vol. 136, pp. 352 –361, 2016. 12

[76] C. Shao, M. Shahidehpour, X. Wang, X. Wang, and B. Wang, "Integrated planning of electricity and natural gas transportation systems for enhancing the power grid resilience," *IEEE Transactions on Power Systems*, vol. 32, no. 6, pp. 4418–4429, Nov. 2017. 12

[77] S. Lei, J. Wang, C. Chen, and Y. Hou, "Mobile emergency generator prepositioning and real-time allocation for resilient response to natural disasters," *IEEE Transactions on Smart Grid*, vol. 9, no. 3, pp. 2030–2041, May 2018. 12

[78] M. Panteli, D. N. Trakas, P. Mancarella, and N. D. Hatziargyriou, "Boosting the power grid resilience to extreme weather events using defensive islanding," *IEEE Transactions on Smart Grid*, vol. 7, no. 6, pp. 2913–2922, 2016. 12, 22, 52, 68

[79] S. Ma, B. Chen, and Z. Wang, "Resilience enhancement strategy for distribution systems under extreme weather events," *IEEE Transactions on Smart Grid*, vol. 9, no. 2, pp. 1442–1451, March 2018. 12

[80] J. Najafi, A. Peiravi, and J. M. Guerrero, "Power distribution system improvement planning under hurricanes based on a new resilience index," *Sustainable Cities and Society*, vol. 39, pp. 592–604, 2018. 12

[81] M. H. Amirioun, F. Aminifar, and H. Lesani, "Resilience-oriented proactive management of microgrids against windstorms," *IEEE Transactions on Power Systems*, vol. 33, no. 4, pp. 4275–4284, July 2018. 12

[82] S. Ma, L. Su, Z. Wang, F. Qiu, and G. Guo, "Resilience enhancement of distribution grids against extreme weather events," *IEEE Transactions on Power Systems*, vol. 33, no. 5, pp. 4842–4853, Sep. 2018. 12

[83] S. Mousavizadeh, M. Haghifam, and M. Shariatkhah, "A linear two-stage method for resiliency analysis in distribution systems considering renewable energy and demand response resources," *Applied Energy*, vol. 211, pp. 443 – 460, 2018. 12

[84] S. Poudel and A. Dubey, "Critical load restoration using distributed energy resources for resilient power distribution system," *IEEE Transactions on Power Systems*, vol. 34, no. 1, pp. 52–63, Jan 2019. 12, 53

[85] D. Luo, Y. Xia, Y. Zeng, C. Li, B. Zhou, H. Yu, and Q. Wu, "Evaluation method of distribution network resilience focusing on critical loads," *IEEE Access*, vol. 6, pp. 61 633–61 639, Oct. 2018. 12

[86] J. Winkler, L. Dueñas-Osorio, R. Stein, and D. Subramanian, "Performance assessment of topologically diverse power systems subjected to hurricane events," *Reliability Engineering & System Safety*, vol. 95, no. 4, pp. 323–336, 2010. 12, 13

[87] A. Barnes, H.Nagarajan, E. Yamangil, R. Bent, and S.Backhaus, "Tools for improving resilience of electric distribution systems with networked," *arXiv:1705.08229v1 [cs.CE]*, May 2017. 13

[88] M. Abdelmalak, J. Thapa, and M. Benidris, "Resilience assessment approach for transmission systems considering uncertainties of ice storms," in *2021 IEEE International Conference on Environment and Electrical Engineering and 2021 IEEE Industrial and Commercial Power Systems Europe (EEEIC / I CPS Europe)*, 2021, pp. 1–6. 13, 16, 17

[89] X. Liu, K. Hou, H. Jia, J. Zhao, L. Mili, X. Jin, and D. Wang, "A planning-oriented resilience assessment framework for transmission systems under typhoon disasters," *IEEE Transactions on Smart Grid*, vol. 11, no. 6, pp. 5431–5441, 2020. 13, 16, 17, 18, 114, 117, 118, 125, 135, 137

[90] M. E. Batts, E. Simiu, and L. R. Russell, "Hurricane wind speeds in the united states," *Journal of the Structural Division*, vol. 106, no. 10, pp. 2001–2016, 1980. 13, 14

[91] P. Vickery, P. Skerlj, and L. Twisdale, "Simulation of hurricane risk in the us using empirical track model," *Journal of structural engineering*, vol. 126, no. 10, pp. 1222–1237, 2000. 14

[92] Y. Wang and D. V. Rosowsky, "Joint distribution model for prediction of hurricane wind speed and size," *Structural Safety*, vol. 35, pp. 40–51, 2012. 14

[93] E. J. Goodwin III, J. D. Mozer, A. DiGioia Jr, and B. Power, "Predicting ice and snow loads for transmission line design," Pennsylvania Power and Light Co Allentown PA, Tech. Rep., 1983. 16

[94] K. F. Jones, "A simple model for freezing rain ice loads," *Atmospheric research*, vol. 46, no. 1-2, pp. 87–97, 1998. 16

[95] H. Nazaripouya, "Power grid resilience under wildfire: A review on challenges and solutions," in *2020 IEEE Power Energy Society General Meeting (PESGM)*, 2020, pp. 1–5. 21, 26

[96] C. Wang, P. Ju, S. Lei, Z. Wang, F. Wu, and Y. Hou, "Markov decision process-based resilience enhancement for distribution systems: An approximate dynamic programming approach," *IEEE Transactions on Smart Grid*, vol. 11, no. 3, pp. 2498–2510, 2020. 21

[97] K. Chawla, P. Bajpai, and R. Das, "Decision support tool for enabling resiliency in an underground power distribution system," *International Journal of Electrical Power & Energy Systems*, vol. 133, p. 107232, 2021. [Online]. Available: https://www.sciencedirect.com/science/article/pii/S0142061521004713 21

[98] C. Wang, Y. Hou, Z. Qin, C. Peng, and H. Zhou, "Dynamic coordinated condition-based maintenance for multiple components with external conditions," *IEEE Trans. on Power Del.*, vol. 30, no. 5, pp. 2362–2370, 2015. 21

[99] Y. Lin, B. Chen, J. Wang, and Z. Bie, "A combined repair crew dispatch problem for resilient electric and natural gas system considering reconfiguration and DG islanding," *IEEE Transactions on Power Systems*, DOI: 10.1109/TPWRS.2019.2895198, 2019. 21

[100] T. R. B. Kushal and M. S. Illindala, "Decision support framework for resilience-oriented cost-effective distributed generation expansion in power systems," *IEEE Transactions on Industry Applications*, vol. 57, no. 2, pp. 1246–1254, 2021. 21

[101] P. Bajpai, S. Chanda, and A. K. Srivastava, "A novel metric to quantify and enable resilient distribution system using graph theory and choquet integral," *IEEE Transactions on Smart Grid*, vol. 9, no. 4, pp. 2918–2929, July 2018. 21

[102] M. Abdelmalak and M. Benidris, "A Markov decision process to enhance power system operation resilience during hurricanes," in *IEEE Power Energy Society General Meeting (PESGM)*, July 2021, pp. 1–5. 22

[103] R. Rocchetta, "Enhancing the resilience of critical infrastructures: Statistical analysis of power grid spectral clustering and post-contingency vulnerability metrics," *Renewable and Sustainable Energy Reviews*, vol. 159, p. 112185, 2022. 22, 52, 68

[104] M. Dabbaghjamanesh, B. Wang, A. Kavousi-Fard, S. Mehraeen, N. D. Hatziargyriou, D. N. Trakas, and F. Ferdowsi, "A novel two-stage multi-layer constrained spectral clustering strategy for intentional islanding of power grids," *IEEE Transactions on Power Delivery*, vol. 35, no. 2, pp. 560–570, 2020. 22

[105] J. Wu, X. Chen, S. Badakhshan, J. Zhang, and P. Wang, "Spectral graph clustering for intentional islanding operations in resilient hybrid energy systems," *arXiv preprint arXiv:2203.06579*, 2022. 22, 52, 68

[106] K. S. A. Sedzro, A. J. Lamadrid, and L. F. Zuluaga, "Allocation of resources using a microgrid formation approach for resilient electric grids," *IEEE Transactions on Power Systems*, vol. 33, no. 3, pp. 2633–2643, May 2018. 22, 68

[107] M. Choobineh, B. Ansari, and S. Mohagheghi, "Vulnerability assessment of the power grid against progressing wildfires," *Fire Safety Journal*, vol. 73, pp. 20–28, 2015. [Online]. Available: https://www.sciencedirect.com/science/article/pii/S0379711215000168 23, 46

[108] S. Mohagheghi and S. Rebennack, "Optimal resilient power grid operation during the course of a progressing wildfire," *International Journal of Electrical Power and Energy Systems*, vol. 73, pp. 843–852, 2015. [Online]. Available: https://www.sciencedirect.com/science/article/pii/S0142061515002409 23

[109] A. Jalilian, K. M. Muttaqi, and D. Sutanto, "A novel voltage clamping-based overvoltage protection strategy to avoid spurious trip of inverter-based resources and eliminate the risk of wildfire following the REFCL operation in compensated networks," *IEEE Transactions on Industry Applications*, pp. 1–1, 2021. 23

[110] M. Abdelmalak and M. Benidris, "A Markov decision process to enhance power system operation resilience during wildfires," in *IEEE Industrial Applications Society Annual Meeting*, Vancouver, BC, Canada, October 2021. 23

[111] S. Xu, Y. Xia, and H.-L. Shen, "Analysis of malware-induced cyber attacks in cyber-physical power systems," *IEEE Transactions on Circuits and Systems II: Express Briefs*, vol. 67, no. 12, pp. 3482–3486, 2020. 23

[112] W. Wang, A. Cammi, F. Di Maio, S. Lorenzi, and E. Zio, "A monte carlo-based exploration framework for identifying components vulnerable to cyber threats in nuclear power plants," *Reliability Engineering & System Safety*, vol. 175, pp. 24–37, 2018. 23

[113] Y. Hayel and Q. Zhu, "Resilient and secure network design for cyber attack-induced cascading link failures in critical infrastructures," in *2015 49th Annual Conference on Information Sciences and Systems (CISS)*, 2015, pp. 1–3. 23

[114] A. Chaves, M. Rice, S. Dunlap, and J. Pecarina, "Improving the cyber resilience of industrial control systems," *International Journal of Critical Infrastructure Protection*, vol. 17, pp. 30–48, 2017. 23

[115] H. Lei and C. Singh, "Non-sequential monte carlo simulation for cyber-induced dependent failures in composite power system reliability evaluation," *IEEE Transactions on Power Systems*, vol. 32, no. 2, pp. 1064–1072, 2017. 24

[116] H. Yuan, G. Li, Z. Bie, and M. Arif, "Distribution system reliability assessment considering cyber-physical integration," *Energy procedia*, vol. 158, pp. 2655–2662, 2019. 24, 51

[117] M. L. Puterman, "Markov decision processes," *Handbooks in operations research and management science*, vol. 2, pp. 331–434, 1990. 29, 71

[118] (2021) New york independent system operator load demand data. [Online]. Available: https://www.nyiso.com/load-data 35, 39, 90, 127, 136

[119] R. Christie. (1993) Power systems test case archive. [Online]. Available: https://labs.ece.uw.edu/pstca/pf30/pg_tca30bus.htm 38, 127

[120] M. Shahidehpour, H. Yamin, and Z. Li, *Market operations in electric power systems: forecasting, scheduling, and risk management*. John Wiley & Sons, 2003. 46

[121] Y. Han, Y. Wen, C. Guo, and H. Huang, "Incorporating cyber layer failures in composite power system reliability evaluations," *Energies*, vol. 8, no. 9, pp. 9064–9086, 2015. 51, 58

[122] W. Liu, Q. Gong, H. Han, Z. Wang, and L. Wang, "Reliability modeling and evaluation of active cyber physical distribution system," *IEEE Transactions on Power Systems*, vol. 33, no. 6, pp. 7096–7108, 2018. 51, 52, 55, 58

[123] R. J. Sánchez-García, M. Fennelly, S. Norris, N. Wright, G. Niblo, J. Brodzki, and J. W. Bialek, "Hierarchical spectral clustering of power grids," *IEEE Transactions on Power Systems*, vol. 29, no. 5, pp. 2229–2237, 2014. 52, 53, 55, 56

[124] S. Hasanvand, M. Nayeripour, S. A. Arefifar, and H. Fallahzadeh-Abarghouei, "Spectral clustering for designing robust and reliable multi-mg smart distribution systems," *IET Generation, Transmission & Distribution*, vol. 12, no. 6, pp. 1359–1365, 2018. 52, 55

[125] A. Ng, M. Jordan, and Y. Weiss, "On spectral clustering: Analysis and an algorithm," *Advances in neural information processing systems*, vol. 14, 2001. 56

[126] Distribution System Analysis Subcommittee, "1992 test feeder cases," IEEE, PES, Tech. Rep., 1992. [Online]. Available: http://sites.ieee.org/pestestfeeders/resources/ 58

[127] W. Liu, Y. Chen, L. Wang, N. Liu, H. Xu, and Z. Liu, "An integrated planning approach for distributed generation interconnection in cyber physical active distribution systems," *IEEE Transactions on Smart Grid*, vol. 11, no. 1, pp. 541–554, 2020. 58, 59

[128] G. Li, P. Zhang, P. B. Luh, W. Li, Z. Bie, C. Serna, and Z. Zhao, "Risk analysis for distribution systems in the northeast u.s. under wind storms," *IEEE Trans. on Power Systems*, vol. 29, no. 2, pp. 889–898, 2014. 58

[129] B. Chen, J. Wang, X. Lu, C. Chen, and S. Zhao, "Networked microgrids for grid resilience, robustness, and efficiency: A review," *IEEE Transactions on Smart Grid*, vol. 12, no. 1, pp. 18–32, 2021. 68

[130] J. Liu, Y. Yu, and C. Qin, "Unified two-stage reconfiguration method for resilience enhancement of distribution systems," *IET Generation, Transmission & Distribution*, vol. 13, no. 9, pp. 1734–1745, 2019. 68

[131] M. Kamruzzaman, M. Abdelmalak, S. Elsaiah, and M. Benidris, "A data-driven shunt dispatch approach to enhance power system resilience against windstorms," in *2021 IEEE Power & Energy Society General Meeting (PESGM)*, 2021, pp. 1–5. 68

[132] X. Zeng, Z. Liu, and Q. Hui, "Energy equipartition stabilization and cascading resilience optimization for geospatially distributed cyber-physical network systems," *IEEE Trans. on Systems, Man, and Cybernetics: Systems*, vol. 45, no. 1, pp. 25–43, 2015. 68

[133] L. Sun, W. Liu, C. Y. Chung, M. Ding, R. Bi, and L. Wang, "Improving the restorability of bulk power systems with the implementation of a wf-bess

system," *IEEE Trans. on Power Systems*, vol. 34, no. 3, pp. 2366–2377, 2019. 68

[134] J. Li, F. Liu, Y. Chen, C. Shao, G. Wang, Y. Hou, and S. Mei, "Resilience control of dc shipboard power systems," *IEEE Trans. on Power Systems*, vol. 33, no. 6, pp. 6675–6685, 2018. 68

[135] Z. Li, M. Shahidehpour, F. Aminifar, A. Alabdulwahab, and Y. Al-Turki, "Networked microgrids for enhancing the power system resilience," *Proceedings of the IEEE*, vol. 105, no. 7, pp. 1289–1310, July 2017. 68, 115

[136] L. T. Marques, A. C. B. Delbem, and J. B. A. London, "Service restoration with prioritization of customers and switches and determination of switching sequence," *IEEE Transactions on Smart Grid*, vol. 9, no. 3, pp. 2359–2370, 2018. 68

[137] N. Xia, J. Deng, T. Zheng, H. Zhang, J. Wang, S. Peng, and L. Cheng, "Fuzzy logic based network reconfiguration strategy during power system restoration," *IEEE Systems Journal*, pp. 1–9, 2021. 68

[138] C. Chen, J. Wang, F. Qiu, and D. Zhao, "Resilient distribution system by microgrids formation after natural disasters," *IEEE Transactions on Smart Grid*, vol. 7, no. 2, pp. 958–966, 2016. 68

[139] A. S. Musleh, H. M. Khalid, S. M. Muyeen, and A. Al-Durra, "A prediction algorithm to enhance grid resilience toward cyber attacks in wamcs applications," *IEEE Systems Journal*, vol. 13, no. 1, pp. 710–719, 2019. 69

[140] Y. Wang, L. Huang, M. Shahidehpour, L. L. Lai, H. Yuan, and F. Y. Xu, "Resilience-constrained hourly unit commitment in electricity grids," *IEEE Transactions on Power Systems*, vol. 33, no. 5, pp. 5604–5614, 2018. 69

[141] B. Taheri, A. Safdarian, M. Moeini-Aghtaie, and M. Lehtonen, "Enhancing resilience level of power distribution systems using proactive operational actions," *IEEE Access*, vol. 7, pp. 137 378–137 389, 2019. 69

[142] M. Abdelmalak and M. Benidris, "A proactive resilience enhancement strategy to electric distribution systems during hurricanes," in *2021 International Conference on Smart Energy Systems and Technologies (SEST)*, 2021, pp. 1–6. 69

[143] H. Farzin, M. Fotuhi-Firuzabad, and M. Moeini-Aghtaie, "Enhancing power system resilience through hierarchical outage management in multi-microgrids," *IEEE Transactions on Smart Grid*, vol. 7, no. 6, pp. 2869–2879, Nov. 2016. 69, 115

[144] J. G. Vlachogiannis and N. D. Hatziargyriou, "Reinforcement learning for reactive power control," *IEEE Trans. on Power Systems*, vol. 19, no. 3, pp. 1317–1325, 2004. 69

[145] Y. Xu, W. Zhang, W. Liu, and F. Ferrese, "Multiagent-based reinforcement learning for optimal reactive power dispatch," *IEEE Trans. on Systems, Man, and Cybernetics, Part C (Applications and Reviews)*, vol. 42, no. 6, pp. 1742–1751, 2012. 69

[146] Q. Yang, G. Wang, A. Sadeghi, G. B. Giannakis, and J. Sun, "Two-timescale voltage control in distribution grids using deep reinforcement learning," *IEEE Trans. on Smart Grid*, vol. 11, no. 3, pp. 2313–2323, 2020. 70

[147] H. Xu, A. D. Domínguez-García, and P. W. Sauer, "Optimal tap setting of voltage regulation transformers using batch reinforcement learning," *IEEE Trans. on Power Systems*, vol. 35, no. 3, pp. 1990–2001, 2020. 70

[148] M. M. Hosseini and M. Parvania, "Artificial intelligence for resilience enhancement of power distribution systems," *The Electricity Journal*, vol. 34, no. 1, p. 106880, 2021. 70

[149] J. Xie, I. Alvarez-Fernandez, and W. Sun, "A review of machine learning applications in power system resilience," in *2020 IEEE Power Energy Society General Meeting (PESGM)*, 2020, pp. 1–5. 70

[150] M. Kamruzzaman, J. Duan, D. Shi, and M. Benidris, "A deep reinforcement learning-based multi-agent framework to enhance power system resilience using shunt resources," *IEEE Transactions on Power Systems*, vol. 36, no. 6, pp. 5525–5536, 2021. 70, 73, 81

[151] L. Tightiz and H. Yang, "Resilience microgrid as power system integrity protection scheme element with reinforcement learning based management," *IEEE Access*, vol. 9, pp. 83 963–83 975, 2021. 70

[152] Z.-c. Zhou, Z. Wu, and T. Jin, "Deep reinforcement learning framework for resilience enhancement of distribution systems under extreme weather events," *International Journal of Electrical Power & Energy Systems*, vol. 128, p. 106676, 2021. 70

[153] H. Nie, Y. Chen, Y. Xia, S. Huang, and B. Liu, "Optimizing the post-disaster control of islanded microgrid: A multi-agent deep reinforcement learning approach," *IEEE Access*, vol. 8, pp. 153 455–153 469, 2020. 70, 100

[154] M. M. Hosseini and M. Parvania, "Resilient operation of distribution grids using deep reinforcement learning," *IEEE Transactions on Industrial Informatics*, pp. 1–1, 2021. 70, 100

[155] A. Zai and B. Brown, *Deep reinforcement learning in action.* Manning Publications, 2020. 70, 101

[156] R. S. Sutton and A. G. Barto, *Reinforcement learning: An introduction.* MIT press, 2018. 71

[157] T. Haarnoja, A. Zhou, P. Abbeel, and S. Levine, "Soft actor-critic: Off-policy maximum entropy deep reinforcement learning with a stochastic actor," *CoRR*, vol. abs/1801.01290, 2018. [Online]. Available: http://arxiv.org/abs/1801.01290 74, 75

[158] Z. Fan, R. Su, W. Zhang, and Y. Yu, "Hybrid actor-critic reinforcement learning in parameterized action space," *CoRR*, vol. abs/1903.01344, 2019. [Online]. Available: http://arxiv.org/abs/1903.01344 75

[159] T. Haarnoja, A. Zhou, K. Hartikainen, G. Tucker, S. Ha, J. Tan, V. Kumar, H. Zhu, A. Gupta, P. Abbeel, and S. Levine, "Soft actor-critic algorithms and applications," *CoRR*, vol. abs/1812.05905, 2018. 76

[160] S. Fujimoto, H. van Hoof, and D. Meger, "Addressing function approximation error in actor-critic methods," *CoRR*, vol. abs/1802.09477, 2018. 76

[161] M. E. Baran and F. F. Wu, "Network reconfiguration in distribution systems for loss reduction and load balancing," *IEEE Power Engineering Review*, vol. 9, no. 4, pp. 101–102, 1989. 80, 107

[162] A. Singhal, V. Ajjarapu, J. Fuller, and J. Hansen, "Real-time local volt/var control under external disturbances with high pv penetration," *IEEE Trans. on Smart Grid*, vol. 10, no. 4, pp. 3849–3859, 2019. 93

[163] G. Qu and N. Li, "Optimal distributed feedback voltage control under limited reactive power," *IEEE Trans. on Power Systems*, vol. 35, no. 1, pp. 315–331, 2020. 93

[164] S. Wang, J. Duan, D. Shi, C. Xu, H. Li, R. Diao, and Z. Wang, "A data-driven multi-agent autonomous voltage control framework using deep reinforcement learning," *IEEE Trans. on Power Systems*, vol. DOI: 10.1109/TPWRS.2020.2990179, pp. 1–11, 2020. 93

[165] R. Lincoln. Pypower. [Online]. Available: https://pypi.org/project/PYPOWER/ 94

[166] A. T. Eseye, X. Zhang, B. Knueven, and W. Jones, "Enhancing distribution grid resilience through model predictive controller enabled prioritized load restoration strategy," in *2020 52nd North American Power Symposium (NAPS)*, 2021, pp. 1–6. 100

[167] J. Zhao, F. Li, X. Chen, and Q. Wu, "Deep learning based model-free robust load restoration to enhance bulk system resilience with wind power penetration," *IEEE Transactions on Power Systems*, vol. 37, no. 3, pp. 1969–1978, 2022. 101

[168] Y. Du and D. Wu, "Deep reinforcement learning from demonstrations to assist service restoration in islanded microgrids," *IEEE Transactions on Sustainable Energy*, vol. 13, no. 2, pp. 1062–1072, 2022. 101

[169] Q. Li, X. Zhang, J. Guo, X. Shan, Z. Wang, Z. Li, and C. K. Tse, "Integrating reinforcement learning and optimal power dispatch to enhance power grid resilience," *IEEE Transactions on Circuits and Systems II: Express Briefs*, vol. 69, no. 3, pp. 1402–1406, 2022. 101

[170] M. Feofilovs, A. Gravelsins, and F. Romagnoli, "Review of disaster resilience assessment methods: (quantitative aspects for renewable energy systems modelling)," in *2020 IEEE 61th International Scientific Conference on Power and Electrical Engineering of Riga Technical University (RTUCON)*, 2020, pp. 1–4. 113

[171] S. N. Naghshbandi, L. Varga, A. Purvis, R. Mcwilliam, E. Minisci, M. Vasile, M. Troffaes, T. Sedighi, W. Guo, E. Manley, and D. H. Jones, "A review of methods to study resilience of complex engineering and engineered systems," *IEEE Access*, vol. 8, pp. 87 775–87 799, 2020. 113

[172] M. A. Haque, G. K. De Teyou, S. Shetty, and B. Krishnappa, "Cyber resilience framework for industrial control systems: Concepts, metrics, and insights," in *2018 IEEE International Conference on Intelligence and Security Informatics (ISI)*, 2018, pp. 25–30. 113

[173] M. Noebels, J. Quirós-Tortós, and M. Panteli, "Decision-making under uncertainty on preventive actions boosting power grid resilience," *IEEE Systems Journal*, pp. 1–12, 2021. 114

[174] E. Ciapessoni, D. Cirio, G. Kjølle, S. Massucco, A. Pitto, and M. Sforna, "Probabilistic risk-based security assessment of power systems considering incumbent threats and uncertainties," *IEEE Transactions on Smart Grid*, vol. 7, no. 6, pp. 2890–2903, 2016. 114

[175] A. Gholami, F. Aminifar, and M. Shahidehpour, "Front lines against the darkness: Enhancing the resilience of the electricity grid through microgrid facilities," *IEEE Electrification Magazine*, vol. 4, no. 1, pp. 18–24, March 2016. 114

[176] M. de Jong, G. Papaefthymiou, and P. Palensky, "A framework for incorporation of infeed uncertainty in power system risk-based security assessment," *IEEE Transactions on Power Systems*, vol. 33, no. 1, pp. 613–621, 2018. 114

[177] E. Brostrom, J. Ahlberg, and L. Soder, “Modelling of ice storms and their impact applied to a part of the swedish transmission network,” in *2007 IEEE Lausanne Power Tech*. IEEE, 2007, pp. 1593–1598. 114

[178] M. Farzaneh and K. Savadjiev, “Statistical analysis of field data for precipitation icing accretion on overhead power lines,” *IEEE Transactions on power delivery*, vol. 20, no. 2, pp. 1080–1087, 2005. 114

[179] H. Yang, C. Chung, J. Zhao, and Z. Dong, “A probability model of ice storm damages to transmission facilities,” *IEEE Transactions on power delivery*, vol. 28, no. 2, pp. 557–565, 2013. 114

[180] A. T. DeGaetano, B. N. Belcher, and P. L. Spier, “Short-term ice accretion forecasts for electric utilities using the weather research and forecasting model and a modified precipitation-type algorithm,” *Weather and forecasting*, vol. 23, no. 5, pp. 838–853, 2008. 114

[181] S. G. Krishnasamy, “Assessment of weather induced transmission line loads on a probabilistic basis,” *IEEE Transactions on Power Apparatus and Systems*, vol. PAS-104, no. 9, pp. 2509–2516, 1985. 114

[182] B. Zhou, L. Gu, Y. Ding, L. Shao, Z. Wu, X. Yang, C. Li, Z. Li, X. Wang, Y. Cao *et al.*, “The great 2008 chinese ice storm: Its socioeconomic–ecological impact and sustainability lessons learned,” *Bulletin of the American meteorological Society*, vol. 92, no. 1, pp. 47–60, 2011. 114

[183] J. Yang, H. Teng, C. Yao, N. Liu, B. Sun, H. Yuan, M. Liu, J. Bai *et al.*, “The reliability evaluation method study of power system communication networks in case of ice storm,” *Engineering*, vol. 5, no. 09, p. 30, 2013. 114

[184] G. Cruse and A. Kwasinski, “Statistical evaluation of flooding impact on power system restoration following a hurricane,” in *2021 Resilience Week (RWS)*, 2021, pp. 1–7. 114

[185] N. T. Bazargani and S. Bathaee, “A novel approach for probabilistic hurricane resiliency assessment of an active distribution system using point estimate method,” in *2018 19th IEEE Mediterranean Electrotechnical Conference (MELECON)*, 2018, pp. 275–280. 115

[186] G. Zhang, F. Zhang, X. Wang, and X. Zhang, “Fast resilience assessment of distribution systems with a non-simulation-based method,” *IEEE Transactions on Power Delivery*, vol. 37, no. 2, pp. 1088–1099, 2022. 115

[187] P. Gautam, P. Piya, and R. Karki, “Resilience assessment of distribution systems integrated with distributed energy resources,” *IEEE Transactions on Sustainable Energy*, vol. 12, no. 1, pp. 338–348, 2021. 115

[188] Storm prediction center. [Online]. Available: https://www.spc.noaa.gov/products/ 119, 127

[189] Storm events database (national centers for environmental information). [Online]. Available: https://www.ncdc.noaa.gov 120, 127

[190] Wind database (national centers for environmental information). [Online]. Available: https://www.ncdc.noaa.gov/cdo$-$web/datatools/lcd 120, 127

[191] Daily U.S. snowfall and snow depth (national centers for environmental information). [Online]. Available: https://www.ncdc.noaa.gov/snow-and-ice/daily-snow 120

[192] M. Abdelmalak and M. Benidris, "Enhancing power system operational resilience against wildfires," *IEEE Transactions on Industry Applications*, 2022. 127

[193] ——, "A Markov decision process to enhance power system operation resilience during hurricanes," in *2021 IEEE Power Energy Society General Meeting (PESGM)*, 2021, pp. 01–05. 128

[194] National Renewable Energy Laboratory Measurement and Instrument Data Center. [Online]. Available: http://www.nrel.gov/midc/ 135